



# UC/CLC CAMPUS EARTHQUAKE PROGRAM



## Initial Source and Site Characterization Studies for the U.C. San Diego Campus



B. Minster, UCSD  
 J. Wagoner, LLNL  
 R. Mellors, SDSU  
 S. Day, SDSU  
 S. Park, UCR  
 S. Elrick, UCR  
 F. Vernon, UCSD  
 F. Heuze, LLNL



July, 1999



UCRL-ID-134785

## DISCLAIMER

This document was prepared as an account of work sponsored by an agency of the United States Government. Neither the United States Government nor the University of California nor any of their employees, makes any warranty, express or implied, or assumes any legal liability or responsibility for the accuracy, completeness, or usefulness of any information, apparatus, product, or process disclosed, or represents that its use would not infringe privately owned rights. Reference herein to any specific commercial product, process, or service by trade name, trademark, manufacturer, or otherwise, does not necessarily constitute or imply its endorsement, recommendation, or favoring by the United States Government or the University of California. The views and opinions of authors expressed herein do not necessarily state or reflect those of the United States Government or the University of California, and shall not be used for advertising or product endorsement purposes.

This report has been reproduced  
directly from the best available copy.

Available to DOE and DOE contractors from the  
Office of Scientific and Technical Information  
P.O. Box 62, Oak Ridge, TN 37831  
Prices available from (423) 576-8401

Available to the public from the  
National Technical Information Service  
U.S. Department of Commerce  
5285 Port Royal Rd.,  
Springfield, VA 22161

## PREFACE

This report was prepared under the UC/CLC Campus Earthquake Program (CEP), which was initiated as part of the Campus-Laboratory Collaboration (CLC) Program created by the University of California Office of the President (UCOP).

The Campus Earthquake Program started in March 1996 as a partnership between four campuses of the University of California - Los Angeles, Riverside, San Diego, and Santa Barbara - and the Lawrence Livermore National Laboratory (LLNL). In 1998, three campuses - Berkeley, Davis, and Santa Cruz - were added to the collaboration. The current CEP studies focus on Riverside, San Diego, and Santa Barbara. Each campus has selected a critical site to demonstrate the methods and procedures used by the CEP. The following sites have been selected: the Rivera Library at UC Riverside, the Thornton Hospital at UC San Diego, and the Engineering 1 building at UC Santa Barbara.

In the first phase of the program, March 1996-April 2000, we are estimating strong ground motions at each critical site. These estimates are obtained by using an integrated geological, seismological, geophysical, and geotechnical approach, bringing together the unique capabilities of the campus and Laboratory personnel. This program is also designed to maximize student participation. Many of the site-specific results are also applicable to risk evaluation of other sites on the respective campuses. In the next phase, the program is planning to extend the integrated studies of strong ground motion effects to other interested UC campuses which are potentially at risk from damaging earthquakes.

This report describes the initial seismic source and site characterization studies performed for the UC San Diego campus where a new seismic station has been installed. The Principal Investigator at San Diego is Professor Bernard Minster.

The Campus Earthquake Program is funded from several additional sources, which leverage the core support provided by the Office of the President and which are gratefully acknowledged. These sources included the University Relations Program at LLNL, directed by Dr. Claire Max, and the offices of the appropriate Vice-Chancellors on the various campuses. At UC San Diego, the Senior Vice-Chancellor for Academic Affairs was Marjorie Caserio and is now Marsha Chandler, the Vice-Chancellor for Resource Management and Planning is John A. Woods, and the Assistant Vice-Chancellor for Design and Construction is Boone Hellmann.

The Director of the UC/CLC Campus Earthquake Program is Dr. Francois Heuze from LLNL.

## TABLE OF CONTENTS

	<b>Page</b>
<b>EXECUTIVE SUMMARY</b> .....	iv
<b>LIST OF TABLES</b> .....	v
<b>LIST OF FIGURES</b> .....	vi
<b>1.0 INTRODUCTION</b> .....	1
<b>1.1 Methods and Philosophy of the CLC Campus Earthquake Program</b> .....	1
<b>1.2 Seismic Hazard Exposure of the UCSD Campus and San Diego Area</b> .....	1
<b>1.3 Selection of a Target Building at UCSD</b> .....	2
<b>1.4 Organization of the report</b> .....	3
<b>2.0 SEISMOTECTONIC SETTING OF THE UC SAN DIEGO CAMPUS</b> .....	3
<b>2.1 Regional Tectonic Setting, and Historical Seismicity Near San Diego</b> .....	3
<b>2.2 Regional Earthquake Sources</b> .....	4
2.2.1 San Andreas Fault .....	4
2.2.2 San Jacinto Fault .....	5
2.2.3 Imperial Fault .....	6
2.2.4 Elsinore Fault .....	7
2.2.5 San Miguel-Vallecitos Fault Zone .....	7
<b>2.3 Earthquake Sources Within the San Diego Area</b> .....	8
2.3.1 Rose Canyon Fault Zone .....	8
2.3.2 San Clemente-San Isidro Fault Zone .....	10
2.3.3 Agua Blanca-Coronado Bank Fault Zone .....	11
<b>3.0 LOCAL UCSD SOURCE AND SITE CHARACTERIZATION</b> .....	12
<b>3.1 Local Geology and Stratigraphy in the San Diego Area</b> .....	12
<b>3.2 Geological and Geotechnical Data from Previous Foundation Studies at Thornton</b> .....	14
<b>3.3 Shallow Seismic Refraction Profiling</b> .....	15
3.3.1 Experiment description .....	15
3.3.2 Seismic refraction line 1 .....	16
3.3.3 Seismic refraction line 2 .....	17
3.3.4 Seismic refraction line 3 .....	18
3.3.5 Seismic refraction line 4 .....	19

<b>3.4 Cone-Penetration Soil Tests, and Downhole Velocity Measurements</b> .....	19
<b>3.5 Deep Hole Drilling and Sampling</b> .....	20
<b>3.6 Geophysical Logging of Hole CLC #1, and Geologic Interpretation</b> .....	20
3.6.1 Electric and Gamma Logs .....	20
3.6.2 Suspension P- and S- Velocity Logs .....	21
3.6.3 Geologic Interpretation .....	21
<b>3.7 Summary of Shear-Wave Data, in the Upper 30 Meters</b> .....	23
<b>3.8 Seismic Background Noise Surveys</b> .....	24
<b>3.9 Instrumentation for the Seismic Station, and Station Installation</b> .....	25
<b>3.10 Initial Recordings from the Thornton Seismic Station</b> .....	26
<b>4.0 REFERENCES</b> .....	28
<b>5.0 ACKNOWLEDGMENTS</b> .....	31

## EXECUTIVE SUMMARY

For each campus and each specific location on campus targeted by the Campus Earthquake Program, the seismic hazard investigation is planned in two phases as follows:

Phase 1 - Initial source and site characterization, drilling, geophysical logging, installation of the seismic station, and initial seismic monitoring

Phase 2 - Extended seismic monitoring, dynamic soil testing, and calculated estimates of site-specific earthquake strong motions at depth and at the surface

The site selected for study by the UCSD administration is the Thornton hospital, which is located on the east side of Interstate 5. This report documents activities for Phase 1 and includes results through July, 1999.

We first address the seismotectonic setting of the UCSD campus and the historical seismicity of San Diego and its region. We then describe both the regional earthquake sources and those around the San Diego area. Estimates are presented for possible sources and magnitudes of future seismic events affecting the campus. The coastal and inner borderland fault system appears to pose several seismic threats to San Diego County's coastal zone. Moderate to strong seismic shaking could result from earthquakes on any of the following faults:

Rose Canyon fault	M 6.2-7.0
La Nacion fault/Point Loma zone	M 6.2-6.6
Coronado Bank fault	M 6.0-7.7
San Diego Trough fault	M 6.1-7.7
San Clemente fault	M 6.6-7.7
Onshore Agua Blanca fault system	M 6.5-7.2
San Miguel fault zone	M 6.0-6.8 (historical event)

A magnitude 6.5 earthquake on the Rose Canyon fault could produce shaking intensities as high as Modified Mercalli VIII or IX in San Diego valleys and along bays. Earthquakes in the ranges shown above for any of the onshore or nearshore (Coronado bank) San Diego faults could subject the coastal zone to shaking intensities of MM VII (at epicenter of M6 earthquakes) or even as high as MM IX-X (at epicenter of M7 earthquakes).

The presentation of seismotectonic data is followed by a detailed description of the studies conducted to date at the Thornton site: additional examination of the local geology, review of existing soil exploration data, shallow seismic refractions, cone-penetration geotechnical tests, seismic background noise survey, deep-hole drilling sampling and geophysical logging, and installation of a new seismic station at the Thornton site. Finally, the report presents uphole and downhole earthquake records obtained by this new CLC seismic station.

## LIST OF TABLES

- Table 1. Active faults near San Diego and their earthquake potential.
- Table 2. Historical seismicity in the San Diego area (Anderson et al, 1989).
- Table 3. Geotechnical data for the UCSD Satellite Medical Facility, San Diego, CA (Geocon Inc., 1989) and for the Charter Psychiatric Hospital and Shiley Eye Center (Geocon Inc., 1989).
- Table 4. Downhole shear-wave velocities from the CPT tests at Thornton hospital.
- Table 5. List of earthquakes recorded at the Thornton CLC station up to July 19, 1999.

## LIST OF FIGURES

- Note: CDMG is the California Department of Mines and Geology  
SCEC is the Southern California Earthquake Center
- Figure 1. Active fault map of Southern California (CDMG, 1994) with UC campus locations.
- Figure 2. Active fault map of Southern California, showing fault names (SCEC, 1994).
- Figure 3. Distribution of the number of times per century that peak acceleration will exceed 0.2g in Southern California (Jackson et al, 1995; adapted by Hudnut, 1997).
- Figure 4. Seismicity of southern California (1932-1996). Data provided by SCEC.
- Figure 5. Map of the U.C. San Diego campus, showing the Thornton hospital location, east of Interstate 5.
- Figure 6. Aerial overview of the Thornton hospital site, looking west. Seismic station holes being drilled (right center). Photo by F. Heuze, June 27, 1997.
- Figure 7. Intensities of felt earthquakes in San Diego (Anderson et al, 1989).
- Figure 8. Segmentation of major faults in southern California (Jackson et al, 1995).
- Figure 9. Map showing the major late Cenozoic fault zones of the inner California Continental Borderland and adjacent areas in the vicinity of San Diego and northern Baja California, Mexico (Legg and Kennedy, 1991).
- Figure 10a. Major strands of the Rose Canyon fault (Lindvall and Rockwell, 1995).
- Figure 10b. Segmentation and activity of the Newport-Inglewood-Rose Canyon fault zone (Fischer and Mills, 1991).
- Figure 11. Index map of bedrock geology of the San Diego coastal area (Kennedy, 1975). Quaternary deposits are not shown.
- Figure 12. Evolving interpretations of the sea cliff exposures along Blacks Beach (Abbott and May, 1991).
- Figure 13. Detailed map of the Thornton Hospital site, showing locations of CLC boreholes, CPT tests, and seismic refraction survey lines.

- Figure 14a. Example of seismic refraction record. Note the dominant frequency of the arrivals in the 20-30 Hz range. Shot point was located 4 m from first geophone.
- Figure 14b. Example of SH records with opposite polarities. Note how SH arrival can be identified by a first break upward on one record and downward on the other.
- Figure 15a. Line 1 travel time plots and velocity models for P waves. A travel time plot at the top, a raypath diagram in the middle, and a velocity model on the bottom.
- Figure 15b. Line 1 travel time plots and velocity models for SH waves.
- Figure 16a. Line 2 travel time plots and velocity models for P waves.
- Figure 16b. Line 2 travel time plots and velocity models for SH waves.
- Figure 17a. Line 3 travel time plots and velocity models for P waves.
- Figure 17b. Line 3 travel time plots and velocity models for SH waves.
- Figure 18a. Line 4 travel time plots and velocity models for P waves.
- Figure 18b. Line 4 travel time plots and velocity models for SH waves.
- Figure 19. The sites of CPT tests 1 through 4
- Figure 20. Cone penetration test results for CPT-1.
- Figure 21. Cone penetration test results for CPT-2.
- Figure 22. Cone penetration test results for CPT-3.
- Figure 23. Cone penetration test results for CPT-4.
- Figure 24. Lithologic section in deep hole CLC#1, as interpreted from cuttings samples, Pitcher samples, and geophysical logs.
- Figure 25. Borehole CLC#1, suspension P and SH wave velocities.
- Figure 26. Fining upwards sequences in the Scripps Formation, along with the shear-wave velocity log.
- Figure 27. Summary depth profile of the various logs and sample locations
- Figure 28. Schematic showing stratigraphy in holes CLC#1, CLC#2, and CLC#3, with locations of Pitcher samples and downhole instrumentation.
- Figure 29. Summary of results of the seismic background noise survey at Thornton hospital.
- Figure 30. P-wave broadband records from an mb 5.2 event at 1840 km, during the noise survey
- Figure 31. Conceptual design of the Thornton hospital seismic station.
- Figure 32. Epicentral locations of seismic events recorded at Thornton up to July 19, 1999.
- Figure 33. Records from a M 3.0 earthquake at a distance of 172 km, on October 22, 1997.
- Figure 34. Records from a M 4.4 earthquake at a distance of 96 km, on July 19, 1999.
- Figure 35. Downhole-to-surface amplification of horizontal spectral accelerations for the July 19, 1999 seismic event.

## 1.0 INTRODUCTION

### 1.1 Methods and Philosophy of the CLC Campus Earthquake Program.

The basic approach of the CLC project is to combine the substantial expertise that exists within the UC system in geology, seismology, geotechnical engineering, and structural engineering to evaluate the effects of large earthquakes on UC facilities. These estimates draw upon recent advances in hazard assessment, seismic wave propagation modeling in rocks and soils, dynamic soil testing, and structural dynamics. The UC campuses currently chosen for applications of our integrated methodology are Riverside, San Diego, and Santa Barbara. The basic procedure is first to identify possible earthquake source regions and local campus site conditions that may affect estimates of strong ground motion. Combined geological, geophysical, and geotechnical studies are conducted to characterize each campus with specific focus on the location of particular target buildings of special interest to the campus administrators. The project will then drill and log deep boreholes next to the target structure, to provide direct in-situ measurements of subsurface material properties and to install uphole and downhole 3-component seismic sensors capable of recording both weak and strong motions. The boreholes provide access to deeper materials, below the soil layers, that have relatively high seismic shear-wave velocities. Analysis of conjugate downhole and uphole records provides a basis for optimizing the representation of the low-strain response of the sites. Earthquake rupture scenarios of identified causative faults are combined with the earthquake records and nonlinear soil models to provide site-specific estimates of strong motions at the selected target locations. The predicted ground motions are then used as input to the dynamic analysis of the buildings.

Thus, for each campus targeted by the CLC project, the seismic effects study will consist of three phases, Phase 1 - Initial source and site characterization, drilling, geophysical logging, installation of the seismic station, and initial seismic monitoring, Phase 2 - Extended seismic monitoring, dynamic soil testing, and calculated estimates of site-specific earthquake strong motions at depth and at the surface, and Phase 3: Calculations of 3-D Building Responses.

### 1.2 Seismic Hazard Exposure of the UCSD Campus and San Diego Area

UCSD is located further from the major inland tectonic structures than the other campuses (**Figure 1**), but differs in its close proximity to the major faults in the inner borderland offshore California. The names of all these active faults in southern California are shown in **Figure 2**, and

an extensive discussion of seismic hazards from onshore faults in Southern California can be found in Jackson et al., 1995 .

UCSD is likely to experience peak acceleration of 0.2g or greater less than once per century (**Figure 3**). Note the relative paucity of significant events in the San Diego region during the past 66 years (**Figure 4**). However, as indicated in **Table 1**, UCSD remains exposed to earthquakes of magnitude exceeding 6.0, from fault segments less than 10km away. The coastal and inner borderland fault system appears to pose several seismic threats to San Diego County's coastal zone. Including the danger of fault rupture on any of the strands of the Rose Canyon fault and perhaps on the onshore portions in the La Nacion-East Point Loma zone, moderate to strong seismic shaking could result from earthquakes on any of the following faults (after Kern, 1988):

Rose Canyon fault	M 6.2-7.0
La Nacion fault/Point Loma zone	M 6.2-6.6
Coronado Bank fault	M 6.0-7.7
San Diego Trough fault	M 6.1-7.7
San Clemente fault	M 6.6-7.7
Onshore Agua Blanca fault system	M 6.5-7.2
San Miguel fault zone	M 6.0-6.8 (historical quakes)

Earthquakes in the ranges shown above for any of the onshore or nearshore (Coronado bank) San Diego faults could subject the coastal zone to shaking intensities of MM VII (at epicenter of M6 earthquakes) or even as high as MM IX-X (at epicenter of M7 earthquakes) (Kern, 1988). An estimate of strong ground motion associated with a M7 event anywhere along the Rose Canyon fault indicates that medium peak horizontal accelerations as high as 0.5-0.6g and Modified Mercalli intensities as high as X can be expected on alluvium in proximity to the fault (Anderson et al., 1989; Sangines, Campbell, and Seligson, 1991).

### 1.3 Selection of A Target Building at UCSD

The critical structure selected by the UCSD administration for a demonstration study is the Thornton hospital. Its location, east of Interstate 5, is shown on the campus map (**Figure 5**) and in an aerial view taken during the drilling of the seismic station holes (**Figure 6**). The 120-bed hospital is a 4-story steel moment frame structure constructed in 1992. The lateral load resisting system consists of special steel moment frames in the perimeter of the building. An X-shaped framing system was used in the south portion of the structure due to the geometry of the building. This created an irregular framing system with complicated dynamic characteristics. Unfortunately, this kind of framing system was found to be vulnerable to brittle fracture at

welded beam-to-column moment connections after the 1994 Northridge earthquake. As a result, the Thornton hospital was strengthened by adding braces to the existing moment frame. With the CLC approach, more realistic ground motions can be generated to reexamine the response of the hospital. The 3-D model of the structure to be analyzed in the next phase of the project would be validated from both passive seismic monitoring of the building itself and from the results of instrumented forced motion tests on the structure. These structural studies will involve additional faculty members from UCSD and other U.C. sites.

#### **1.4 Organization of the Report**

The report first addresses the general seismotectonic setting of the UCSD campus and reviews the historical seismicity of San Diego and its region. Then, we describe both the regional earthquake sources and those in the San Diego area. Estimates are presented for possible sources and magnitudes of future seismic events affecting the campus. This is followed by a detailed description of the studies conducted to date at the Thornton site: additional examination of the local geology, review of existing soil data, shallow seismic refractions, cone-penetration geotechnical tests, deep-hole drilling sampling and geophysical logging, and seismic background noise survey. Finally, the report presents uphole and downhole earthquake records obtained by the new CLC seismic station.

## **2.0 SEISMOTECTONIC SETTING OF THE UC SAN DIEGO CAMPUS**

### **2.1 Regional Tectonic Setting and Historical Seismicity Near San Diego**

The San Diego region is located within the broad shear zone that forms the transform boundary between the North American and Pacific plates. This plate boundary zone is more than 225 km wide in southern California, extending from the San Clemente fault to the San Andreas fault. The right lateral relative motion between the two plates is largely accommodated by northwest-trending strike-slip faults. The total amount of relative plate motion is estimated at 48 mm/year (De Mets et al., 1990). A portion of the plate motion is being absorbed by faults along the western part of the shear zone, including the Coronado Bank, San Diego Trough, Rose Canyon, and San Clemente faults.

The historical record of earthquakes is as good for San Diego as for any other part of California (**Table 2**). For intensity high enough to cause serious damage (VII or above), the record is probably complete from 1769, when the mission and presidio were established (Agnew, 1991). The quality of reporting became much better in 1850 when an Army post was established.

Additional descriptive material can be found in newspaper reports. **Figure 7** shows all intensities reported for San Diego through the end of 1982 (Anderson et al, 1989)

Although northern Baja California is a region of high seismicity, no moderate or large magnitude ( $M > 5$ ) historical earthquakes can be readily associated with the Agua Blanca fault (Kern, 1988). Along the offshore portion of the Agua Blanca fault zone, M3-M5 earthquakes and swarms of smaller magnitude events have been centered west of Punta Salsipuedes and within Todos Santos Bay (Gonzales and Suarez, 1984). The Coronado Bank fault zone is characterized by a linear trend of M3-M5 events offshore from San Diego (Rockwell, Hatch, and Schug, 1987).

The San Diego Trough fault zone has been active in the recent past. It generated a magnitude 5.3 event in July, 1986 (Hauksson and Jones, 1988).

The San Clemente fault zone also has high seismicity. The largest earthquake (magnitude 5.9) occurred in 1951. The most recent significant event on the fault was ML3.7, occurring 96 km west/southwest of Thornton hospital on November 26, 1997. Unfortunately, the Thornton seismic station was not on line at the time.

Earthquake activity has been low in onshore coastal San Diego during the past 200 years (Magistrale, 1993; Kern, 1988; Simons, 1977). From 1932 to 1982, the largest earthquake in the immediate vicinity of San Diego was a M3.4 in 1964. Beginning in 1983, however, there was a dramatic change in seismicity. Between June 1983 and July 1986, there were 4 events with magnitudes  $> 4.0$ .

The historical earthquake record of the Rose Canyon fault system is ambiguous because of the uncertainty of epicentral locations of the 1800 and 1862 quakes. Both produced Mercalli intensities of VI to VII in San Diego and probably were located on either the Rose Canyon fault (with magnitudes of  $\sim 6.5$  and 6.0) or on the Coronado Bank fault (Kern, 1988).

## **2.2 Regional earthquake sources**

### **2.2.1 San Andreas Fault**

The 325 km-long southernmost portion of the San Andreas fault extends from the Cajon Pass to the Salton Sea (No. 30, **Figure 2**) and is divided into the Mojave, San Bernardino Mountains, and Coachella Valley segments. In the Salton Trough, the San Andreas Fault splays into a broad zone that includes the San Jacinto, Imperial, and other major faults further to the south. While there has been high seismicity on some of the associated faults in this region, the San Andreas has not had a major earthquake in historical times (Kern, 1988). Between 1934 and 1961, there were only four earthquakes of M5.0 or greater. The only surface rupture during this time was about 1 cm of right slip in the Mecca Hills, and this displacement was triggered by the Borrego Mountain earthquake on the San Jacinto fault in 1968 (Kern, 1988). Jackson et al (1995) suggest

a maximum magnitude of 7.45 for the 114 km southern segment of the San Andreas. Anderson et al (1989) estimated a maximum plausible magnitude of 7.3 for this segment, but up to M8.2 for multiple segment events. A magnitude 8 earthquake on the southern segment of the San Andreas could produce Mercalli Intensities of VI-VII in the coastal areas of San Diego county (Kern, 1988).

**Mojave Segment:** The Mojave segment extends southeastward 78 km from about Three Points to a few kilometers northwest of Cajon Creek (No. 5, **Figure 8**). The northwest end of the segment is not well-defined and represents a 40 km-long transition zone where slip increased from about 3 to 7 m in 1857; the southeastern end is the southern limit of the 1857 rupture. A primary characteristic of the Mojave segment is a relatively consistent 3 to 4 m of slip during the 1857 earthquake, although Salyards et al (1992) estimate slip during the 1857 and two prior events at about 6 m per event near the south end. Based on a slip rate of  $30 \pm 5$  mm/yr and a characteristic displacement of  $4.5 \pm 1.0$  m, the recurrence interval is 150 years.

**San Bernardino Mountains Segment:** This segment is a structurally complex zone between the Mojave and Coachella Valley (No. 6, **Figure 8**). The San Bernardino Mountains segment has received the most study since the 1988 Working Group report (1988). New paleoseismic data provide several important constraints for estimating behavior of the San Bernardino Mountains segment. It appears that the most recent event was in 1812, which defines an elapsed time of 181 years. New observations of offset define a characteristic displacement of  $3.5 \pm 1.0$  m (Jackson et al., 1995). A slightly modified slip rate of  $24 \pm 5$  mm/yr results in an average recurrence interval of 145(+143,-60) years.

**Coachella Valley Segment:** The Coachella Valley segment (No. 7, **Figure 8**) comprises the southern 114 km of the fault and extends from the San Geronio Pass on the northwest to the Salton Sea on the southeast. This segment has the longest elapsed time of any on the fault zone, last experiencing a large event around 1680. The 1988 Working Group (1988) used the paleoseismological event times at Indio of 1680, 1450, 1300, and 1020 to arrive at an average recurrence interval of 220 years. As of 1995, there had been no additional paleoseismic study of this segment (Jackson et al., 1995)

### 2.2.2 San Jacinto Fault

The San Jacinto fault system has been an important source of moderate to large earthquakes in southern California this century. The fault zone is a complex system that is 10 km wide and 250-km long, extending from its junction with the San Andreas fault near Wrightwood to the northern edge of the Gulf of California (No. 16, **Figure 2**). The San Jacinto fault passes diagonally across the northeastern corner of San Diego County, where the zone includes numerous named fault segments, as well as many smaller, unnamed Quaternary faults.

Jackson et al (1995) divided the San Jacinto Fault into segments using information on fault geometry, historical seismicity, and slip rate. The segments were named San Bernardino Valley (No. 8), San Jacinto Valley (No. 9), Anza (No. 10), Coyote Creek (No. 11), Borrego Mountain (No. 12), Superstition Mountains (No. 13), and Superstition Hills (No. 14) segments (**Figure 8**).

During the past century, the San Jacinto fault zone has been the most active seismic feature in southern California. Since 1899, there have been ten earthquakes of magnitude close to 6.0. From this short historical record, it appears that earthquakes of magnitude 6-7 are characteristic of the entire San Jacinto zone and that these events occur at an average interval of 8-11.5 years throughout the zone. The Anza segment has had no earthquakes since the 1890's at least, thus it presumably poses a more imminent seismic threat than the others (Kern, 1988).

McEuen and Pinckney (1972) estimated a maximum probable earthquake for the San Jacinto fault of M6.9-7.3, and a maximum credible event of M7.6. As the Coyote Creek and Borrego Mountain segments are only 100-105 km from San Diego, earthquakes of magnitude 6.0 would produce Mercalli scale shaking intensities of IV-V in the city. Events of magnitude 6.5 to 7.0 could shake San Diego at Mercalli V-VI and VI-VII respectively.

### 2.2.3 Imperial Fault

The Imperial Fault is located in the southern part of the Salton Trough, and trends from east of El Centro, about 35 km into northern Mexico (No. 14, **Figure 2**; No. 23, **Figure 8**). The Imperial fault is a complex structure with multiple modes of slip behavior. It has produced two large historical surface faulting earthquakes -- an M6.9 in 1940 and an M6.4 in 1979. The 1979 event broke the northern 25 km of the 1940 rupture with a similar amount of surface offset. The 1988 Working Group (1988) noted that the long-term slip rate for the fault is not well determined, but assumed a value of  $30 \pm 5$  mm/yr, estimated a characteristic displacement of  $1.2 \pm 0.4$  m, and calculated a recurrence interval of 44 years for the northern section only. This interval was adopted by Jackson et al (1995). Repeat times of 1940-type events are unknown. It is possible that the northern part of the fault, which had significantly lower slip than the southern part in 1940, is failing repeatedly at shorter intervals to fill a slip deficit.

Subsurface investigations at the U.S.-Mexico border led Sharp (1981) to suggest that several hundred years had passed between the penultimate event and the 1940 earthquake. A recent trenching study by Thomas and Rockwell (1996) confirms this observation. Based on relations between the fault and deposits of the last high stand of Lake Cahuilla, they conclude that only the 1940 Imperial Valley earthquake produced significant surface offset during the past 300 years and that the penultimate event dates to about 1670. Thomas and Rockwell (1996) also suggest that the slip rate on the Imperial fault for the past 300 years is only about 15 to 20 mm/yr, which is substantially less than the geodetic estimates.

#### 2.2.4 Elsinore Fault

This major northwest trending strike-slip fault (No. 11, **Figure 2**) accommodates 5 to 10 percent of the plate boundary slip in southern California and could produce earthquakes of magnitude 7 or larger. The fault can be traced about 250 km from Los Angeles on the north across the U.S.-Mexico border into northern Baja California. Jackson et al (1995) divided the fault into five segments (from north to south): Whittier (No. 15), Glen Ivy (No. 16), Temecula (No. 17), Julian (No. 18), and Coyote Mountain (No. 19, **Figure 8**). Slip rates vary from about 2.5 mm/yr at the north end to about 5 mm/yr at the south end. The lower apparent slip rate on the Whittier segment may be related to branching of the fault or strain partitioning due to the more westerly trend of this segment. The San Andreas, San Jacinto, and Imperial faults are the only northwest trending strike-slip faults in southern California having higher slip rates. Segment-specific mean repeat times range from 240 years to about 760 years and average around 400 years. With the possible exceptions of the M7 earthquake of 1892 on the Laguna Salada segment in Mexico and the M6 1910 Temescal Valley event on the Glen Ivy segment, the Elsinore fault has not produced an earthquake with surface faulting during the past 200 years.

The fault zone crosses eastern San Diego County on its 200 km path from the Mexican border to the northern end of the Santa Ana Mountains in Los Angeles County. Near its northwestern end in Riverside County, it apparently splits into the Whittier and Chino faults. Near the southeastern end of the Coyote Mountains in eastern San Diego County, the fault steps left to the Laguna Salada fault, which continues at least 60 km more into Mexico (Magistrale and Rockwell, 1996; Kern, 1988; Lamar and Rockwell, 1986; Mueller, 1985).

Lamar and Rockwell (1986) summarized previous studies that include total slip estimates ranging from 5 to 40 km in San Diego County. Wesnousky (1986) assumed 4mm/yr average rate of slip, supposing that the fault is characterized by moderate earthquakes that rupture individual segments rather than the entire fault zone. McEuen and Pinckney (1972) estimated the maximum probable earthquake for the Elsinore fault zone at M6.9 to 7.3, with a recurrence interval of 60 years. They suggested a maximum credible earthquake at M7.6.

#### 2.2.5 San Miguel-Vallecitos Fault Zone Trend

The San Miguel-Vallecitos fault zone strikes southeastward for a distance of ~160 km from the vicinity of Tijuana (**Figure 9**). The fault zone, located within the peninsular ranges of Baja California, has produced moderate to large earthquakes in historic time. The fault zone is composed of the Vallecitos, Calabasa, and San Miguel fault strands and it accommodates a fraction of the relative motion between the Pacific and North American plates. The fault zone displays right lateral strike slip motion and may be the southeastern extension of the Rose

Canyon fault. However, there are some structural complexities that separate the Rose Canyon and San Miguel fault zones (Hirabayashi et al, 1996).

The San Miguel fault zone has been the most seismically active structure of the Baja California peninsula this century (Reyes et al, 1975), producing six moderate earthquakes of about M6 or greater in a sequence from 1954-1956 on the San Miguel segment alone. The slip rate for the San Miguel-Vallecitos fault zone is quite low (0.1-0.5 mm/yr), relative to other strike-slip faults in northern Baja California and southern California (Petersen and Wesnousky, 1994), and the consequent return time for large earthquakes is long (Hirabayashi et al, 1995). Dividing the slip expected for rupture of the entire 160 km length of the fault zone by the fault slip rate yields an estimated return time for M7.8 earthquakes of about 80 ka (Hirabayashi et al, 1996).

## 2.3 Earthquake sources within the San Diego area

### 2.3.1 Rose Canyon Fault Zone

The Rose Canyon fault zone (**Figure 10a**; **Figure 10b**) comprises a complex set of anastomosing and en echelon fault strands that include the Rose Canyon, Mount Soledad, Country Club, Mission Bay, Old Town, Spanish Bight, Coronado, and Silver Strand faults, in addition to several other secondary faults (Lindvall and Rockwell, 1995; Kennedy, 1975; Kennedy and Welday, 1980). Although the displacement on the Rose Canyon fault is generally considered to be right-lateral strike-slip, individual strands within the fault zone display various combinations of dip slip and strike slip. The variable sense of dip-slip motion along this fault is characteristic of many strike-slip faults that have variations in strike or dip along their length. These changes have locally resulted in the uplift of Mount Soledad and the depression of San Diego Bay (Lindvall and Rockwell, 1995).

Geomorphic expression of the fault zone from Mount Soledad south to Mission Bay indicates that the Mount Soledad strand is the most active. Based on trenching studies, Lindvall and Rockwell (1995) estimate a slip rate of 1.07 +/- 0.03 mm/yr on the strand. In a study of offset streams, West (1987) suggested a slip rate of 0.7 to 1.2 mm/year on the principal strand on Mount Soledad. Wesnousky (1986) suggested a rate of 1.5 mm/year based on the scant geologic data in the literature. Seismicity is quite low and diffuse along the fault zone, with most of the seismicity located near the San Diego Bay, along the southern portion of the fault zone. The left bend of Mount Soledad may be locking the fault, perhaps accounting for its low seismic profile during the past century, yet there is no genuine evidence for this suggestion (Kern, 1988). However, earthquake swarms in 1985 and 1986 included 3 M4 events (Treiman, 1993). Topozada et al (1981) also found evidence from historical reports of damage in San Diego from two pre-1900 earthquakes in 1862 (M5.9) and 1800 (M6.5) (Petersen and Wesnousky, 1994).

Anderson et al (1989) identified potential fault segments of the Rose Canyon fault zone that might rupture in single earthquakes, based on segments that were defined by large-scale changes in fault orientation and structural discontinuities. The Mission Bay segment is 24-km long and extends from the restraining bend of the fault north of Mount Soledad to the major releasing step in the fault at San Diego Bay (**Figure 10a**). Immediately north is the 34-km long Del Mar segment that extends from the restraining bend at Mount Soledad to the structural complexities and step in the fault zone near Oceanside (**Figure 10b**). Based on an estimated fault width of 12 km, the Mission Bay and Del Mar segments are estimated to be capable of generating M6.4 and M6.6 earthquakes, respectively. If the adjacent segments ruptured together, the resulting earthquake would register M6.9 (Anderson, et al, 1989). Based on an assumed slip rate of 1.2 mm/yr (which is similar to the estimate of Lindvall and Rockwell, 1995), Anderson, et al (1989) estimated average recurrence times of 720 years for the M6.4 event and 1800 years for the M6.9 event (Lindvall and Rockwell, 1995). Treiman (1993) suggested a maximum credible earthquake of M6.5 to 7.2, but a maximum expected earthquake of only M5.4 to 6.7.

To the southeast of San Diego, the Rose Canyon fault zone has been interpreted as being related to, or possibly extending to, the Vallecitos and San Miguel fault zones in Baja California (**Figure 9**). The San Miguel fault has been the most seismically active structure in that region this century, producing a sequence of M6-6.8 earthquakes in 1954 and 1956. However, recent paleoseismic investigations along the 1956 San Miguel surface rupture (Hirabayashi et al, 1995) indicate a slip rate of only 0.1 to 0.5 mm/yr, which is much less than that determined for the Rose Canyon fault zone. Thus much of the Rose Canyon fault slip apparently is accommodated by the Descanso fault in the near offshore of Tijuana (Legg, 1985). The Rose Canyon fault zone makes a right bend and splays across San Diego Bay as the Silver Strand, Coronado, and Spanish Bight faults toward the Descanso fault zone, thereby producing the extension and subsidence associated with the San Diego Bay area. These observations imply that the Descanso fault transfers over 1mm/yr of slip southward to the Agua Blanca fault zone (Lindvall and Rockwell, 1995).

The Rose Canyon fault zone is the dominant element of active deformation onshore in coastal San Diego County (Kern, 1988). The Rose Canyon fault, a right-slip wrench fault, includes several subparallel strands (some of which are active) that cross the zone from south-southeast to north-northwest. It is enveloped by an extensive array of associated, but largely inactive, shorter secondary fractures. There is a broad zone of apparently active north-south faults of intermediate length that include the La Nacion-Sweetwater Group east of San Diego Bay, several offshore faults across Coronado and North Island, and Point Loma's eastern boundary faults (Kern, 1988). The main onshore trace of the Rose Canyon fault extends 20 to 25 km from the north end of San Diego Bay to the sea cliffs at La Jolla. Its northward path continues at least another 40 km to the

offshore zone west of Oceanside. Further continuity with the Newport-Inglewood fault in Los Angeles (**Figure 10b**) has been argued by Moore (1972), Legg and Kennedy (1979), and Fischer and Mills (1991). The offshore Newport Inglewood-Rose Canyon fault zone between Newport Beach and La Jolla is subdivided into 3 major segments and several subsegments (Fischer and Mills, 1991). From north to south the 3 segments are the Dana Point, Oceanside, and Del Mar segments (**Figure 10b**). Onshore and south of La Jolla and offshore of San Diego Bay, Fischer and Mills (1991) proposed 2 additional divisions, called the San Diego and offshore Silver Strand segments.

As many as five or more subparallel strands constitute the main onshore fault zone. Some of these strands are discontinuous, and one of them may break into several right-lateral stepping en-echelon segments. The secondary faults are pervasive in the fault zone at a range of scales. Dense clusters of faults are conspicuous at quadrangle scale (Kern, 1988).

The zone of intermediate-length north-south faults crossing the San Diego Bay region appears to be an active one. Terrace deformation on the east side of Point Loma suggests activity of the faults bounding Point Loma's eastern shore. The Spanish Bight, Coronado, and Silver Strand faults apparently cut Pleistocene and probably Holocene sediments offshore (Kennedy and Welday, 1980). Though the evidence is ambiguous, faulting in the Sweetwater-La Nacion system may also be active (Woodward-Clyde Consultants, 1986). The entire zone seems to be of extension across the southern end of the onshore section, as there are substantial normal separations on several of these faults (Elliott, 1970, Woodward-Clyde Consultants, 1986).

### 2.3.2 San Clemente-San Isidro Fault Zone

The inner continental borderland west of San Diego is crossed by a complex system of faulting that is continuous with onshore faults in northern Baja California and in coastal southern California (**Figure 9**). Both offshore and onshore parts of this system pose potential seismic hazards to San Diego. The major offshore fault zones are the San Clemente-San Isidro, San Diego Trough-Bahia Soledad, and Palos Verde Hills-Coronado Bank. Late Quaternary and probably Holocene activity are indicated on all three zones by ocean-floor scarps, offset submarine canyons, and offsets of uppermost ocean-floor sediments (Kern, 1988). Recent seismicity also clearly delineates these structures and further attests to their activity.

The San Clemente fault system defines the western edge of the inner California Continental Borderland (**Figure 9**). The San Clemente-San Isidro fault zone is a long (>300 km), continuous, zone of dextral shear that marks the axis of the San Clemente fault system. The fault zone is generally narrow (<2 km), although locally, major branch faults broaden its width (5-10 km). To the northwest, the San Clemente fault zone has been mapped past San Clemente Island (Vedder et al, 1974; Ford and Normark, 1980) and may continue as far north as Santa Cruz Island

(Corbett, 1984). Through a major left bend along the western edge of the Descanso Plain, it is linked to the San Isidro fault zone (Legg et al, 1991). The San Isidro fault zone is mapped to the southeast as far as 31°N latitude, but data are not available to map its southernmost extent. Swarms of earthquakes, with magnitudes as great as 5.0 and located off the Baja California coast a few kilometers northwest of San Quintin, may show modern activity along the southern continuation of the San Clemente fault system (Brune, et al, 1979). The San Isidro fault zone has an overall N30W trend, which is about 10° more northerly than the trend of the San Clemente fault zone.

The San Clemente-San Isidro fault zone does not pass onshore in Baja California, and appears from offset geomorphic features to have a slip rate of 4mm/yr (Legg, 1985). Anderson et al (1989) give a rate of .5 to 5.0 mm/yr. Woodward-Clyde Consultants (1986) suggested that the San Clemente-San Isidro fault zone is capable of a maximum credible magnitude of 7.7, while Anderson et al (1989) give a range of M6.7 to 7.7.

### 2.3.3 Agua Blanca-Coronado Bank Fault Zone

The Agua Blanca fault system is a complex northwest-trending zone of dextral shear, delineated by three or more subparallel, wrench fault zones. All of these wrench fault zones terminate or merge into the Agua Blanca fault which cuts across the Baja California peninsula (**Figure 9**). In the offshore area, all of these zones have a similar N30+5W trend. Also, a region of north-south trending faults is located in the area southwest of San Diego. To the north, the major fault zones of the Agua Blanca trend more westerly as they approach the Transverse Ranges.

The Agua Blanca fault system is a major active tectonic element in Baja California that is capable of producing moderately large earthquakes. Initial movement along this structure may have begun during the Cretaceous Period. The fault may have a maximum displacement of 11 to 22 km. Onshore studies of the Agua Blanca fault system indicate that about 6mm/yr of dextral slip is distributed among three faults that trend offshore to connect with the inner borderland faults. The main Agua Blanca fault accounts for most of this with at least 4mm/yr (Anderson, Rockwell, and Agnew, 1989; Kern, 1988; Rockwell, Hatch, and Schug, 1987).

The Palos Verde Hills-Coronado Bank and San Diego Trough-Bahia Soledad fault zones are continuous with the onshore Agua Blanca fault. The San Diego Trough-Bahia Soledad fault zone marks the western edge of the Agua Blanca fault system (**Figure 9**). The fault zone consists of relatively long and continuous (~50 km) fault traces. The main trace of the Bahia-Soledad fault zone trends approximately N50W and passes onshore near the Punta Santo Tomas where it is inferred to link with the south branch of the Agua Blanca fault. Faulting is complex along the eastern edge of the Descanso Plain where the San Diego Trough and Bahia Soledad fault zones

connect. The San Diego Trough fault trends more northerly than the Bahia Soledad fault and lies near the axis of the San Diego Trough (Legg et al, 1991).

The Coronado Bank-Agua Blanca fault zone is complex, with numerous discontinuous, subparallel right and left-stepping, en echelon fault segments, commonly associated with substantial structural relief. This fault zone disrupts surficial sediments presumed to be of late Quaternary to Holocene age along the shelf and nearshore slopes; faults offset the seafloor locally (Legg et al, 1991).

Nearshore faults associated with the Agua Blanca fault system include the Newport-Inglewood-Rose Canyon fault zone to the north and the Descanso-Estero fault zone to the south (**Figure 9**). These fault zones trend subparallel to the coast and pass onshore near San Diego and Ensenada. Numerous north-trending faults in the San Diego Bay are inferred to be associated with right-stepping, en echelon faulting between the Rose Canyon and Descanso fault zones (Legg et al, 1991).

Leighton and Associates (1983) estimated a maximum probable earthquake on the Coronado Bank fault of M5.8 to 6.2, with a recurrence interval of 100-200 years. A M6.2 quake typically would cause a Modified Mercalli shaking intensity of VII within a radius of 8 to 40 km and perhaps VIII within a few kilometers of the epicenter. Woodward-Clyde Consultants (1986) suggested a maximum earthquake range of M6.25 to 7.25. Anderson et al, (1989) give a range of M6.5 to 7.0 for the onshore Agua Blanca and a maximum plausible earthquake of M6.1 to 7.7 for earthquakes rupturing multiple segments of the Coronado Bank fault (Kern, 1988). Woodward-Clyde Consultants (1986) suggested a maximum plausible event of M6.25 to 6.75 for the San Diego Trough fault, while Anderson et al (1989). give a range of M6.1 to 7.7, as the result of multiple segment rupture.

### **3.0 LOCAL UCSD SOURCE AND SITE CHARACTERIZATION STUDIES**

#### **3.1 Local Geology and Stratigraphy Near U.C. San Diego**

The University of California at San Diego is located northwest of the Scripps Institution of Oceanography (**Figure 11**), on a broad, regional mesa known informally as Torrey Pines Mesa. Across Torrey Pines Mesa, Eocene sedimentary formations of the La Jolla Group (Kennedy, 1975) are unconformably overlain by early Pleistocene to late Pliocene sediments, which were deposited across a wave-cut marine terrace.

These marine terraces are wave-abraded platforms that have been preserved from subsequent erosion and deposition. Each marine terrace was cut during a Pleistocene sea-level high stand. Continuous slow uplift raised each terrace clear of wave action. Each terrace is mantled by a

regressive sequence of marine and nonmarine sediments that were deposited during sea-level high stand and retreat. As sea level dropped after each high stand, sand and gravel were spread across the terrace surface by shoreline and alluvial processes. These coarse sedimentary deposits form the most commonly observed rock type resting directly on the terrace surface.

The Tertiary sediments were deposited unconformably on an irregular surface of Mesozoic basement rocks. The pre-Eocene basement rocks are subdivided into 4 major units, which from oldest to youngest are the Bedford Canyon Formation, Santiago Peak Volcanics, southern California Batholith, and the Rosario Group. The pre-Eocene basement terrane is locally decomposed to depths of 49 m. In most areas where Eocene sediments rest directly on the basement rock, the early Tertiary surface is marked by residual clay deposits of montmorillonite that grade downward into fresh basement rock and upward into the Eocene sedimentary rock (Kennedy, 1975).

The Santiago Peak Volcanics comprise an elongate belt of mildly metamorphosed volcanic, volcanoclastic, and sedimentary rocks. The volcanic rocks range in composition from basalt to rhyolite, but are predominantly dacite and andesite and are hard and extremely resistant to weathering and erosion. Most of the volcanic rocks are dark greenish gray when fresh, and weather from grayish red to dark reddish brown. Age estimates for this group range from Late Triassic to mid-Cretaceous.

The Upper Cretaceous Rosario Group is composed of clastic sedimentary rocks of marine and non marine origin. The sediments range from cobble and boulder conglomerate to fine-grained sandstone and shale.

The Eocene La Jolla Group ranges from deep water, fine-grained claystone to coarse-grained continental sandstone and conglomerate. These units include 6 formations, which from the oldest to youngest are the Mount Soledad Formation, Delmar Formation, Torrey Sandstone, Ardath Shale, Scripps Formation, and Friars Formation (**Figure 12**).

This Eocene section in San Diego was put into a stratigraphic framework by Kennedy and Moore (1971), who recognized a major Eocene transgressive and regressive cycle. Later work by May and Warne (1991) identified additional smaller-scale cycles and refined these cycles into a sequence stratigraphic context. They recognized an older shallow water facies (Delmar Formation and Torrey Sandstone), separated by a major widespread erosion surfaces. These formations are dissected by a submarine canyon complex north of La Jolla, called the Torrey Submarine Canyon. Parts of the formations mapped as Torrey, Ardath, and Scripps all occur within the canyon fill. Although these individual formations and their boundaries were originally defined using lithologic criteria, sedimentologic relationships indicate that they form a genetically related canyon-fill sequence (Abbott and May, 1991).

Internally, the canyon complex is composed of multiple cross-cutting channels on a multitude of scales and with widely diverse lithologies. Individual channels range from subtly scoured and only a few meters deep, to greater than 1-km wide and up to 100-m deep. As a whole, the canyon system displays large-scale fining-upwards trends. This is very apparent in the Scripps Formation, where coarse-grained sediments of the Scripps scoured into the underlying, fine-grained Ardath Shale. Thinning-upward and fining-upward channels prevail above the unconformable surface at the base of the Scripps (Abbott and May, 1991).

***Ardath Shale:*** The Eocene Ardath Shale is a predominantly weakly fissile olive-gray shale which is exposed in several areas near the UCSD campus. The Ardath Shale is estimated to be 70-m thick at its type locality, and is unconformably overlain by the Scripps Formation. Based on fossil content, this unit has been assigned a Middle Eocene age.

***Scripps Formation:*** The Eocene Scripps Formation underlies much of the area around the UCSD campus and consists primarily of sandstone and local cobble conglomerate interbeds. The basal contact with the Ardath Shale is conformable.

The Scripps Formation generally consists of light gray-yellow, very fine, silty sandstone, interbedded with siltstone. This formation is also characterized by thinly laminated, silty fine sand beds, with occasional interbeds of cobble conglomerate, highly cemented concretionary zones and silty clays. The soils possess low expansion potential characteristics. There are some very well cemented sandstone lenses in the subsurface at the campus, but these are generally thin (<3 m) and pinch out laterally. The Scripps Formation is exposed on the campus roughly between elevations 88-98 m above sea-level, and has an estimated thickness of 67 m.

***Lindavista Formation:*** The Lindavista Formation is exposed on the ridge top, above 98 m elevation and consists of nearshore marine and non marine Pleistocene sediments deposited on wave-cut terraces. This formation is characterized by reddish-brown, interbedded sandstone and conglomerate, and has an estimated variable thickness of 3-15 m.

### **3.2 Geological and Geotechnical Data from Previous Foundation Studies at Thornton**

The UCSD Facility Management group has catalogued all the available soils reports that were generated for building construction at the hospital. A good summary of the data acquired prior to construction of the facility is given in a report prepared by Geocon Inc., of San Diego, which drilled 17 holes at the hospital site in 1989. **Table 3** summarizes the lithologic information. The elevations are those measured prior to construction. The maximum borehole depth was just short of 19 m. Most of the holes terminate in the Scripps Formation, and none seems to penetrate the underlying Ardath Formation. The units appear to dip gently toward the west-southwest.

All SPT blow counts reported for holes under the building footprint were high (>50). The bulk dry density of the materials at these locations was from 1.6 to 2.0 (unit weights 100 to 125 lbs/cuft).

### 3.3 Shallow Seismic Refraction Profiling

#### 3.3.1 Experiment Description

Four seismic refraction surveys were performed in the vicinity of Thornton Hospital at UC San Diego (**Figure 13**), primarily to obtain data on the shear-wave velocity structure of the site. Both compressional (P), and shear (S) sources and geophones were used, so the velocities of P and horizontally polarized S waves (SH) were measured.

All four lines used 24 geophones, spaced 4 m apart. For Lines 2 to 4, shotpoints were placed at a distance of 1 to 4 m from the first and last geophones, making the lines 100-m long from shot to shot. This would give a ground penetration of a least 20 m. For Line 1, there was enough space to place additional shot points 50 m from the first and last geophones, thus giving a total line length of 196 m and a ground penetration of more than 30m. Geophones were planted in 15-30 cm deep holes dug through the ground cover. This depth allowed the phones to be below the root mass of the vegetation. Both P- and horizontal S-phones were placed in the same hole with the axes of the S-phones aligned transverse to the seismic line. All S-phones were set up so that they had the same polarity. They were then covered to prevent any wind noise.

Two seismic sources were used for the refraction surveys. The first was an SH-source constructed by and on loan from Dr. Craig Pearson of Los Alamos National Laboratory. This unit used compressed gas to fire two 45 kg weights against stops, thereby imparting an impulsive horizontal ground motion. This source was held firmly to the ground by parking the front end of a Suburban truck on it. The source was operated on dirt for all four lines. The SH source was aligned transverse to the seismic line and thus parallel to the SH geophones. The second source, used to generate P waves, consisted of a 7.2 kg sledgehammer and a metal plate. This latter source was emplaced by digging through the root mass at the surface and placing the metal plate on the dirt below. Then, the plate was struck several times in order to seat it in the soil. Despite these preparations, the P source could not generate observable first arrivals beyond 100 m. The SH source, on the other hand, was clearly visible at distances of up to 200 m.

Data were recorded digitally on a Geometrics Strataview 24-bit seismic recorder. The recorder was triggered by a geophone (P or SH) placed within 3 cm of the P or SH source. A total of 8192 points in a record 1024 msec long were recorded for each channel, yielding a sample rate of 0.125 msec per point. The only filtering used a 250-Hz high cut filter and a 180-Hz notch filter. A notch filter at 60 Hz was tried, but it attenuated the seismic arrivals as well. As shown

in **Figure 14a**, the dominant frequency of the arrivals was in the 20 to 30 Hz range. One advantage of digital recording was that multiple shots could be stacked in order to improve the signal-to-noise (S/N) ratio. A minimum of 16 repeated shots were stacked for each SH source location, and 32 stacks were used for the shot points located 50 m from the ends of the lines. Different numbers of repeated shots were used with the P source, but no difference was found in the record quality with more than 8 stacks. Thus, P sources were stacked 8 times for each shot. The SH source was capable of generating a polarized signal, depending on which side the weights were fired. Thus, we obtained records with both polarities, and we used the polarizable nature of the signal to differentiate between SH and other arrivals. Because the shear-wave velocity in soils typically ranges from 200 to 600 m/s, it is possible to confuse the SH first arrivals with the arrival of the ground roll (a surface wave) or of the air wave traveling at the speed of sound in air (330 m/s). One may also get SH-P wave conversions off of nearby structures which are parallel to the seismic line. Most of these other waves will have the same polarity, regardless of which way the SH source is fired. For example, the air wave is a sound wave resulting from the impact of the weights against the stops and is always a compressional wave traveling outward from the source. The polarity of its arrival at the geophone (i.e., which way the geophone moves first) is the same whether the SH source is fired to the right or to the left. By collecting records of first arrivals with both polarities from the SH source, one can overlay the two and clearly identify the SH arrival (**Figure 14b**).

First arrivals were picked from the digital records using the analysis software SIPC (RimRock Geophysics, 1995). First arrivals and quality factors based on the uncertainties in the arrival times were stored in files. Uncertainties in arrival times increased with shot-receiver distance. For distances less than 100 m, uncertainties were typically less than 5 msec. At longer distances (150-200 m), uncertainties were typically 10 msec. Larger uncertainties were assigned to particularly noisy geophones or unclear arrivals. In a few cases, arrivals were not clear at all and the first arrival could not be picked.

Data were interpreted via trial-and-error forward modeling using the 2-D ray tracing program, MacRay (Luetgert, 1992). This program is based on a block model which allows both horizontal and vertical velocity gradients within individual blocks. Interfaces between layers of differing velocities can be placed between layers of blocks, and these interfaces can be irregular. Because the P and SH arrivals are modeled separately by this program, we took special care to ensure that structural discontinuities (interfaces between layers) were common to both models. Unless otherwise noted, the P and SH lines were fit with structures which were consistent with each other.

### 3.3.2 Seismic Refraction Line 1

This line, 196 m long, was recorded to the south of the hospital along a sidewalk parallel to the road (**Figure 13**). Four SH shot points (two at the ends of the line and two offset 50 m to the north and south of the line) were recorded. Two P shot points at the ends of the line were recorded. The first P arrivals are fit to within the uncertainties ( $< 5$  msec) with the velocity model shown in **Figure 15a**. Compressional wave velocities in the upper 10 m varied from 430m/s to 700 m/s. The planar interface at a depth of 10 m was placed in the model in order to match the structure from the SH profile; a modest velocity contrast of only 20 m/s exists for this interface in the P model. Alternate velocity models had no layer interface to which the data were sensitive. Based on the ray paths, the maximum depth of penetration with the P waves was approximately 20 m. Velocities at 20 m increased to 800 m/s. The deeper ray paths shown in **Figure 15a** would be recorded beyond the region spanned by the geophones.

The SH arrivals (**Figure 15b**) penetrated deeper into the section because of the offset shot points. The arrival times from these records are matched to within 5 msec except at greater shot-receiver offsets where the mismatch may be as much as 10 msec. Based on the ray diagrams, these waves penetrated to depths between 30 and 40 m. This is consistent with a maximum shot-receiver offset of 150 m.

This model required a planar interface at a depth of 10 m, with a more substantial velocity contrast of up to 150 m/s across it. Shear wave velocities in both the upper and lower layers had lateral variations. Values in the first layer ranged from 270 m/s at the west end of the line to 350 m/s in the middle section (**Figure 15b**). Velocities at the eastern end dropped to 310 m/s. Note that appreciable vertical gradients of 7 m/s/m were observed in this layer. At the western end of the line, there is a significant lateral variation in the upper layer; this is reasonable for soil layers. The deeper layer also shows horizontal velocity variations. At a depth of 30 m, velocities change from 620m/s beneath the western end to 440 m/s beneath the eastern end. This lateral change occurs abruptly (**Figure 15b**). The extreme values of shear-wave velocities at this line range from 270 m/s at the surface to 620 m/s at 30 m and fall within a range expected for well-consolidated soils and lithified older sediments.

### 3.3.3 Seismic Refraction Line 2

Line 2 was located on the archery range southwest of Thornton Hospital and was limited to a maximum length of 94 m (**Figure 13**). This area was bulldozed to prepare the range; so, we expected a thinner weathered layer at the surface. Shot points were located 1 m to the north and south of the ends of the seismic line. With the shorter line, ray penetration reached to depths of only 15 to 20 m. P-wave travel times were all fit to within the picking uncertainty of 5 msec (**Figure 16a**). The resulting velocity structure has a surface layer approximately 3-m thick overlying a deeper layer. Velocities in the surface layer range from 400 to 500 m/s, with a

velocity increase across the interface to values of 640 to 840 m/s. Velocities beneath the southwestern end are much lower (640 m/s) in this deeper layer than elsewhere along the profile (840 m/s). Values of 920 to 1000 m/s are obtained at a depth of 20 m.

The SH arrivals (**Figure 16b**) were also picked and fit with uncertainties of 5 msec with a similar geometric structure as that in **Figure 16a**. Rays penetrated slightly deeper, 20 m, because of the different shear-wave velocity structure. The model also had a surface layer with velocities increasing from 200 m/s at the surface to 400 m/s at 3-m depth. A modest velocity contrast with the underlying layer exists, with values increasing from 400 m/s above to 410-440 m/s below the interface. Velocities increase from 410 m/s at 3 m in the lower layer to 520-640 m/s at a depth of 20 m. Modest lateral changes are also present in this layer, with velocities beneath the center of the line being about 10% higher than at the ends.

It is likely that the 3-m thick layer is a section of fill and/or disturbed soil. Comparison of the topographic map of the archery range and observations of surface geology show that at least 6 m of consolidated sediments were cut in order to construct the range. It is therefore unlikely that this 3-m thick layer is the result of simple weathering.

#### 3.3.4 Seismic Refraction Line 3

Line 3 was located in the wetlands to the south of Thornton Hospital and in the gully below Line 1. Taken together, these two lines can provide a composite cross section. This line also had a total length of 94 m, with shot points 1m off the ends of the line. Rays on this profile penetrated about 20 m (**Figure 17a**). P- wave arrival times were picked and matched by the model to within 5 msec. The resulting velocity model (**Figure 17a**) has a 3.5 m thick layer of material overlying a much faster material. Velocities are 200-450 m/s in the upper layer, and an average of 1100 m/s in the lower layer. Velocities at 20 m depth increased to 1370 m/s. No lateral velocity gradients were needed to fit the P-wave data.

The resulting model from the S-wave measurements is substantially the same, but there is a modest lateral velocity gradient in the lower layer from either end of the line towards the middle (**Figure 17b**). Rays penetrated only to about 15 m, and the predicted arrival times matched the observed ones to within the 5 msec uncertainties. Velocities were 200-300 m/s in the upper layer, and 590 to 660 m/s at a depth of 15 m in the lower layer (**Figure 17b**). The upper layer is likely a section of fill or disturbed soil with undisturbed consolidated sediments beneath. Line 3 is about 16 m lower than Line 1, in elevation. Thus, the values in excess of 600 m/s from Line 3 compare favorably to the values of 620 m/s seen at the deepest levels of Line 1. A composite section at the west end of Line 1 shows a gradually increasing shear-wave velocity profile from 270m/s at the surface to 660 m/s at depths of 31 m under Line 1.

### 3.3.5 Seismic Refraction Line 4

Line 4 was located west of the hospital. It straddled the location of the new seismic station, and spanned 94 m. P-waves penetrated to a depth of 20 m (**Figure 18a**). The resulting velocity model fits the observed arrival times to within the 5msec picking uncertainties. This model also consists of two layers. The shallow layer extends to depths of 1.5 to 2 m and has velocities ranging from 200 m/s at the surface to 470 m/s at the bottom. The upper surface of the second layer has velocities of 640-680 m/s with an apparent increase to 930 m/s at its western end (**Figure 18a**). However, this higher velocity structure is poorly constrained because it is at the margins of the line. Velocities at 20 m depth reached 930 to 1250 m/s.

The model for shear waves is geometrically similar to the one for the P-waves (**Figure 18b**). Rays also penetrated to a depth of 20 m, and matched the observed travel times to within the 5 msec uncertainty. Velocities in the upper layer range from 200 to 400 m/s, while values at the upper surface of the lower layer range from 440 (east) to 470 m/s (middle). Velocities reach 580 (east) to 630 m/s (middle) at a depth of 20 m. The upper layer is likely to be disturbed soil, or fill used to build up the helipad area. The lower layer consists of more consolidated sediments, and the velocities are similar to those found on Lines 1 and 2.

## 3.4 Cone-Penetration Soil Tests, and Downhole Velocity Measurements

Four Cone-Penetration Tests (CPT) were conducted at the Thornton site. The locations are marked on Figure 13, as CPT-1 through 4. The program was carried out by Gregg In-Situ Company of Signal Hill, CA. **Figures 19 a to 19 d** picture the equipment at the four locations and provide a tour of the Thornton site a ground level. A 10-ton capacity, integrated electronic cone system was used. The cone has a tip area of 10 cm<sup>2</sup> and friction-sleeve area of 150 cm<sup>2</sup>. Downhole shear-wave velocity measurements were made at each location.

The results of penetration and the interpretation in terms of soil types are given in **Figures 20 to 23**. A significant characteristic of the site is the presence of cemented sand layers which prevented deep penetration of the cone. Depth of refusal was from 3.85 to 8.20 m. The figures also show the strong heterogeneity of the near-surface materials. However, some caution should be exercised when looking at the layering profiles implied by the CPT data. Occasionally, the automated interpretation may not be accurate, as seems to be the case for a “cemented sand” between 0.6 m and 2.4 m at CPT-1. This is not supported by the data from the deep holes, drilled next to this CPT site. The cone may simply have encountered a local concretion.

The results of the S-wave velocity measurements are given in **Table 4**. Where the hardest layers stopped the CPT cone, the velocities range from 339 to 528 m/s. The S-wave velocity measurements across the site are compared in section 3.7.

### 3.5 Deep Hole Drilling and Sampling

Three boreholes, CLC#1, CLC#2, and CLC#3, were drilled at the Thornton Hospital site (**Figure 6**). They were located about 50 m west of the hospital; see the 3 small circles in **Figure 13**. All three were 12.38cm (4.875”) in diameter. A standard rotary system was used with bentonite for holes CLC#1 and CLC#2, and polymer for hole CLC#3. The contractor was Pitcher Drilling Company of Palo Alto, CA.

The purpose of hole CLC#1 was several-fold: to emplace the deeper downhole seismometer, to provide soil samples, and to allow for geophysical logging to a depth greater than 90 m at the Thornton site. Drilling started on 6/24/97 and reached a total depth of 91.4 m on 6/25/97. The top of the Scripps Formation was encountered at 3.6 m depth. Five Pitcher samples were collected, down to a depth of 7.6 m. The upper 3.6 m is artificial fill and was too coarse-grained to sample.

The Scripps Formation was drilled easily in the sandstone and siltstone, and with more difficulty in the conglomerate and concretionary zones. Numerous cobble zones were encountered between 3.6 and 59.4 m. The clasts were primarily composed of detrital siliceous chert and quartzite, with distinct abraded surfaces. The driller changed to tri-cone drill bits in these hard cobble zones, with moderate success. The number of cobble zones appeared to increase toward the base of the Scripps Formation, suggesting an overall fining upward sequence in the Scripps.

The top of the Ardath Shale was encountered at ~59.4 m depth (**Figure 24**). The unit is mainly a dark gray, very fine grained claystone or shale. It drilled very rapidly. Several thin (0.15-0.3 m thick) siliceous interbeds were encountered in the Ardath. Two Pitcher samples were collected between 90.5 and 91.4 m depth.

Borehole CLC#2 was drilled on 6/26/97 to a depth of 46 m. The purpose of this hole was for emplacement of the second, shallower downhole seismometer. No samples were collected. The hole location is about 3 m west of CLC#1.

Borehole CLC#3 was drilled also to a depth of 46 m on 9/24/97. It was located about 5 m west of CLC#2. The purpose of the hole was to collect additional high-quality soil samples, at pre-selected depths in the hole. Pitcher samples were obtained at 13.7 to 14.2 m, 19.8 to 20.4 m, 30.2 to 30.5 m, 36.6 to 37.3 m, 42.7 to 43.0 m, and 45.3 to 45.5 m. There was no instrumentation or geophysical logging in this hole.

### 3.6 Geophysical Logging of Hole CLC #1, and Geological Interpretation

#### 3.6.1 Electric and Gamma Logs

Two geophysical logs, an electric log and natural gamma log, were run in CLC#1. They were performed by Agbabian and Associates Company of Pasadena, CA, on 6/25/97. These logs were extremely useful for interpreting the stratigraphy encountered in the hole. The log profiles and stratigraphy are shown jointly in **Figure 24**. The scales of the logs are not given because the absolute values have no bearing upon ground motion estimates, and their absence makes the figure clearer.

### 3.6.2 Suspension P- and S- Wave Velocity Logs

In-situ velocity measurements of compressional (P) and horizontal shear (SH) waves were performed in hole CLC#1, also by Agbabian Associates, on 6/25/97. The OYO Model 170 Suspension Logging Recorder and Suspension Logging Probe were used to obtain records at 0.5-m intervals. Data were collected to a maximum depth of 87.0 m. This information is essential for the modeling of site response to seismic wave excitation. Among other things, it provides an estimate of the in-situ shear modulus of soils at very low strains ( $G_{max}$ ). This “undisturbed” value of  $G_{max}$  can be used to calibrate the results of laboratory soil dynamics tests showing the decay of shear modulus with increasing shear strain. P and SH velocity profiles with depth are shown in **Figure 25**.

The site was located in an suburban environment, adjacent to the Thornton Hospital, and approximately 0.3 km from Interstate 5. Vibration from vehicular traffic was apparent in the data from the upper 30 m, though it was not a significant problem. Occasionally, very high amplitude, 600 Hz interference was observed on the vertical receivers. This appeared to be caused by some equipment within the adjacent hospital, and data were not collected while the interference was present. The measurements started below the 3.5-m long steel surface conductor casing placed by the drilling contractor to support the near-surface fill.

P-wave velocities reach 1650 m/sec at a depth of approximately 28 m. The rapid increase in velocity seen at this depth is accompanied by a corresponding increase in SH-wave velocity, indicating that this is a layer of faster material, rather than saturated soil. Just below this fast layer, at 31 m, the P-wave velocity again drops, tracking the SH-wave velocity to approximately 34 m. At this depth the P-wave velocity again reaches 1650 m/sec, but with no corresponding change in SH-wave velocity. This appears to be a perched water table, as the P-wave velocity again drops at 43 m. There is a noticeable fast layer between 48 and 55 m, which was identified during drilling as a cobble bed. Then, the ground is clearly saturated below 55 m, based on the marked increase in P-wave velocity which is not reflected in the S-wave profile.

### 3.6.3 Geological Interpretation

The top of the Ardath Shale shows up well on the electric log, as evidenced by the distinct change in character of the signature and general low resistivity of the fine-grained material. Note also the numerous thin high resistivity “blips” in the Ardath. These are interpreted to be the thin concretionary zones in the shale. The depths of these zones correlate well with areas of difficult drilling.

The Scripps Formation has much more heterogeneity as evidenced from the character of the electric log. The highly resistive zones are interpreted as coarse grained sediments, while the lower resistive zones are relatively finer grained (**Figure 24**). This interpretation is supported by the drilling rates, as well as by the cuttings collected during the drilling. The basal cobble zone likely represents the erosional contact between the Scripps and the underlying Ardath Shale. There are 3 obvious high resistivity beds (cobbles zones) overlain by a sequence of decreasing resistivity (decreasing clast size). These are interpreted as fining upward sequences and probably represent nested channels. This interpretation fits well with the description of the Scripps Formation by Abbott and May (1991), who describe the submarine canyon complex as composed of multiple cross-cutting channels, displaying large-scale fining-upwards trends. This is very apparent in the Scripps Formation, where coarse-grained sediments of the Scripps scoured into the underlying, fine-grained Ardath Shale. Four fining upward channel-fill sequences are identified in the Scripps Formation, above the unconformable surface at its base. These fining upward channel-fill sequences are even more apparent when related to the shear-velocity log (**Figure 26**). Assuming that the relative increase in the velocity of thin zones is a function of the high velocity of the detrital cobbles, the velocity log reflects the relative grain size of the sediments.

The new data we generated at the Thornton site raise some questions regarding previously published results. Kennedy (1975) mapped the geology of the site and showed the contact of the Scripps and the underlying Ardath at about the 85.3 m elevation (the units are supposedly generally flat in this area). The collar elevation of CLC#1 is about 104.2 m above sea level. If the 85.3 m elevation for the Scripps-Ardath interface is correct, then we should have encountered it at a depth of 18.9 m in the first borehole. In fact, the top of the Ardath was intersected at a depth of 59.4 m (44.8 m elevation). There are several possible explanations for this discrepancy :

- 1) The contact between the formations is at 18.9 m, and the Ardath simply contains coarse-grained sediments at this location. This does seem likely since, since the Ardath, as defined by Kennedy et al, is mainly a very fine grained clastic deposit, with very subordinate sandstone and conglomerate. The sediments from 18.9 to 59.4 m are much more Scripps-like than Ardath-like.
- 2) The mapping in the Thornton Hospital area is incorrect. This is possible, since much of this mapping was probably done on a regional scale, and possibly only “spot-checked” in places. All

of the nearby Ardath would actually be Scripps Formation and the Ardath would probably not be exposed in this area, at least not above ~45.7 m elevation.

3) The borehole fortuitously intersected a deep channel, in which Scripps scoured down into the Ardath.

For the seismic evaluation of the Thornton site we will rely on the data we obtained directly in the CLC deep holes. **Figure 27** illustrates the relationship between the various logs, as a function of depth, and shows the location of the samples and the downhole seismometers. **Figure 28** is our working diagram of the stratigraphy encountered in the boreholes.

### 3.7 Summary of Shear-Wave Data in the Upper 30 Meters

Three types of tests gave shear-wave velocity data at the Thornton site: seismic refraction, CPT, and suspension logging. This offers an opportunity to evaluate the correlations between their results, and the degree of redundancy achieved. Of particular interest are the materials in the upper 30 m (100 ft) or so below the surface. More and more data are being obtained from vertical seismic arrays in the U.S. (California), Japan (Chiba and Kobe), and Taiwan (Lotung). They show that, in many cases, it is in this depth range that the most significant seismic ground motion modification takes place. It is appropriate that the S-wave refraction data were obtained down to such a depth at the Thornton site.

Refraction line 1 is on an alignment between CPT-3 to the west and CPT-4 to the east. Both of these cones met refusal at shallow depths, 3.85 and 5.20 m respectively, which are within the definition of the upper layer for that refraction line. This refraction survey does not provide as detailed a velocity structure in the upper 5 m as the CPT does. At the west end, toward CPT-3, line 1 shows S-wave velocities going from 210 to 330 m/s between the surface and 10-m depth (**Figure 15b**). CPT-3 shows about 290 m/s between 1.5 and 3m (**Table 4**). At the east end, toward CPT-4, line 1 shows S-wave velocities from 310 to 430 m/s between the surface and 10-m depth. CPT-4 shows 372 to 447 m/s in the interval from 1.5 to 4.7 m. While these velocities are generally consistent in the upper layer, there appears to be some amount of lateral variability in the geologic structure.

Refraction line 3 overlaps the location of CPT-2, which met refusal at 5.35 m. The refraction interpretation had a 3.5-m thick top layer overlying a much faster layer. In the top layer, the shear velocities were from 200 to 300 m/s (**Figure 17b**). This is consistent with the CPT velocities of 255 to 272 m/s between 1.5 and 3 m (**Table 4**).

Refraction line 4, at its east end, overlapped the location of CPT-1 and hole CLC#1. The CPT refusal depth was 8.20 m, and the shear velocity increased abruptly below a depth of about 2 m, to reach about 500m/s from 6 m to 8 m (**Table 4**). Again, this is consistent with the refraction

interpretation of a 1.5 to 2-m thick softer layer overlying a faster material. In that faster material, at the east end, the depth-interpolated velocity from refraction was 470 to 485 m/s between 6 and 8 m respectively (**Figure 18b**). The suspension log in CLC#1 also shows a shear velocity nearing 500m/s at 8-m depth (**Figure 25**).

In summary, the comparison of data from linear measurements such as the CPT's and the deep borehole CLC # 1 with areal data from the refraction surveys shows that there is some lateral variability in the near-surface geology around the Thornton site. However, the various S-wave velocities obtained at Thornton hospital are generally consistent, indicating that the refraction results can be used as a basis to describe the areal shear velocity structure in the upper 30 meters or so, around the hospital. This is advantageous, considering the low cost of refraction surveys.

### **3.8 Seismic Background Noise Surveys**

Two noise surveys were conducted on the grounds of Thornton Hospital, prior to the drilling and deployment of the borehole seismometers. The goal of these noise surveys was to assess the level of seismic noise within the frequencies of interest (roughly 100 to 0.01 Hz). Because highway I-5 is located a few hundred meters west of the site, it was important to verify that useful data could be collected prior to drilling the boreholes. It was also important to check for intermittent sources of seismic noise, such as air compressors.

The initial survey was conducted using high-frequency geophones and a seismic reflection recording unit (Geometrics StrataView recorder). We deployed the geophones in two configurations: a square grid centered around the proposed site and a line roughly perpendicular to I-5 along the back of the hospital. Data were recorded in approximately one-minute segments. The time of the recording was on a weekday morning. Visual examination of the linear deployment results showed no obvious localized noise sources from the hospital itself and no obvious reduction of noise levels with distance from the highway, possibly because the highway is a linear source. In addition, locations that were the farthest from I-5 were closer to other noise-producing streets (i.e., La Jolla Village Drive). It was concluded that seismic noise levels were high over much of the hospital grounds and that situating the borehole in an alternate site (farther away from the highway) would not greatly reduce the noise levels.

In May 1997, a broadband (flat response between approximately 0.008 and 50 Hz) Streckeisen STS-2 seismometer was deployed for several days about 50 meters west of the proposed borehole site and CPT#1. Examination of the records showed no large intermittent sources of noise during the time of the deployment at the site. The noise spectra of the data collected are shown in **Figure 29**. BHZ, BHN, and BHE respectively are the vertical, north-south, and east-west components. They are compared to the high- and low-noise models of the USGS (Peterson,

1993), which are shown as dashed lines. During the day, they were above the high-noise model, but they decreased approximately 10 dB at night at higher frequencies (above 1 Hz), as expected for the cultural noise.

On May 1, while doing the second survey, we obtained broadband records of the P-wave from a magnitude (mb) 5.2 event in the Gulf of California (distance: 1840 km; lat. 18.7N; long. -107.3W); see **Figure 30**. The P-arrival time is shown by an arrow. It is visible as higher-amplitude lower-frequency energy starting at 11:41:30. Amplitude is in counts and has not been converted to ground motion.

Although an STS-2 has a significantly broader frequency response than a Wilcoxon sensor, filtering of the broadband data to approximate the Wilcoxon response showed similar results. In conclusion, although noise levels at the site are high, moderate-size regional events will be recorded with sufficient signal-to-noise ratio to provide useful data. This second survey confirmed that locating the borehole elsewhere on the Thornton site (i.e. not at the helicopter pad) would not significantly reduce noise levels.

### **3.9 Instrumentation of the Seismic Station, and Installation**

The conceptual design of the Thornton station is shown in **Figure 31**. Each borehole (CLC#1 and CLC#2) contains a sonde package designed and built by Lawrence Berkeley National Laboratory (LBNL). The packages were emplaced at 91 m in CLC#1 and 46 m in CLC#2. The sonde contained three Wilcoxon seismometers and three 4 Hz geophones for redundancy. Both the Wilcoxons and the geophones appeared to be functioning after installation, i.e. a signal that varied with time was received. It was impossible to determine at the time whether this was true seismic signal or instrumental noise.

Implementation of the permanent recording system was done in three stages. The first stage was construction of the surface seismometer pad, instrument bunker, and laying of cable conduit to Thornton hospital. The second stage was an instrument shakedown stage intended to verify that all seismometers and associated electronics (power circuitry, digitizers, and clocks) worked well. The third and final stage was the implementation of the asynchronous telemetry link between the instrument bunker and a computer in the Thornton hospital. This computer is connected through the campus Internet to the Scripps Institute of Oceanography.

The first stage began immediately after completion of the boreholes and was largely completed by late August 1997. A landscaping company dug trenches between the boreholes, the surface instrument site, and the nearby lithotripter electronics output box and laid PVC pipe. The instrument cables were run through this pipe to the instrument pad and fishlines were laid throughout the other pipes. The lithotripter electronics box was already connected to the main

switch-room at Thornton Hospital and we therefore had a connection from the surface instrument site to the hospital. Standard irrigation pipe covers covered the boreholes. A 10- to 15-cm thick pad of concrete was poured. The pad was coupled to the ground with rebars spaced about 30 cm apart and driven 15 to 30 cm into the ground. The top of the pad protruded 2 to 5 cm above ground to prevent pooling of water. A fiberglass hut (Western Power Products) was bolted on the concrete pad. We later found (during the passage of Hurricane Nora) that this structure leaked slightly around the door during heavy rain. A rubber gasket was installed in order to solve the leakage problem. We are continuing to monitor the water tightness of the hut.

On completion of the instrument hut, stage two (instrument shakedown) began. A metal plate was fabricated to hold the surface Wilcoxon (731-4A) and Kinometrics FBA-23 (2g range) and power circuitry was built to power the Wilcoxons. Two Reftek DAS (model 72A-07, 6 channels, and 24-bit digitizer, no DSP chip) were used to sample the data. Two Reftek GPS clocks supply timing. For this stage of the project we elected to store the data directly on disk at the site and use batteries for power. Recording began in this mode August 26, 1997. Due to problems with circuitry (partially due to water damage) and testing of the instruments, full data recovery was not achieved. The recorders were removed on December 16, 1997.

The third stage was to implement the real-time telemetry link to Scripps Institution of Oceanography. In this stage, the instruments in the outside instrument bunker were connected to a basement room in the hospital through the existing conduits. This provides a reliable data and power link for the instruments. Power is provided by a low voltage DC current, which is low-cost and requires no additional permits (as an outside higher voltage AC line would, for example). The station went back in operation in July 1998. The data from the Refteks are being sent to a Sun Sparcstation in Thornton which in turn sends them over an ethernet link to IGPP at Scripps using the already existing UCSD ethernet campus-wide network. Once at IGPP, the data are archived and associated with existing catalogs in near real-time, and the system allows rapid access to those data via Internet.

### **3.10 Initial Recordings at the New Thornton Seismic Station**

The station code for the Thornton Hospital seismic station is “**THSB**”. The channel codes for the deep borehole sensor, a three-component Wilcoxon seismometer located at 91-m depth, are **HL1** for the vertical component, **HL2** for the first horizontal component, and **HL3** for the second horizontal component. The channel codes for the intermediate depth sensor, a three-component Wilcoxon located at 46 meters, are **HL4** for the vertical component, **HL5** for the first horizontal component, and **HL6** for the second horizontal component. The orientations of **HL2**, **HL3**,

**HL5**, and **HL6** are not precisely known at this time, and will be determined by polarization analysis of seismic waves generated by earthquakes or man-made sources.

The Wilcoxon surface sensor also has three channels with the following designations: vertical **HL7**, north-south horizontal **HL8**, and east-west horizontal **HL9**. Finally, the Kinometrics FBA-23 surface sensor has three channels designated as: vertical **HLZ**, north-south horizontal **HLN**, and east-west horizontal **HLE**.

Records of twenty four regional events have been obtained at the Thornton station between September 1997 and July 1999. They have *M<sub>L</sub>* magnitudes between 1.6 and 4.9 and are located at epicentral distances from 8 to 194 km. The locations of the epicenters are shown on **Figure 32**. The source parameters of these events are shown in **Table 5**. The seismic sources are well distributed in azimuth over land, but are scarce from offshore.

For illustration, the records of two events - no. 4 in October 1997 and no. 24 in July 1999 - are given in **Figures 33** and **34**. They show 9 channels of acceleration time-histories from the three Wilcoxon instruments, two downhole and one at the surface. The records from the other surface instrument, the Kinometrics FBA, are not shown as they are consistently identical to the Wilcoxon surface records. The FBA originally was selected as a potentially useful second sensor at the surface, since it has a much higher linear recording range (up to 2 g's, vs. 0.5 g for the Wilcoxon). All seismograms were filtered with a 1-Hz high-pass filter to remove a DC offset. These seismograms are available in digital form for further processing and analysis of site response.

The Thornton records indicate that the ground motion does not change very much between depths of 91 m and 46 m, but is strongly modified between the deep locations and the surface. To further illustrate the response of the ground at the Thornton site, we calculated the amplification of horizontal spectral accelerations from 91-m depth to the surface for the earthquake of July 19, 1999. This is shown in **Figure 35**. Because the sensor orientations are not known exactly, as discussed earlier, we are using the amplification of the Fourier spectrum of the total complex horizontal motion. We focus on the period range between 0.1 and 1 second (frequencies between 10 Hz and 1 Hz), because it is the range of fundamental periods for buildings from 1 to 10-stories high (the fundamental period of a building, in seconds, is roughly the number of stories divided by 10). At weak motions, under which soils tend to stay linear, the maximum site amplification of horizontal acceleration is about 12, at about 0.46 sec (2.2 Hz). This would be most noticeable for buildings 4 or 5-stories tall. Clearly, this behavior may be modified under strong motions, because of the nonlinear response of the soils. The actual amplifications under moderate to strong earthquakes will be determined when our strong motion estimates of surface accelerations are completed. They will be described in the Phase 2 report.

#### 4.0 REFERENCES

Abbott, P.L. and May, J.A. (eds.), 1991, Eocene Geologic History, San Diego Region: Soc. Economic Paleontologists and Mineralogists, Pacific Section, v. 68, 229 p.

Agnew, D. C., 1991, How complete is the pre-instrumental record of earthquakes in southern California?, In Abbott, P. L. and Elliott, W. J., eds., Environmental Perils/San Diego Region, published for the Geological Society of America by the San Diego Association of Geologist, October 20, pp. 75-88.

Anderson, J. G., Rockwell, T. K., and Agnew, D. C. 1989, Past and possible future earthquakes of significance to the San Diego region, Earthquake Spectra, v. 5, n. 2, pp. 299-335.

Brune, J. N., Simons, R. S., Rebollar, C., and Reyes, A., 1979, Seismicity and faulting in northern Baja California, in Abbott, P. L., and Elliott, W. J., (eds.), 1979, Earthquakes and Other Perils, San Diego Region: Geological Society of America Guidebook, San Diego Association Geologists Publication, pp 83-100

Corbett, E. J., 1984, Seismicity and crustal structure studies of southern California--Tectonic implications from improved earthquake locations, unpublished PhD. dissertation, California Institute of Technology, Pasadena, California, 231 p.

De Mets, C., Gordon, R.G., Argus, D.F., and Stein, S., 1990, Current plate motions, Geophysical Journal Int., v. 101, pp 425-478

Elliott, W. J., 1970, Gravity survey and regional geology of the San Diego embayment, southwest San Diego County, California, in Pacific Slope Geology of Northern Baja California, Pac. Sect. A.A.P.G., S.E.P.M, S.E.G., Guidebook for 1970 Fall Field Trip, pp. 10-22.

Fischer, P. J. and Mills, G. L., 1991. The offshore Newport-Inglewood-Rose Canyon Fault Zone: Structure, segmentation and tectonics, In Abbott, P. L. and Elliott, W. J., eds., Environmental Perils/San Diego Region, published for the Geological Society of America by the San Diego Association of Geologist, October 20, pp. 17-36.

Ford, G. A. and Normark, W. R., 1980, Map showing a Deep-Tow geophysical study of the north end of the San Clemente fault, California Borderland, United States Geological Survey, Miscellaneous Field Studies, Map MF-1230.

Geocon Inc., San Diego, CA., 1989, Consultation for phase I, UCSD Satellite Medical Facility, San Diego, CA for UCSD Facilities Design Construction.

Gonzales, J.J. and Suarez, F., 1984, Geological and seismic evidence of a new branch of the Agua Blanca Fault, Geophysical Research Letters, v. 11, pp. 42-45.

Hauksson, E., and Jones, L.M., 1988, The July 1986 Oceanside (ML=5.3) earthquake sequence in the continental borderland, southern California, Bulletin Seismological Society of America, v. 78, pp 1885-1906

Hirabayashi, C. K., Rockwell, T. K., Wesnousky, S. G., Stirling, M. W., and Suarez-Vidal, F., 1996, A neotectonic study of the San Miguel Vallecitos fault, Baja California, Mexico: Bulletin Seismological Society of America, v. 86, pp. 1770-1783.

- Jackson, et al 1995, Seismic hazards in southern California: Probable earthquakes 1994-2004, The Phase II report, Southern California Earthquake Center, Bulletin Seismological Society of America, v.85, n.2, pp. 379-439.
- Kennedy, M. P., 1975, Geology of the San Diego metropolitan area, California: California Division of Mines and Geology Bulletin 200, 56 p.
- Kennedy, M. P. and Moore, G. W., 1971, Stratigraphic relations of Upper Cretaceous and Eocene Formations, San Diego Coastal Area, California, Bulletin American Association of Petroleum Geologists, v. 55, pp. 709-722.
- Kennedy, M. P., and Welday, E. E., 1980, Recency and character of faulting offshore metropolitan San Diego, California: California Division of Mines and Geology, Map Sheet 40, Scale 1:50,000.
- Kern, P., 1988, Earthquake shaking and fault rupture in San Diego County. A report to the San Diego County Earthquake Preparedness Committee, 58p.
- Lamar, D. L. and Rockwell, T. K., 1986, An overview of the tectonics of the Elsinore fault zone, in, Ehlig, P. (ed) Guidebook and volume on neotectonics and faulting in southern California, Cordilleran Section, Geological Society of America, pp. 149-158.
- Legg, M. R., 1985, Geologic Structure and tectonics of the inner continental borderland offshore northern Baja California, Mexico; unpublished Ph.D. dissertation, University of California, Santa Barbara, 410 p.
- Legg, M. R., Wong, V., and Suarez, F., 1991 Geologic structure and tectonics of the Inner Continental Borderland of northern Baja California. In Dauphin, P. and B.S.T. Simoneit, eds., The Gulf and Peninsular Province of the California, AAPG Memoir 47.
- Legg, M. R., and Kennedy, M. P., 1979, Faulting offshore San Diego and northern Baja California: in Abbott, P. L., and Elliott, W. J., eds., Earthquakes and other perils - San Diego Region: San Diego Association of Geologists Guidebook, pp. 29-46.
- Legg, M. R., and Kennedy, M. P., 1991, Oblique divergence and convergence in the California Continental Borderland, In Abbott, P. L. and Elliott, W. J., eds., Environmental Perils/San Diego Region, published for the Geological Society of America by the San Diego Association of Geologist, October 20, pp. 1-16.
- Leighton and Associates, 1983, Seismic safety study for the city of San Diego, 39 pp.
- Lindvall, S. C. and Rockwell, T. K., 1995, Holocene activity of the Rose Canyon fault zone in San Diego, California, J. Geophysical Research, v. 100, p. 24,121-24,132.
- Luetgert, J. H., 1992. MacRay 1.0.9, Interactive two-dimensional seismic ray-tracing for the Macintosh. USGS Open-file Report 92-356, Computer disk.
- Magistrale, H., 1993, Seismicity of the Rose Canyon fault zone near San Diego, California, Bulletin Seismological Society of America, v. 83, pp 1971-1978
- Magistrale, H., and Rockwell, T. K., 1996, The central and southern Elsinore fault zone, southern California, Bulletin Seismological Society of America, v. 86, pp 1793-1803

May, J. A. and Warme, J. E., 1991, Marine sedimentology of the early to middle Eocene La Jolla Group, in Abbott, P.L. and May, J.A. (eds.), 1991, Eocene Geologic History, San Diego Region: Soc. Economic Paleontologists and Mineralogists, Pacific Section, v. 68, p. 73-88.

McEuen, R. B. and Pinckney, C. J., 1972, Seismic risk in San Diego, Transactions San Diego Society Natural History , v. 17, no. 4, pp. 33-62.

Moore, G. W., 1972, Offshore extension of the Rose Canyon Fault, United States Geological Survey Professional Paper 800-C, pp. 113-116.

Mueller, M.J., 1985, Neotectonics, alluvial history, and soil chronology of the southwestern margin of the Sierra de los Cucapas, Baja California Norte, unpublished M.S. thesis, San Diego State University.

Petersen, M. D. and Wesnousky, S. G., 1994, Fault slip rates and earthquake histories for active faults in Southern California, Bulletin Seismological Society of America, v. 84, pp. 1608-1649.

Peterson, J., 1993, Observations and modeling of seismic background noise. USGS Open-file report 93-322.

Reyes, A., Brune, J. N., Barker, T., Canales, L., Madrid, J., Revollar, J., and Munguia, L., 1975, A microearthquake survey of the San Miguel fault zone, Baja California, Mexico, Geophysical Research Letters, v. 2, n. 2, pp. 56-59.

RimRock Geophysics, 1995, User's Guide to SIP Shell, RimRock Geophysics, Inc., Englewood, Colorado.

Robertson, P. K., and Campanella, R. G., 1988, Guidelines for use, interpretation, and application of the CPT and CPTU, University of British Columbia, Civil Engineering, Soil Mechanics Series, No. 105, Vancouver, B.C., Canada, V6T 1W5

Rockwell, T. K., Hatch, M.E., and Schug, D.L., 1987, Late Quaternary Rates of Agua Blanca and Borderland faults, United States Geological Survey Final Technical Report, Contract No. 14-08-0001-22012, 65 p., 2 plates.

Salyards, S.L., Sieh, K.E., and Kirschvink, J.L., 1992, Paleomagnetic measurement of nonbrittle coseismic deformation across the San Andreas fault at Pallett Creek. J. Geophysical Research, v. 97, n. B9, pp. 12457-12470.

Sangines, E. M., Campbell, K. W., and Seligson, H. A., 1991, Ground motion, intensity, and damage expected in the metropolitan San Diego area as a result of a M=7 earthquake on the Rose Canyon Fault, In Abbott, P. L. and Elliott, W. J., eds., Environmental Perils/San Diego Region, published for the Geological Society of America by the San Diego Association of Geologists, October 20, pp. 101-108.

Sharp, R. V., 1981, Variable Rates of late Quaternary strike slip on the San Jacinto fault zone, southern California, J. Geophysical Research, v. 86, pp. 1754-1762.

Simons, R. S., 1977, Seismicity of San Diego, 1934-1974. Bulletin Seismological Society of America, v. 67, pp. 809-826.

Thomas, A. P., and Rockwell, T.K., 1996, A 300- to 550-year history of slip on the Imperial fault near the US-Mexico border. Missing slip at the Imperial fault bottleneck. J. Geophysical Research, Solid Earth, v.101, Mar. 10, pp. NB3: 5987-5997

Thomas, A. P., and Rockwell, T.K., 1996, A 300- to 550-year history of slip on the Imperial fault near the US-Mexico border. Missing slip at the Imperial fault bottleneck. *J. Geophysical Research, Solid Earth*, v.101, Mar. 10, pp. NB3: 5987-5997

Topozada, T. R., Parke, D. L., and Real, C., 1981, Preparation of isoseismal maps and summaries of reported effects for pre-1900 California earthquakes, California Division of Mines and Geology Open File Report 81-11, Sacramento, CA.

Treiman, J. A., 1993, The Rose Canyon fault zone, southern California, California Division of Mines and Geology, Open File Report 93-02, 45p.

Vedder, J. G., Beyer, L. A., Junger, A., Moore, G. W., Roberts, A. E., Taylor, J. C., and Wagner, H. C., 1974, Preliminary report on the geology of the Continental Borderland of southern California: U.S. Geological Survey, Miscellaneous Field Studies Map MF-624, Scale 1:500,000.

Wesnousky, S. G., 1986, Earthquakes, Quaternary faults and seismic hazard in California, *J. Geophysical Research*, v.91, pp. 2587-12632

West, R. B., 1987, Tectonic geomorphology of the Mount Soledad segment of the Rose Canyon fault zone. Unpublished senior thesis, San Diego State University.

Woodward-Clyde Consultants, 1986, Evaluation of liquefaction opportunity and liquefaction potential in the San Diego, California urban area, Final technical report for U.S.G.S. Contract No. 14-08-001-20607.

Working Group on California Earthquake Probabilities, 1988, Probabilities of large earthquakes occurring in California on the San Andreas fault: U.S. G.S. Open File Report 88-398.

## 5.0 ACKNOWLEDGMENTS

This work was funded by the University of California Office of the President, by the University Relations Program at Lawrence Livermore National Laboratory, and by the Office of the Vice-Chancellor for Resource Management and Planning at the University of California San Diego. Their support is gratefully acknowledged.

At UCSD, we are particularly indebted to Assistant Vice-Chancellor Boone Hellmann, the Campus Architect, for his early and strong support of our efforts to provide the University with improved evaluations of its exposure to earthquakes.

We thank Macan Doroudian, UCLA, for his geological logs of hole CLC#1. We are grateful to James Batti and John Unwin of UCSD/IGPP, and Norm Lash and Rick Martin of Thornton hospital for their contributions to the construction of the seismic station. In addition, we want to express our appreciation to James Batti, Jennifer Eakins, Glen Offield, and John Unwin, all of IGPP, at U. C. San Diego, who contributed to the initial testing of the station.

Table 1. Active faults near San Diego , and their earthquake potential (Anderson et al, 1989)

Fault name	Primary Style of Faulting	Closest Approach to Thornton Hospital (km)	Maximum Credible Magnitude	Peak Site Acceleration in San Diego (g)	Estimated Slip Rate (mm/yr)	Estimated Recurrence Interval (yr)	Segment Length (km)
<b>Rose Canyon-Newport Inglewood Fault Zone</b>							
1933 event	FS	105	6.6	0.02	0.5-3.0	555	37
Camp Pendleton segment	FS		7	0.07	0.5-3.0	1050	70
Coronado	FS	19					
Country Club	FS	4.7					
Del Mar segment	FS		6.6	0.16	0.5-3.0	1020	34
Descanso	FS						
La Nacion segment	FS	17.5	6.5	0.39	.02-.08	10080	28
Mission Bay + Del Mar segments	FS		6.9	0.65	0.5-3.0	1800	60
Mission Bay segment	FS	6	6.4	0.48	0.5-3.0	720	24
Mount Soledad	FS	4					
Multiple segments	FS		6.8	0.41	0.5-3.0	9000	50
Multiple segments	FS		6.2	0.29	0.5-3.0	295	18
Old Town	FS	14					
Rose Canyon	FS	3.8					
Silver Strand	FS	21.5					
Spanish Bight	FS	15					
<b>Agua Blanca-Coronado Bank Fault Zone</b>							
		25					
Multiple segments	FS		7.7	0.25	2-6.0		>250
Multiple segments	FS		7.1	0.18	2-6.0	1020	>85
Multiple segments	FS		6.1	0.10	2-6.0	180	>15
Punta Banda Ridge segment	FS		6.5	0.02	4-5.0	130	29
Santo Tomas segment	FS		6.5	0.01	4-6.0	96	32
Valle Trinidad segment	FS		7	0.01	4-6.0	195	65
<b>San Diego Trough Fault Zone</b>							
Multiple segments	FS		7.7	0.15	.05-1.0		>250
Multiple segments	FS		7.1	0.11	.05-1.0	3060	>85
Multiple segments	FS		6.1	0.06	.05-1.0	540	>15
<b>San Clemente-San Isidro fault zone</b>							
		80					
Multiple segments	FS		7.7	0.06	.5-5.0	1440	>250
Multiple segments	FS		7.6	0.06	.5-5.0	252	>200
Multiple segments	FS		6.6	0.03	.5-5.0		>35
<b>Sierra Madre-Cucamonga and related central Transverse Ranges faults</b>							
San Miguel-Vallecitos	FS				0.1-0.5	80,000	160
Multiple segments	FS		8.2	0.02	1-10.0		>250

Table 2. Historical seismicity in the San Diego Area (Kern, 1988; Anderson et al, 1989)

Date	Magnitude	Location	Epicentral Peak Intensity (MM)	Damage	Distance to Thornton Hospital (km)
22 November 1800		?	VII?	Adobe walls at the Presidio of San Diego were damaged, and the walls of the new church at San Juan Capistrano were cracked.	
25 May 1803		?	VI?	The mission church at San Diego was slightly damaged.	
8 December 1812		San Andreas?	?	This event was possibly on the San Andreas Fault, was felt in San Diego but caused no damage there.	
12 April 1852		?	VII?	An adobe house was destroyed by a severe shock. This earthquake was not mentioned in any other source.	
29 November 1852		Mexicali Valley?			210.
20 September 1856		Santa Ysabel?			
9 January 1857	7.9	Cajon Pass to Parkfield	V	7.9M event on the San Andreas Fault caused intensity V in San Diego, but with little damage.	425.
25 March 1859		Nearby?			
27 May 1862		South or west of San Diego	VII	Appears to have been closer to San Diego than any other damaging earthquake.	20.
29 May 1862		Nearby?			
13 June 1862		Nearby?			
21 October 1862		?			
13 September 1885		?			
8 October 1886		?			
5 February 1890		?			
9 February 1890	6?	San Jacinto?			105.
30 July 1891	7??	Colorado Delta			
23 February 1892	6.8?	Southeast of San Diego?	VII	Caused widespread minor damage in San Diego. Possible a 7.5M on the Laguna Salda fault?	
24 February 1892		Northern Baja?			155.
23 October 1894	5.5	East of San Diego	VI	Less strong than the 1892 event; possibly in the mountains east of San Diego.	
22 July 1899	6.5	Cajon Pass			
25 December 1899	6.5	San Jacinto	V-VI		105.
23 January 1903	7	Colorado Delta			
18 April 1906	6	Imperial Valley			

Table 2 (cont.)

20 November 1915	7.1	Mexicali Valley			
29 September 1916		East San Diego County?			
21 April 1918	6.8	San Jacinto FZ			105.
23 July 1923	6.2	San Jacinto FZ	V-VI		
2 December 1929		Northern Baja			
30 December 1934	6.5	Laguna Salada	?		180.
31 December 1934	7.1	Cerro Prieto?	?		225.
25 March 1937	6	San Jacinto FZ	IV-V		105.
1 May 1939	5	San Clemente FZ	V		100.
24 June 1939	5	San Clemente FZ	III		100.
19 May 1940	6.7	Imperial Fault	IV-V		160.
21 October 1942	6.5	San Jacinto FZ	IV-VI		110.
29 August 1943	5.5		IV		155.
15 August 1945	5.7	San Jacinto FZ	V		110.
10 April 1947	6.2		V		240.
4 December 1948	6.5		VI		140.
4 November 1949	5.7	Vallecitos FZ	VI		100.
26 December 1951	5.9		VI		105.
21 July 1952	7.7		V		285.
19 March 1954	6.2	San Jacinto FZ	V		105.
24 October 1954	6	San Miguel FZ	V		175.
12 November 1954	6.3	San Miguel FZ	V		170.
9 February 1956	6.8	San Miguel FZ	VI		175.
14 February 1956	6.3	San Miguel FZ	V		220.
15 February 1956	6.4	San Miguel FZ	V		220.
22 December 1964	5.6	San Isidro FZ	VI		120.
9 April 1968	6.4	San Jacinto FZ	VI		105.
28 April 1969	5.8	San Jacinto FZ			
9 February 1971	6.4		VI		205.
15 October 1979	6.6	Imperial Fault	?		180.
25 February 1980	5.5	San Jacinto FZ			95.
8 May 1985	5	San Miguel FZ			170.
8 July 1986	5.6				140.
13 July 1986	5.3	30 Mile Bank			60.
29 October 1986	4.7	Rose Canyon			30.
23 November 1987	6.2	San Jacinto FZ			
24 November 1987	6.6	San Jacinto FZ			

Table 3: Geotechnical data for Phase 1, UCSD Satellite Medical Facility, San Diego, CA  
(Geocon Inc., 1989)

Boring #	Elevation (ft)	TD (ft)	Northing	Easting		
Boring 1	333	2 5. 5	260 322.	1700 520.		Topsoil (0-0.5') Scripps Fm (.5-25.5')
Boring 2	330	4 0. 5	260 144.	1700 650.		Topsoil (0-0.5') Scripps Fm (.5-40.5')
Boring 3	334	4 0. 5	260 456.	1700 724.		Topsoil (0-1.0') Scripps Fm (1.0-40.5')
Boring 4	332	2 5. 5	260 250.	1700 876.		Topsoil (0-0.5') Scripps Fm (.5-25.5')
Boring 5	335	2 5. 5	260 520.	1700 870.		Scripps Fm (0-25.5')
Boring 6	334	2 5. 5	260 532.	1700 792.		Topsoil (0-0.5') Scripps Fm (.5-25.5')
Boring 7	331	4 1	260 454.	1700 340.		Scripps Fm (0-41.0')
Boring 8	325	1 2. 5	260 472.	1700 285.		Topsoil (0-2.0') Scripps Fm (2.0-12.5')
Boring 9	325	2 1	260 514.	1700 336.		Topsoil (0-2.0') Scripps Fm (2.0-21.0')
Boring 10	329	1 5	260 128.	1700 810.		Scripps Fm (0-15.0')
Boring 11	328	1 0	260 118.	1700 886.	Fill (0-5.0')	Topsoil (5-6.0') Scripps Fm (6-10.0')
Boring 12	328	8	260 086.	1700 830.		Topsoil (0-2.0') Scripps Fm (2.0-8.0')
Boring 13	328	1 7	260 090.	1700 916.	Fill (0-8.0')	Topsoil (8-15.0') Scripps Fm (15-17.0')
Boring 14	328	1 0	260 046.	1700 860.	Fill (0-5.0')	Topsoil (5-7.0') Scripps Fm (7-10.0')
Boring 15	327	5	260 010.	1700 815.		Scripps Fm (0-5.0')
Boring 16	327	5	259 968.	1700 760.		Scripps Fm (0-5.0')
Boring 17	330	5	260 206.	1700 840.		Topsoil (0-1.0') Scripps Fm (1.0-5.0')

Table 4 : Summary of Shear-Wave Velocity Measurements from the CPT Tests at Thornton

<u>Test</u>	<u>Refusal Depth (m)</u>	<u>Geophone Depth (m)</u>	<u>S-Wave Velocity (m/s)</u>
CPT-1	8.20	1.52	356
		2.13	280
		3.32	552
		4.48	438
		6.07	497
		7.87	499
CPT-2	5.35	1.46	255
		3.02	272
		4.51	290
		5.19	339
CPT-3	3.85	1.52	291
		3.02	287
		3.69	528
CPT-4	5.20	1.52	372
		3.02	385
		3.97	447
		4.73	393

Table 5 : Source parameters of the seismic events recorded at the Thornton station up to July 19

Event #	Lat	Lon	Depth (km)	Origin Time	Azim
1	31.862	-115.572	5.21	9/13/1997 (256) 22:26:33.034	125.59°
2	34.141	-116.856	10.25	9/19/1997 (262) 22:37:14.468	13.665°
3	34.301	-116.452	7.69	9/28/1997 (271) 15:57:22.949	24.199°
4	31.901	-115.802	6.00	10/22/1997 (295) 16:36:52.893	128.72°
5	32.784	-116.812	14.69	11/14/1997 (318) 19:31:34.214	105.1°
6	33.582	-116.943	12.72	12/12/1997 (346) 14:08:03.309	18.582°
7	34.374	-117.648	8.99	8/20/1998 (232) 23:49:58.442	346.92°
8	34.111	-116.920	4.41	10/01/1998 (274) 18:18:15.959	11.649°
9	32.058	-115.406	6.00	10/20/1998 (293) 2:48:57.103	117.62°
10	31.840	-115.721	6.00	10/20/1998 (293) 9:25:24.094	128.83°
11	32.085	-115.404	6.00	10/20/1998 (293) 23:14:20.176	116.81°
12	32.933	-117.159	0.00	10/22/1998 (295) 19:00:37.327	46.269°
13	33.966	-117.176	14.11	10/25/1998 (298) 11:40:48.952	2.2237°
14	34.323	-116.844	5.90	10/27/1998 (300) 1:08:40.647	12.347°
15	34.324	-116.851	4.52	10/27/1998 (300) 7:16:06.969	12.12°
16	34.320	-116.850	4.29	10/27/1998 (300) 15:40:17.064	12.185°
17	31.896	-115.772	6.00	11/02/1998 (306) 10:16:05.707	128.27°
18	32.274	-118.363	6.00	11/10/1998 (314) 14:13:28.438	238.02°
19	32.719	-115.921	9.35	1/13/1999 (013) 10:02:05.430	97.929°
20	32.727	-115.926	2.58	1/13/1999 (013) 13:20:56.021	97.551°
21	32.746	-118.111	6.00	5/03/1999 (123) 16:18:58.756	260.11°
22	34.062	-116.366	1.85	5/14/1999 (134) 7:54:03.189	31.019°
23	32.374	-115.242	6.00	6/01/1999 (152) 15:18:02.629	106.27°
24	33.627	-116.717	17.27	7/19/1999 (200) 22:09:26.612	29.528°

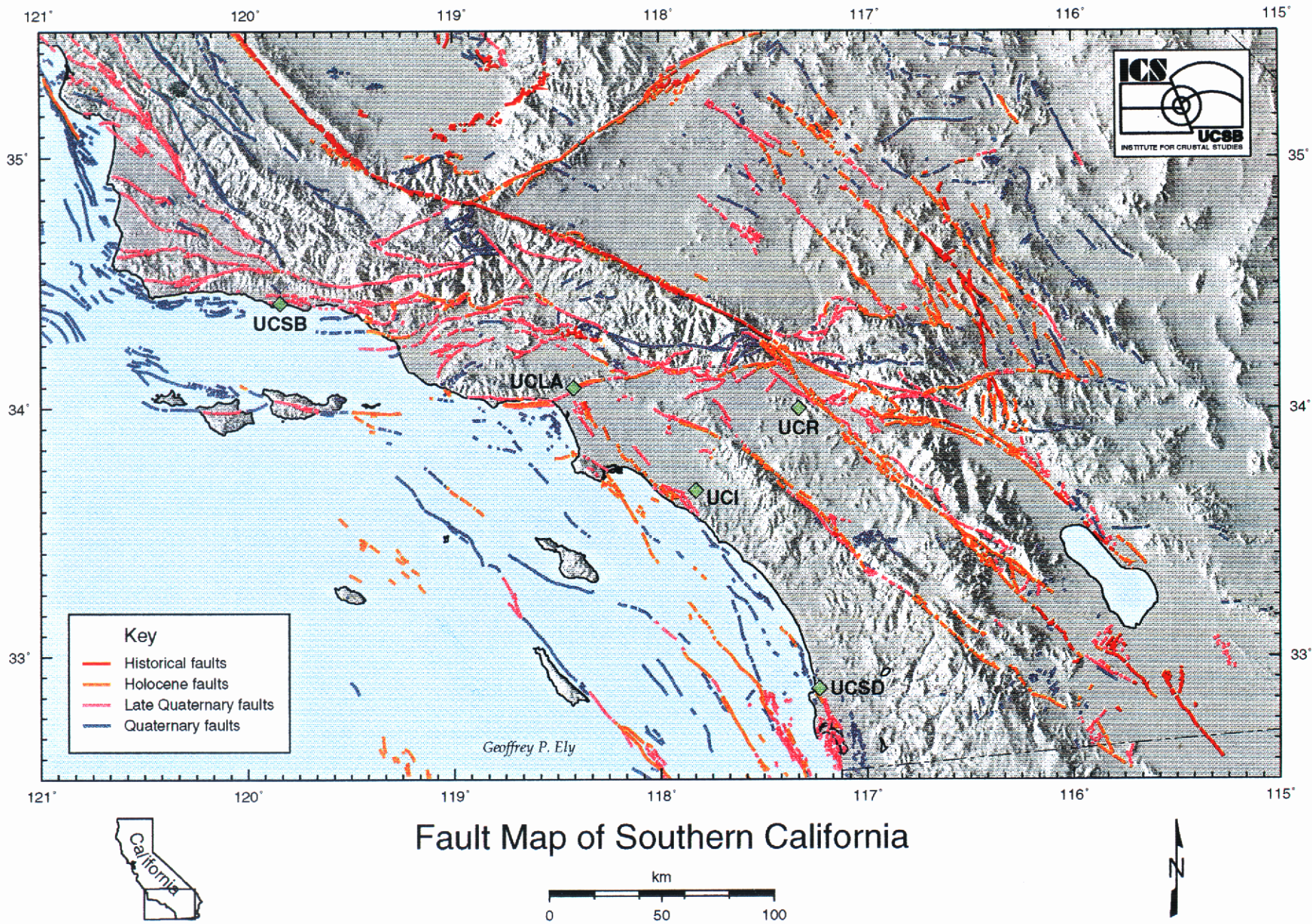


Figure 1. Active fault map of Southern California (CDMG, 1994) with UC campus locations.

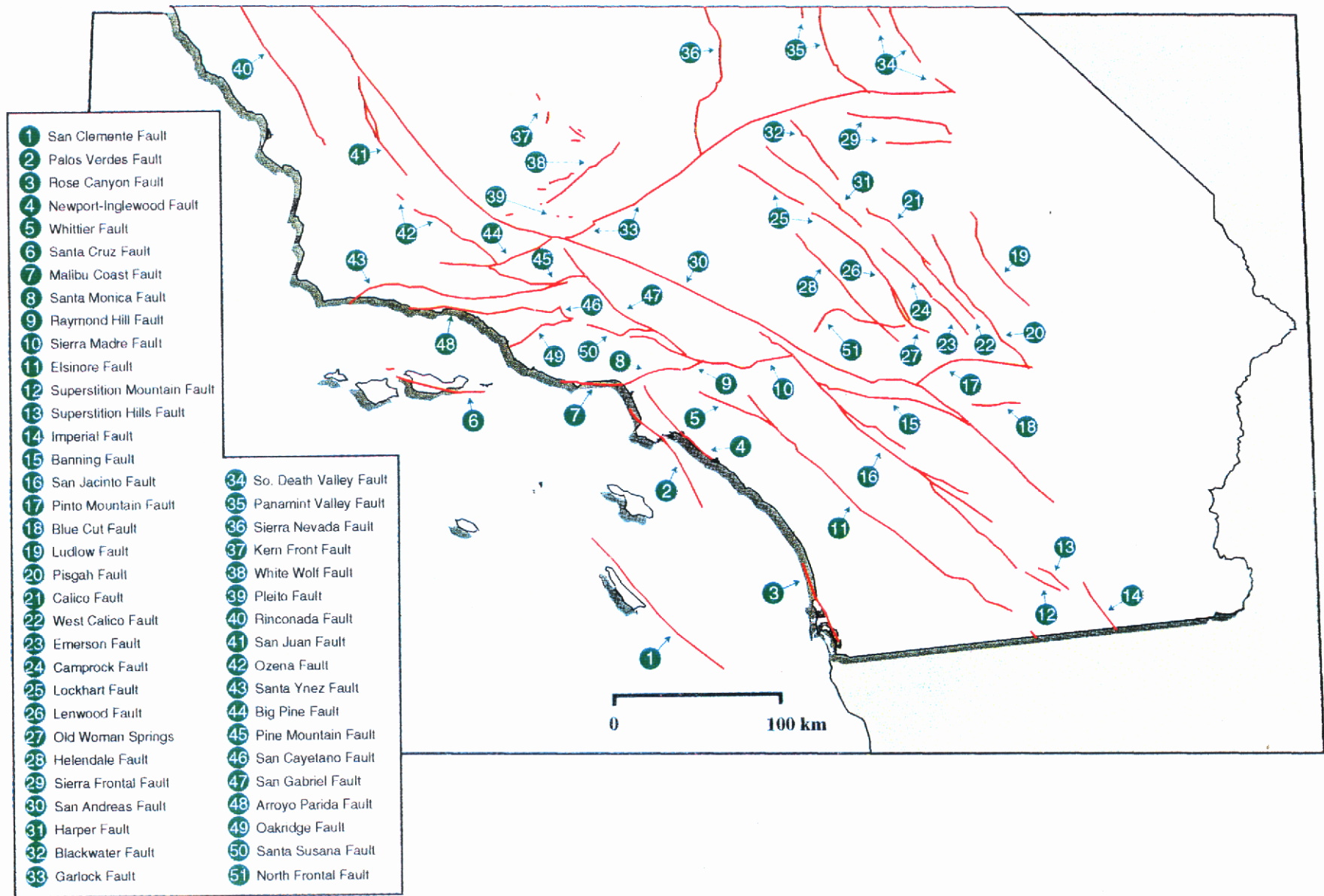
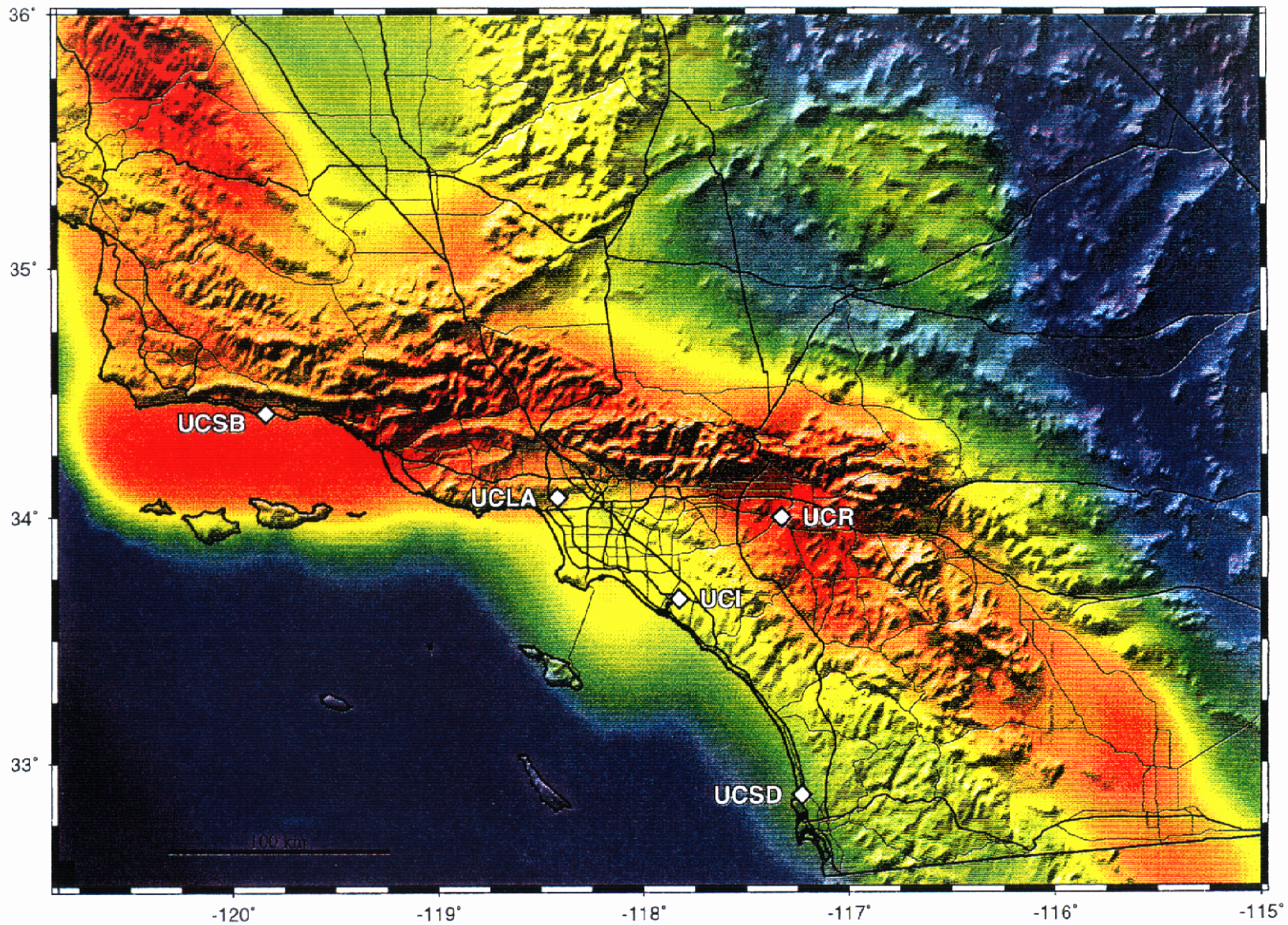
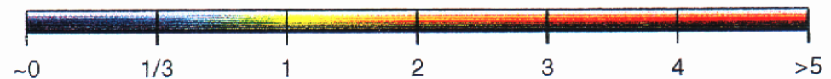


Figure 2. Active fault map of Southern California, showing fault names (Jackson et al, 1995)



**So. Calif. Earthquake Center (SCEC)**



Key - Number of times per century the shaking from earthquakes will exceed 20% the force of gravity. Significant damage to older buildings begins at this level.

Figure 3. Estimated number of times per century for the peak surface acceleration to exceed 0.2g, in Southern California ( adapted from Jackson et, 1995, by K. Hudnut, 1997)

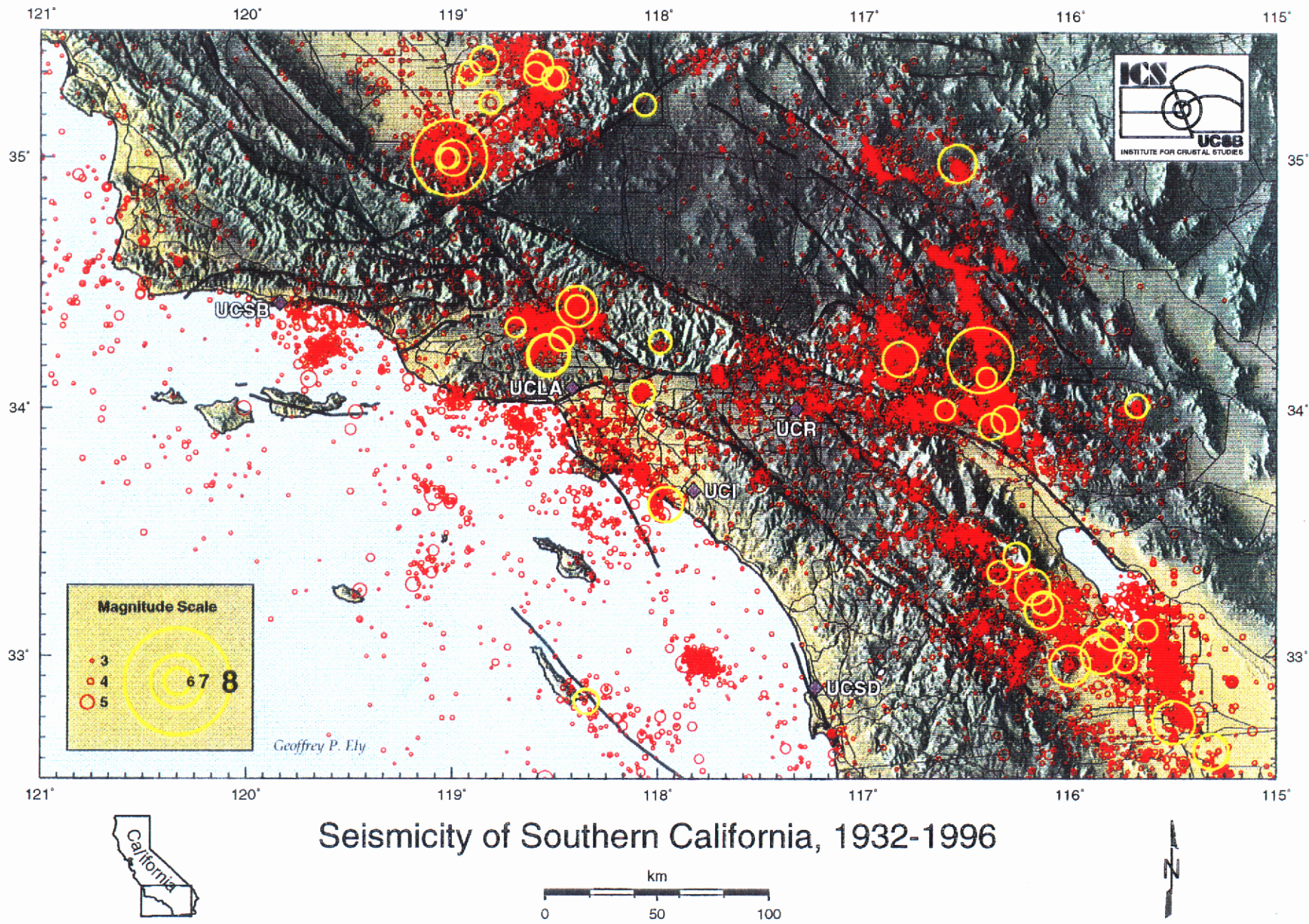


Figure 4. Seismicity of southern California (1932-1996). Data provided by SCEC.

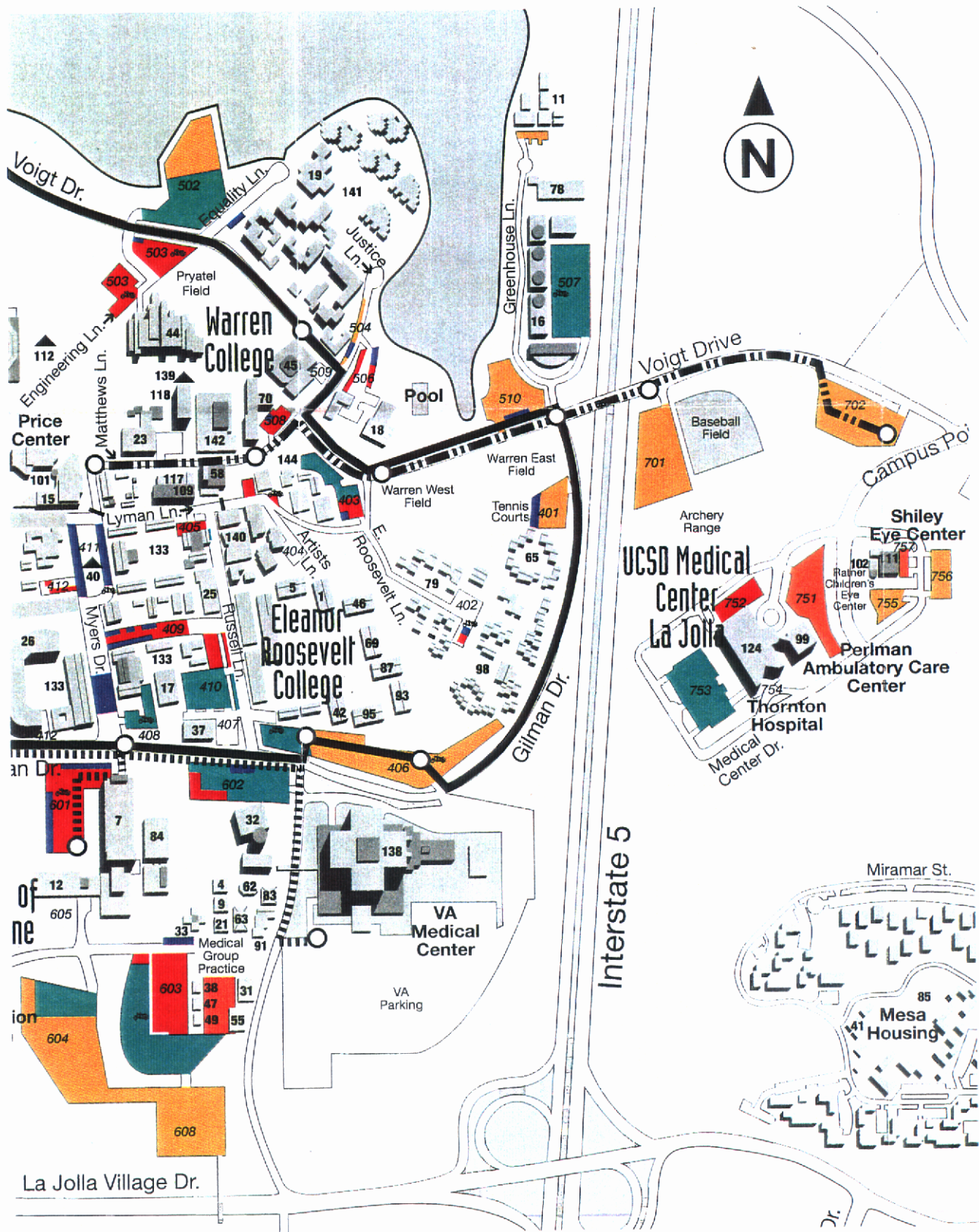


Figure 5. Map of the U.C. San Diego campus, showing the Thornton hospital location, East of Interstate 5.

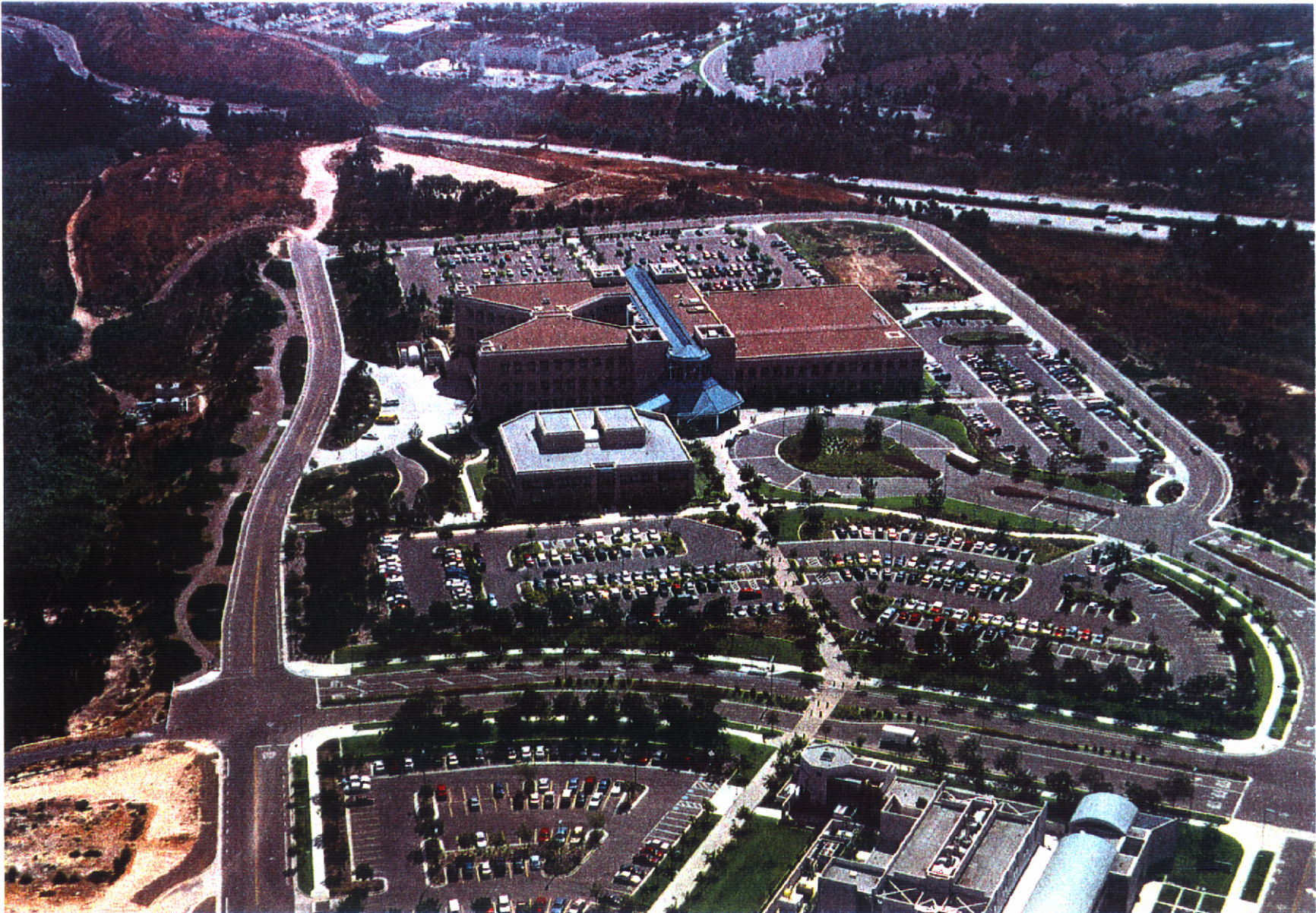


Figure 6. Aerial overview of the Thornton hospital site, looking west, . Seismic station holes being drilled (right upper quadrant). Photo by F. Heuze, June 26, 1997.

# Felt Earthquakes in San Diego

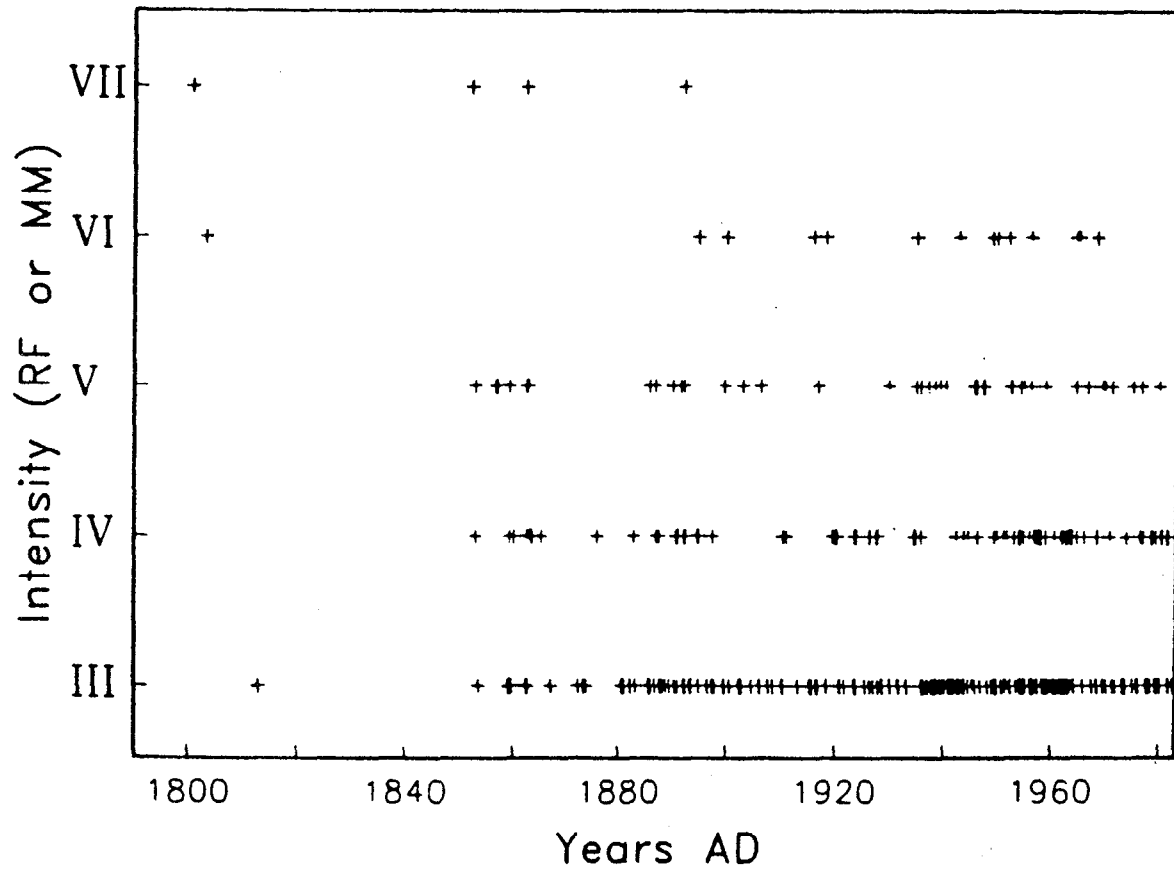


Figure 7. Intensities of felt earthquakes in San Diego (Anderson et al, 1989)

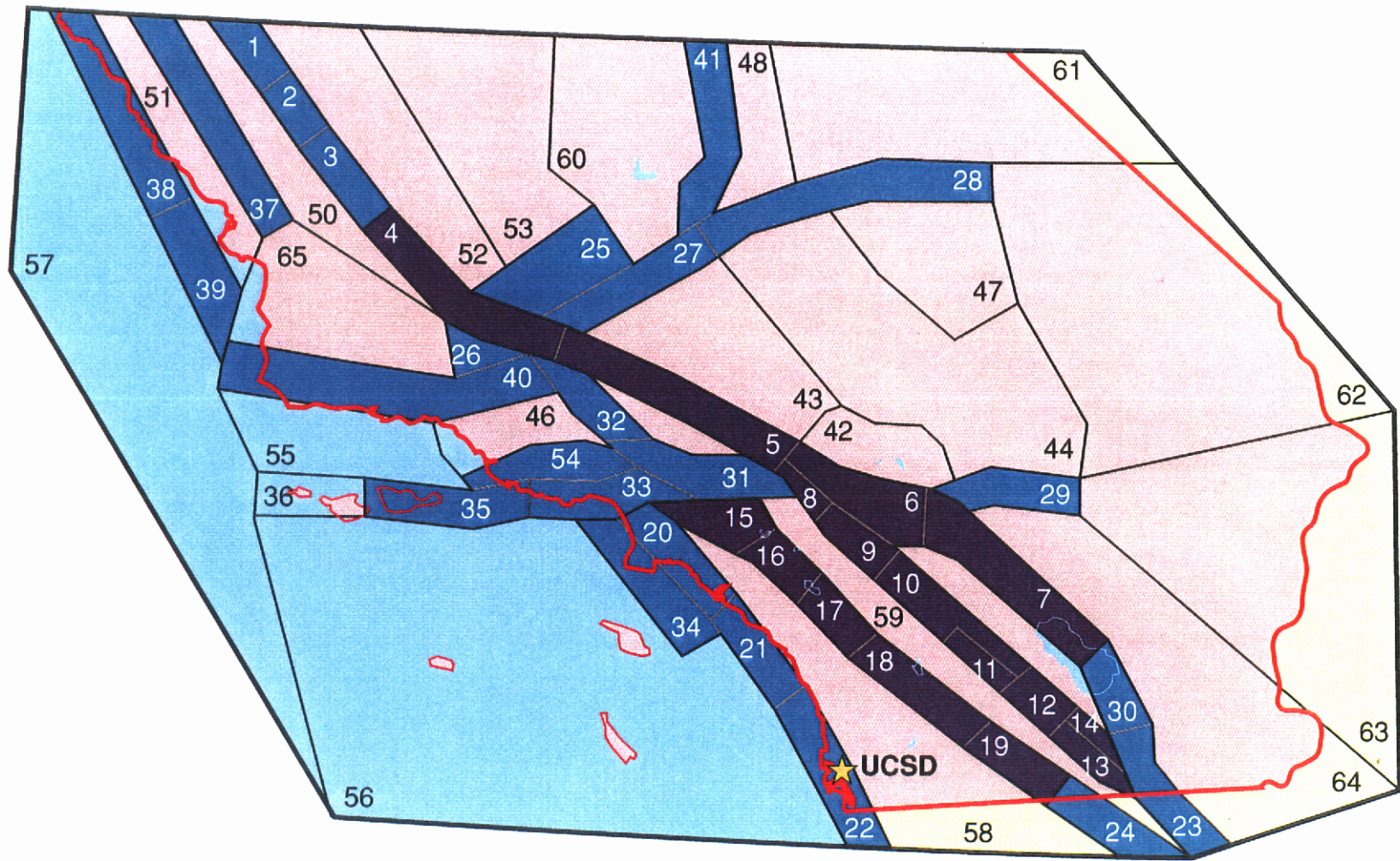


Figure 8. Segmentation of faults in Southern California (adapted from Jackson et al, 1995)

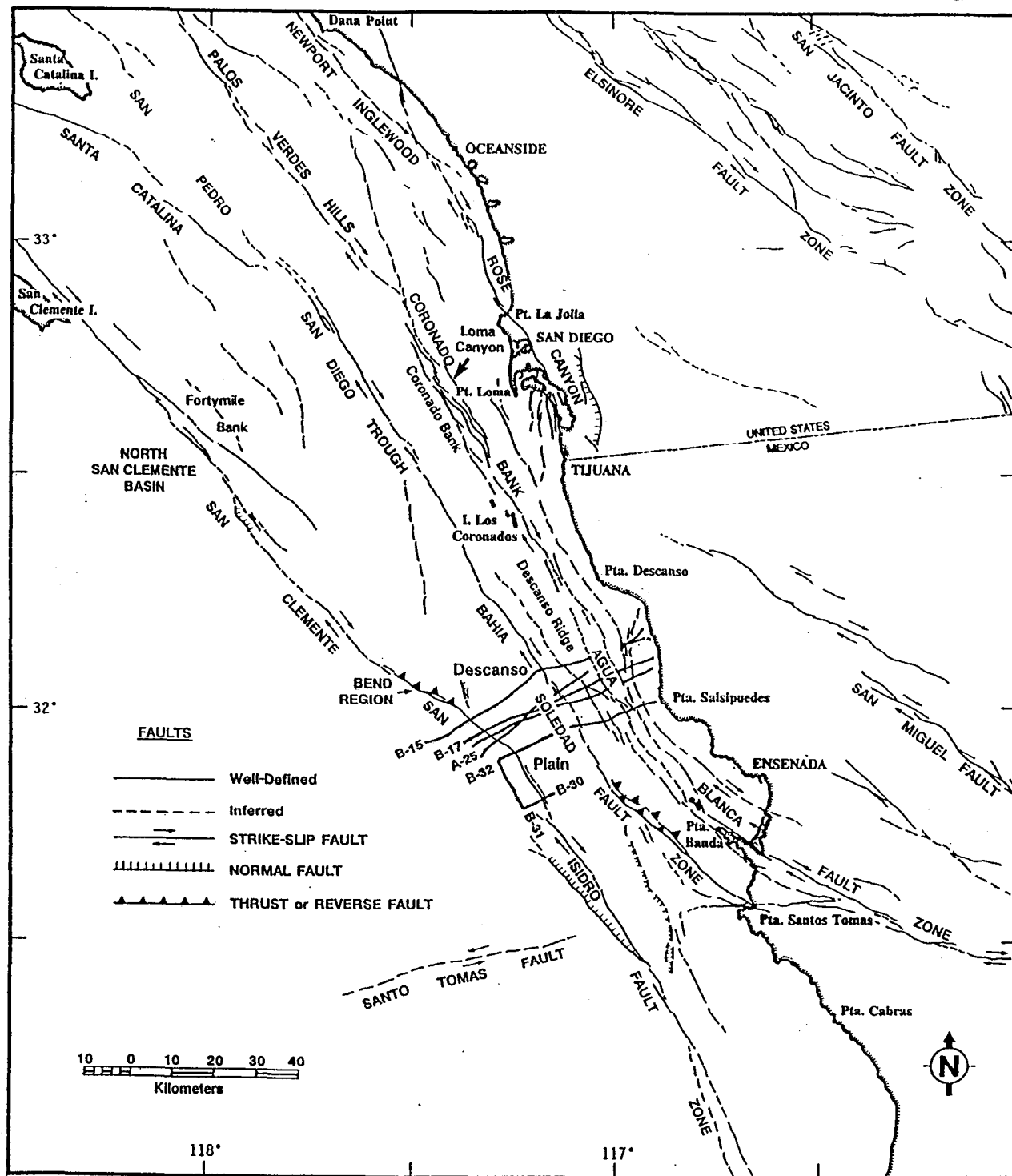


Figure 9. Major late Cenozoic fault zones of the inner California Continental Borderland and adjacent areas in the vicinity and San Diego and northern Baja California, Mexico (Legg and Kennedy, 1991)

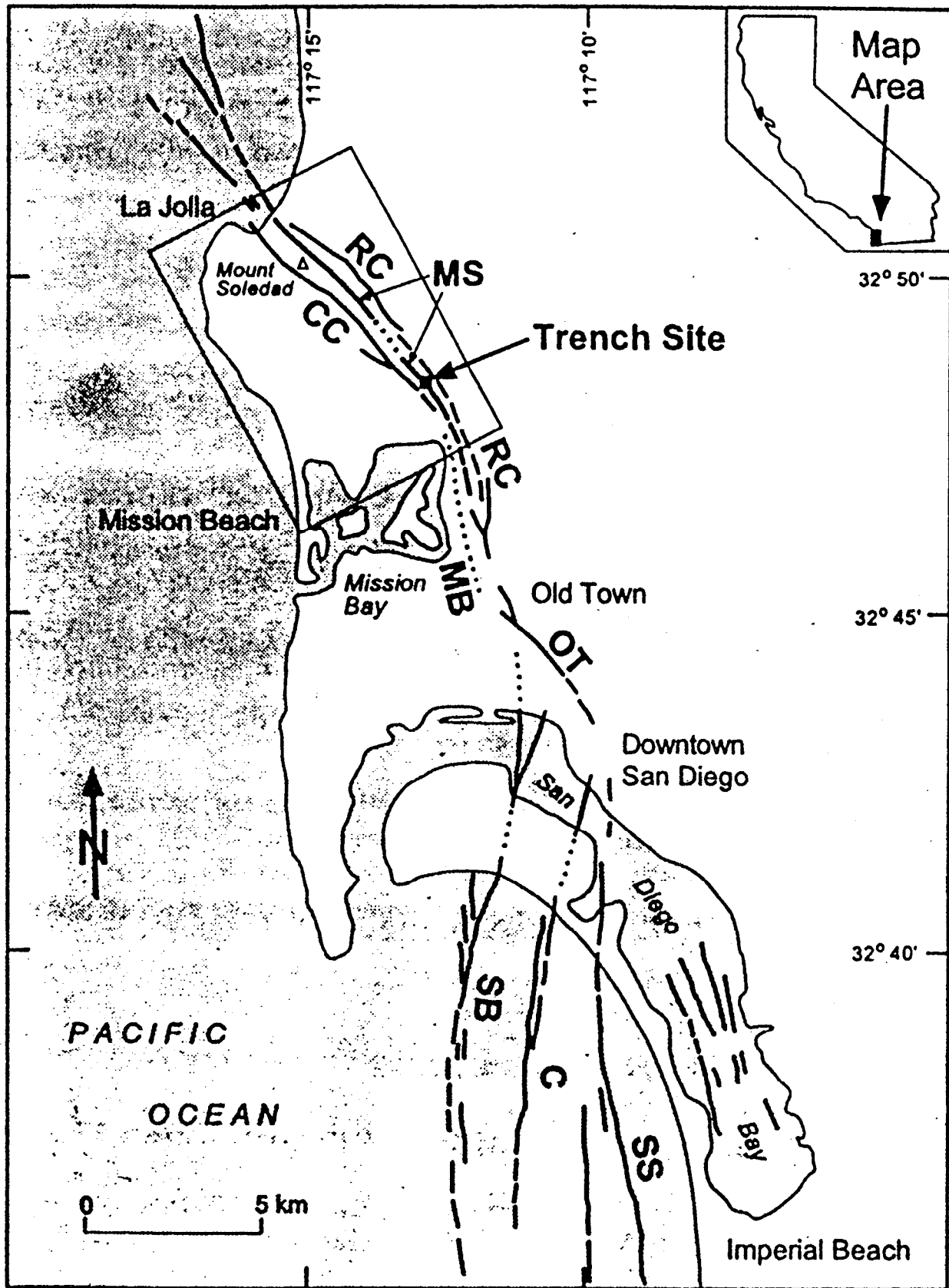


Figure 10a. Major strands of the Rose Canyon fault (Lindvall and Rockwell, 1995)

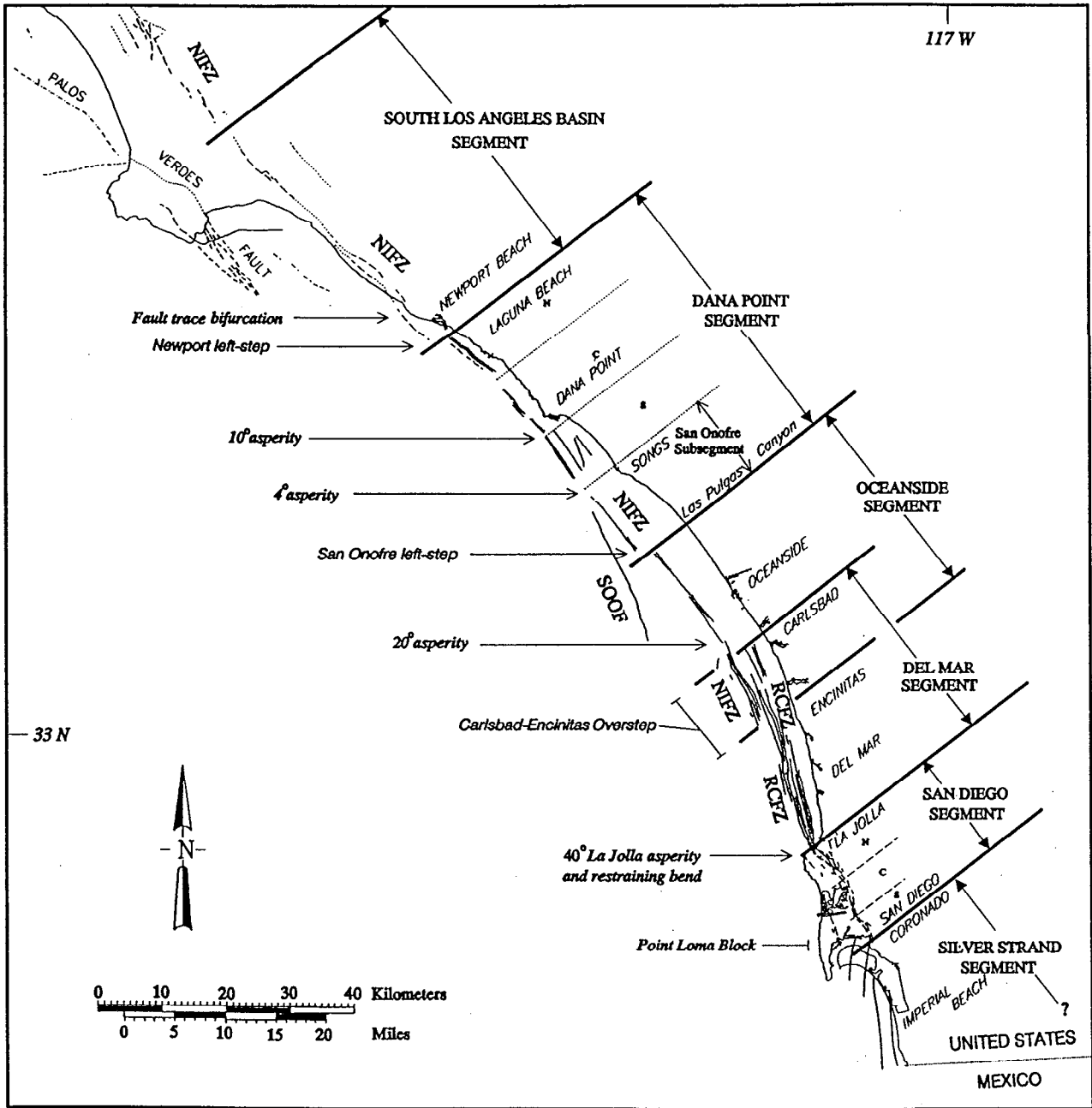


Figure 10b. Segmentation of the Newport-Inglewood - Rose Canyon fault zone  
(Fischer and Mills, 1991)

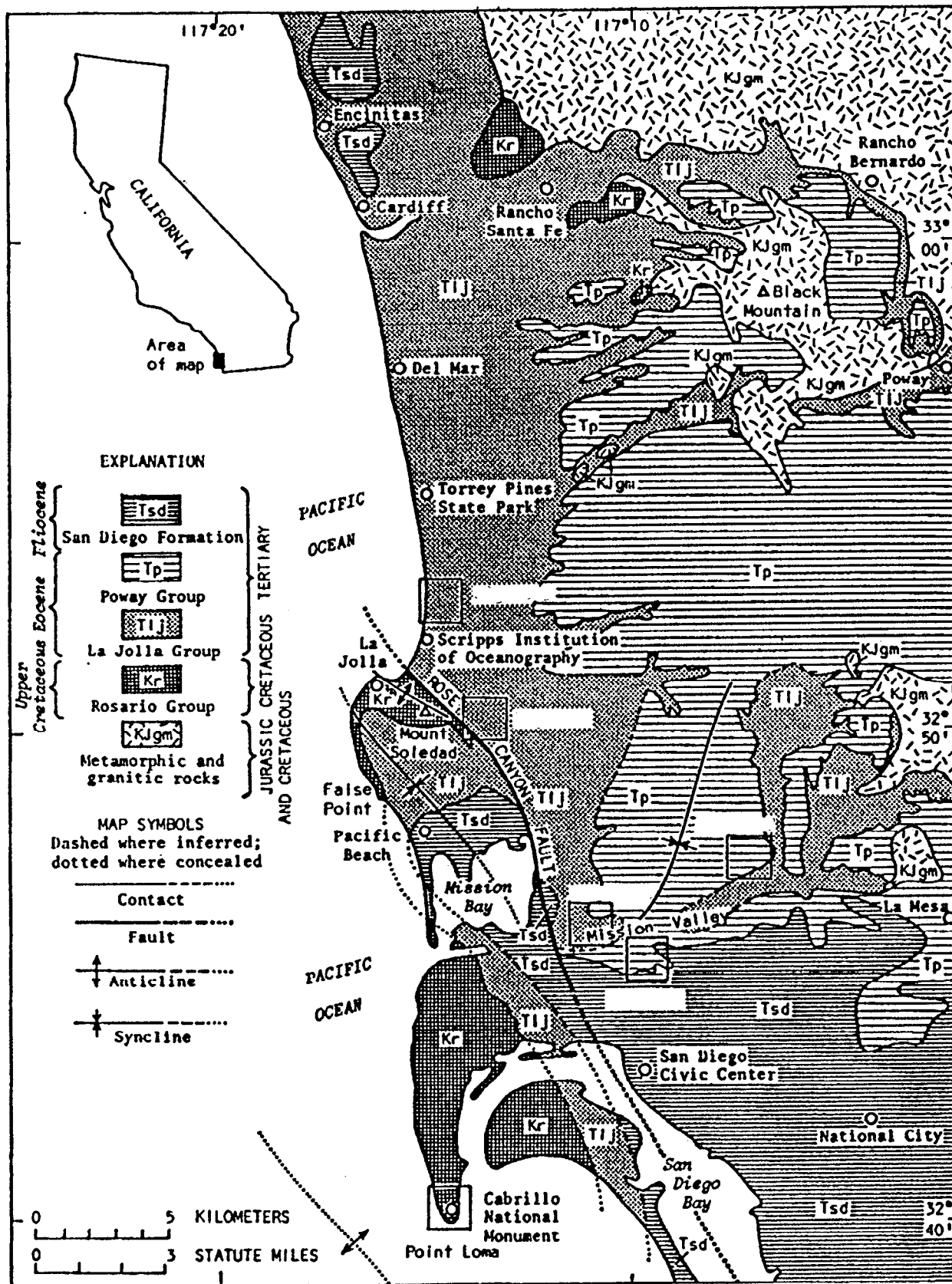


Figure 11. Index map of bedrock geology of the San Diego coastal area (Kennedy, 1975). Quaternary deposits are not shown.

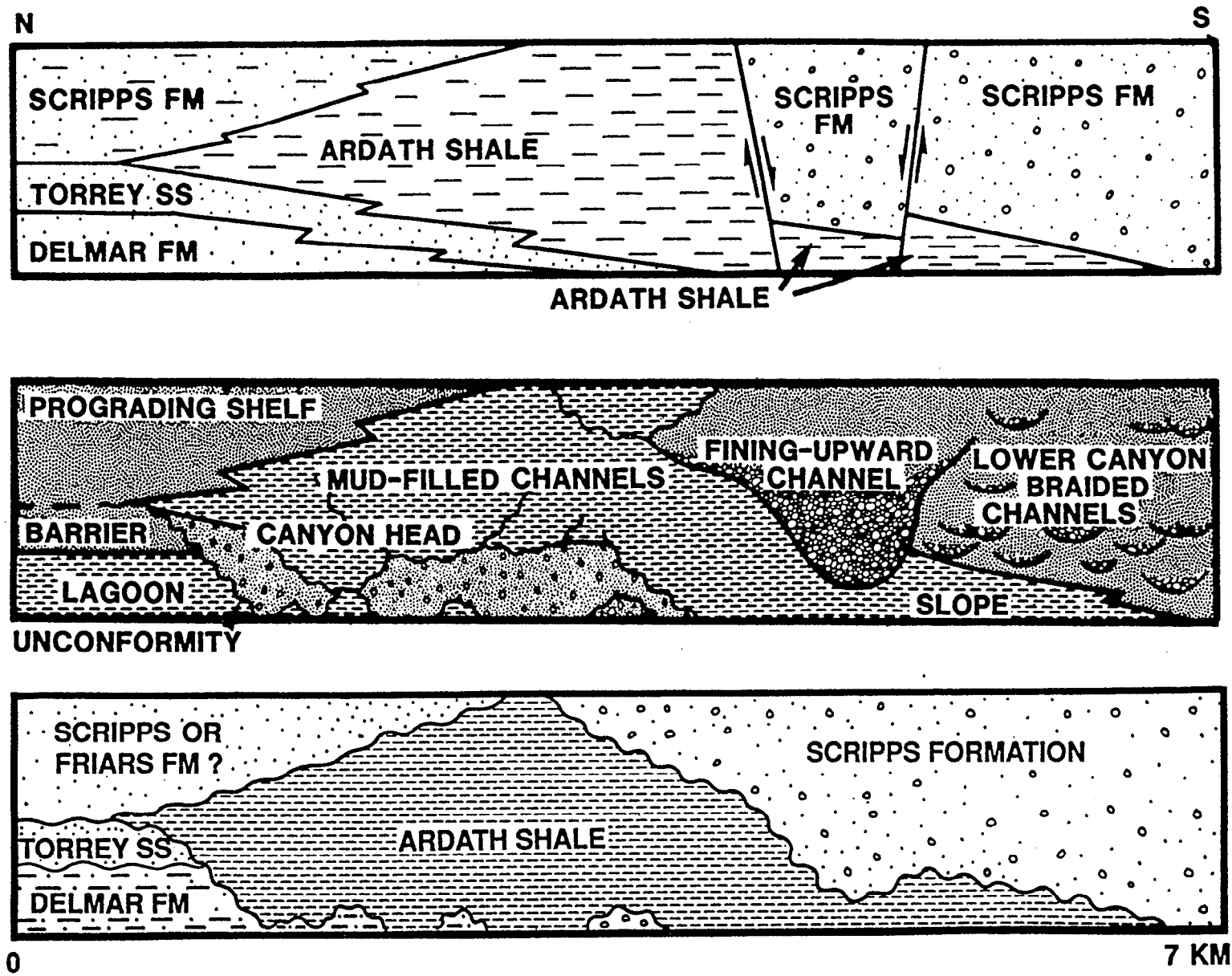


Figure 12. Evolving interpretation of the sea cliff exposures along Black's Beach (Abbott and May, 1991)

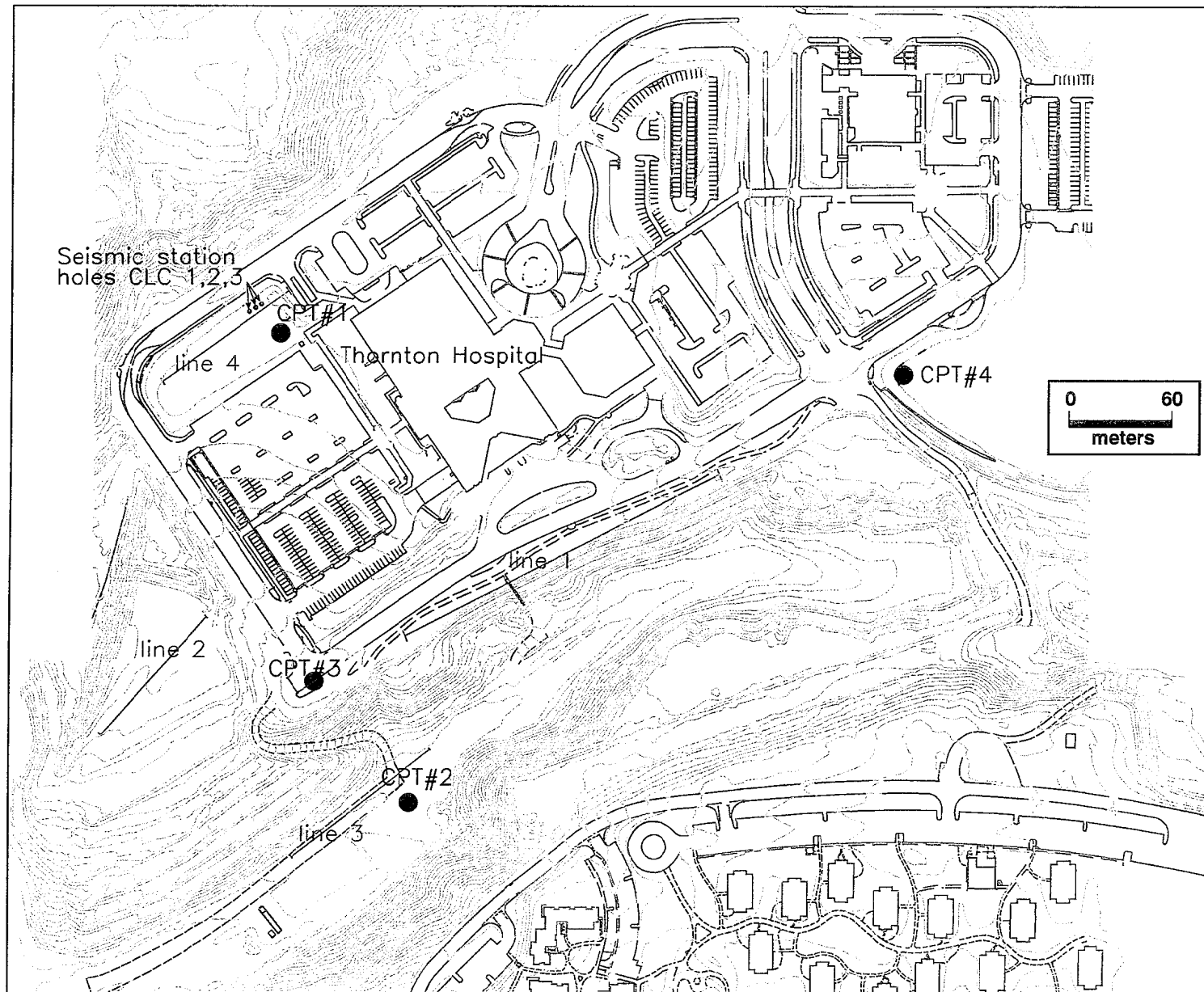


Figure 13. Detailed map of the Thornton Hospital site, showing locations of CLC boreholes, CPT, and seismic refraction survey lines.

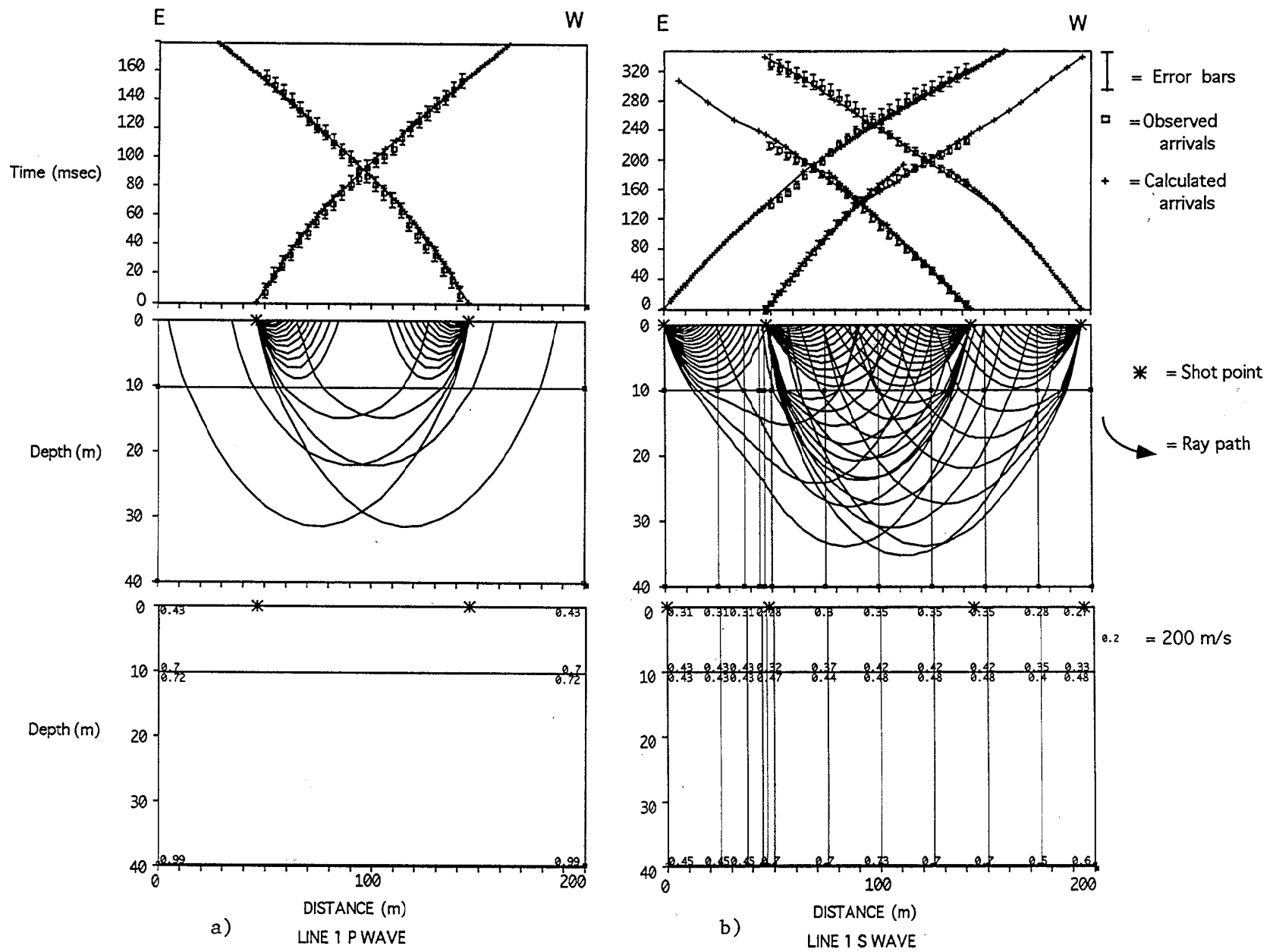
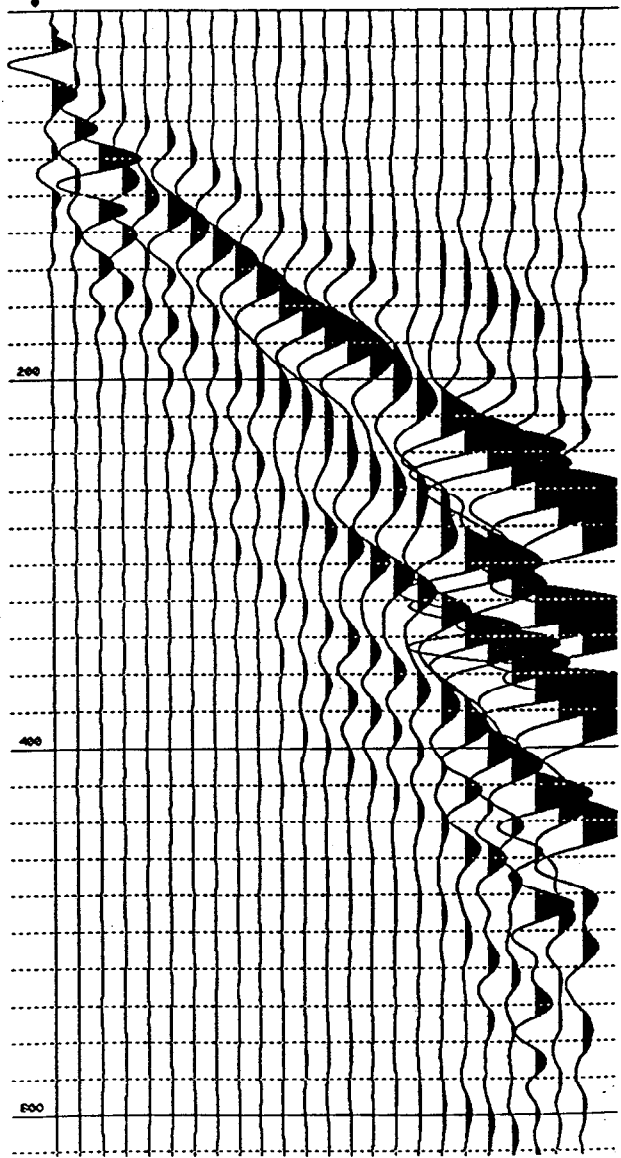
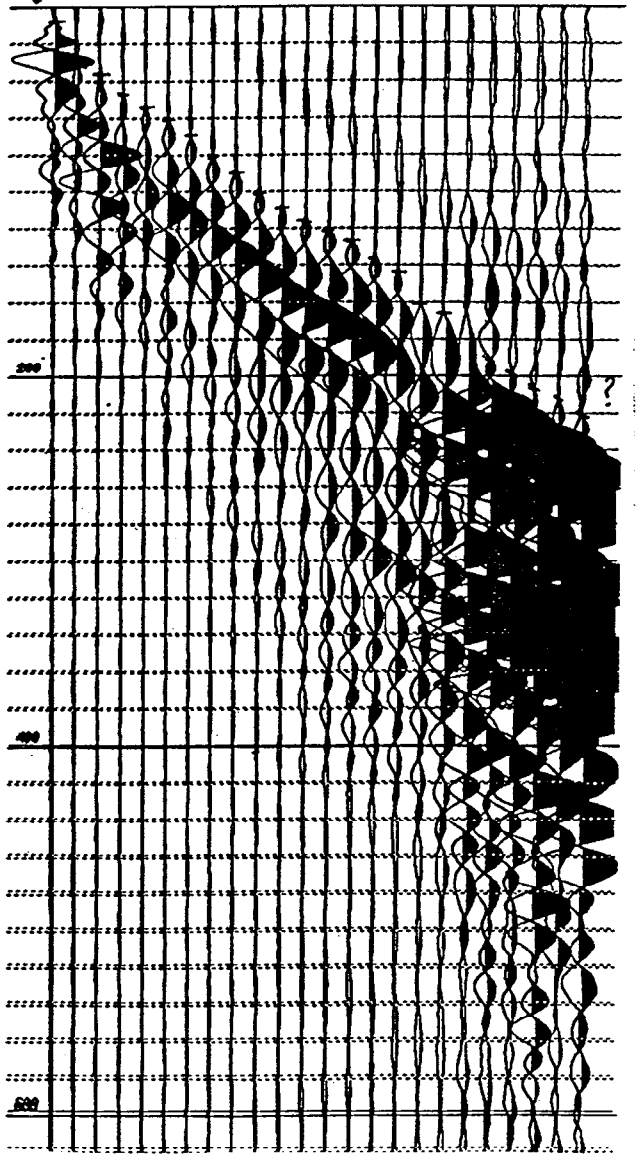


Figure 15 : Line 1 travel-time plots, ray-paths, and velocity model (km/sec)

**GEOMETRICS**  
 StrataView  
 9:51:3025/JAN/1997  
 SAVED AS 040202.DAT  
 LINE NUMBER 04  
 SHOT LAG -1.00  
 SAMPLE INTERVAL 125 us  
 ACR FILE OUT  
 DISP FILE NI CUT 250HZ NOTCH 100HZ  
 GROUP INTERVAL 4.00  
 PHONE 1 LAG 0.00  
 RECORD LEN 1024 MS  
 SHOT INTERVAL 0.00  
 PHONE 24 LAG 92.00  
 DELAY 0 MS  
 STACKS 16  
 FIXED GAIN  
 1 2 3 4 5 6 7 8 9 10 11 12 13 14 15 16 17 18 19 20 21 22 23 24  
 0 0 4 4 16 21 21 21 24 27 30 33 36 39 39 39 42 45 48 48 48



**GEOMETRICS**  
 StrataView  
 9:51:3025/JAN/1997  
 SAVED AS 040202.DAT  
 LINE NUMBER 04  
 SHOT LAG -1.00  
 SAMPLE INTERVAL 125 us  
 ACR FILE OUT  
 DISP FILE NI CUT 250HZ NOTCH 100HZ  
 GROUP INTERVAL 4.00  
 PHONE 1 LAG 0.00  
 RECORD LEN 1024 MS  
 SHOT INTERVAL 0.00  
 PHONE 24 LAG 92.00  
 DELAY 0 MS  
 STACKS 16  
 FIXED GAIN  
 1 2 3 4 5 6 7 8 9 10 11 12 13 14 15 16 17 18 19 20 21 22 23 24  
 0 0 4 4 16 21 21 21 24 27 30 33 36 39 39 39 42 45 48 48 48



a) Example of seismic refraction record. Velocities were estimated by picking the arrival times of wave travelling from the left side of the record. Travel time in ms is plotted on the vertical axis. Note the dominant frequency of the arrivals in the 20-30 Hz range, eliminating the need for filtering 60 Hz noise.

b) Example of SH records with opposite polarities. Note how the SH arrival can be identified by a first break upward on one record and downward on the other.

Figure 14

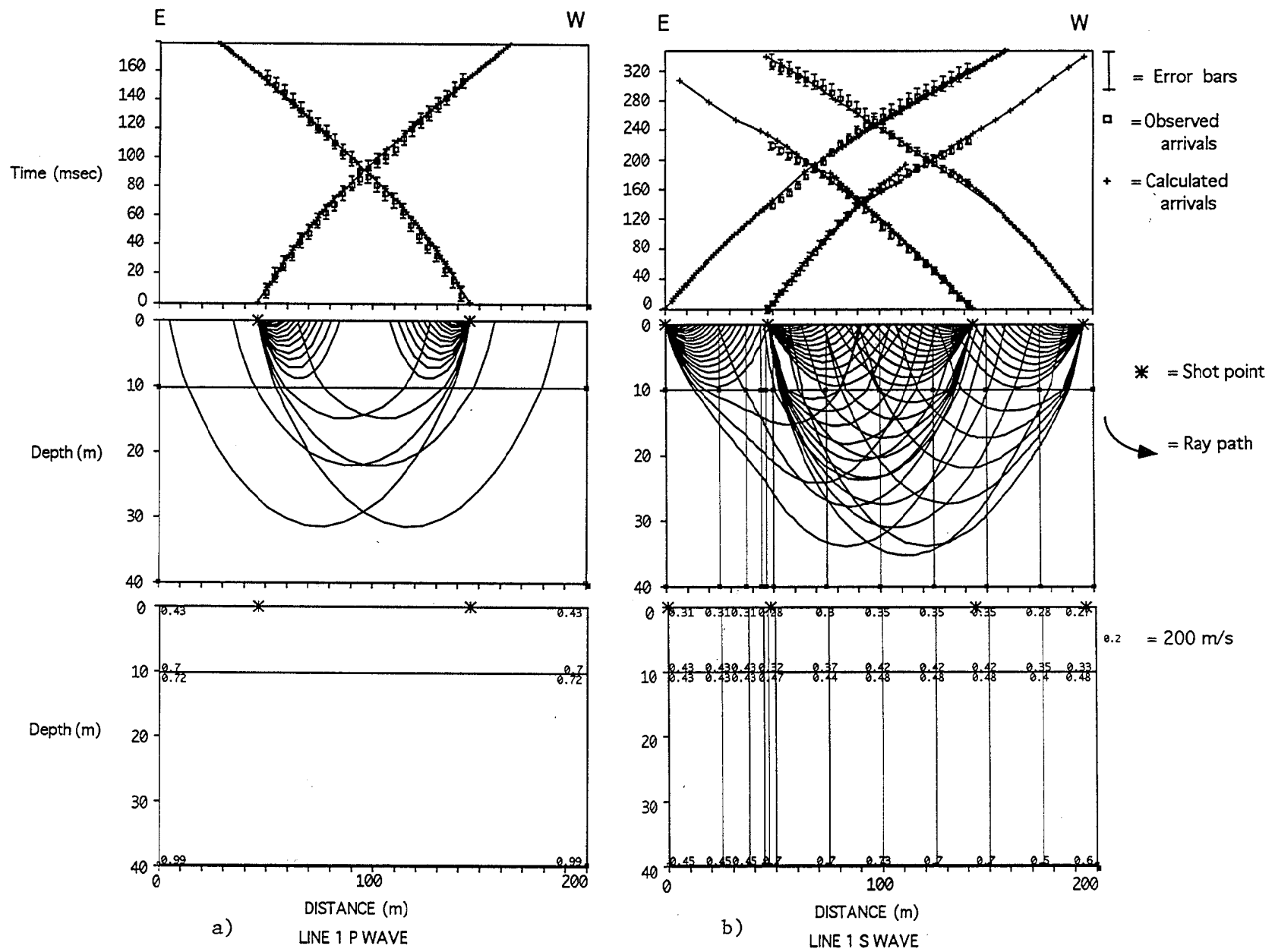


Figure 15 : Line 1 travel-time plots, ray-paths, and velocity model (km/sec)

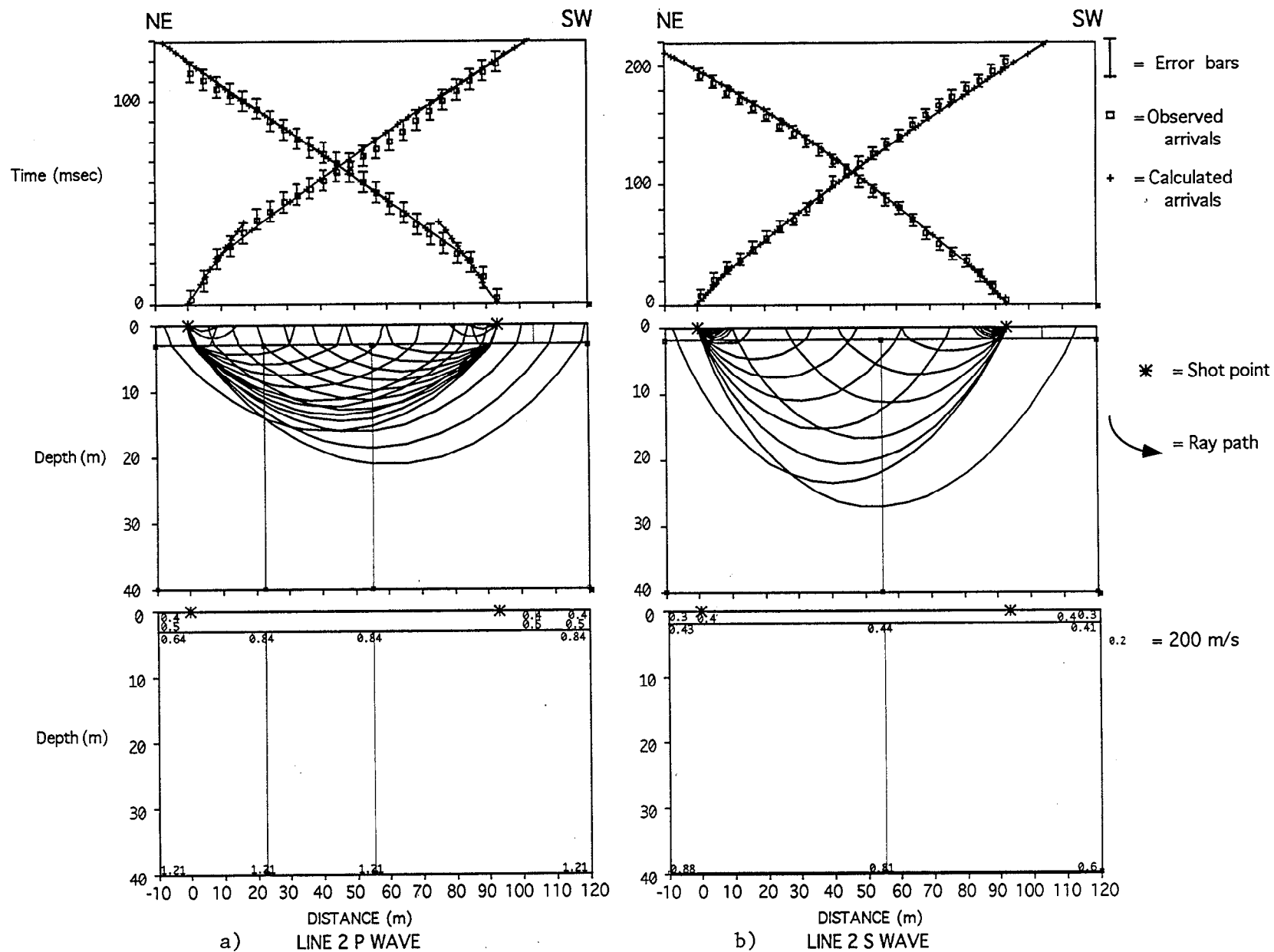


Figure 16 : Line 2 travel-time plots, ray paths, and velocity model (km/sec)

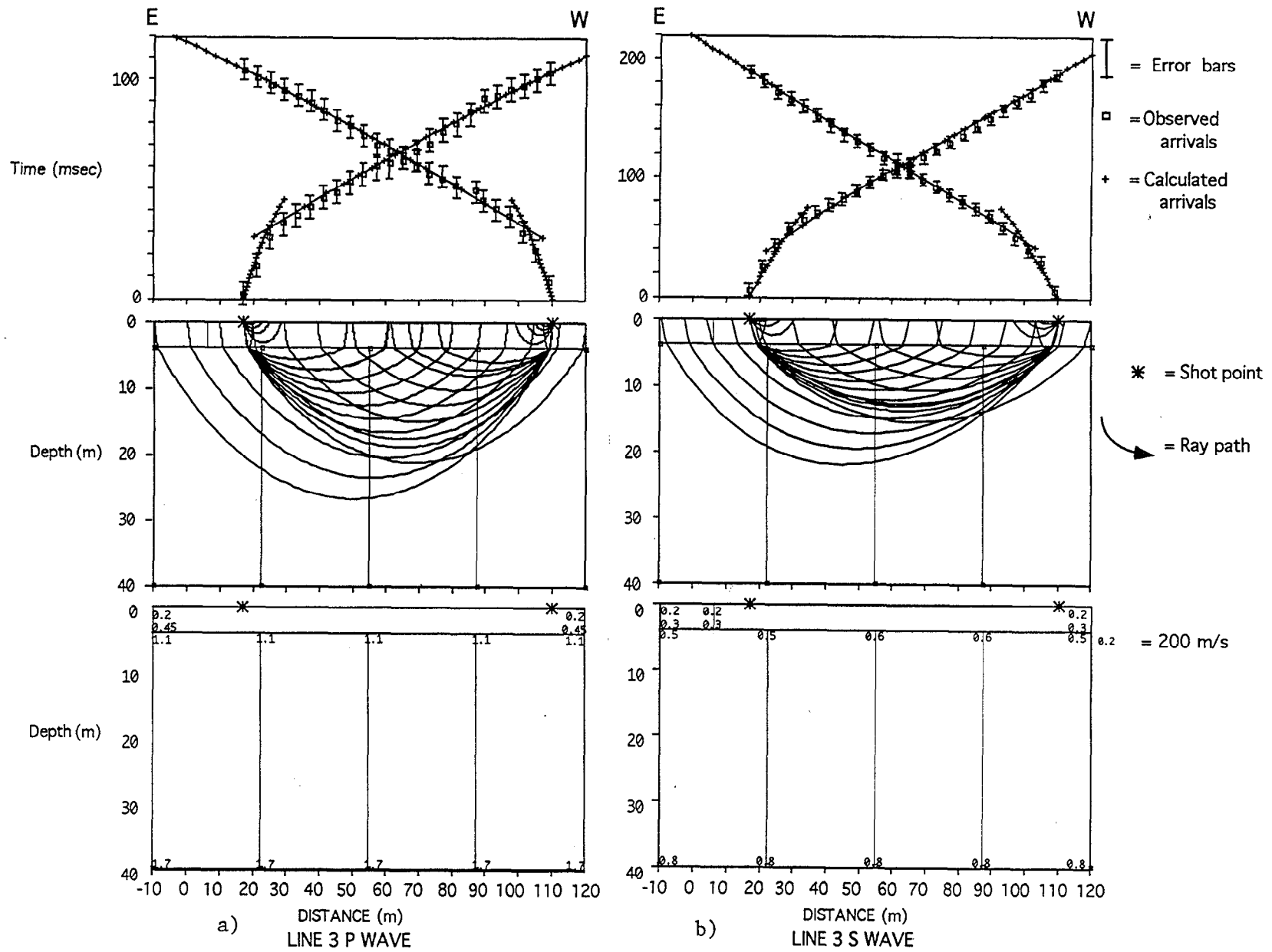


Figure 17 : Line 3 travel-time plots, ray paths, and velocity model (km/sec)

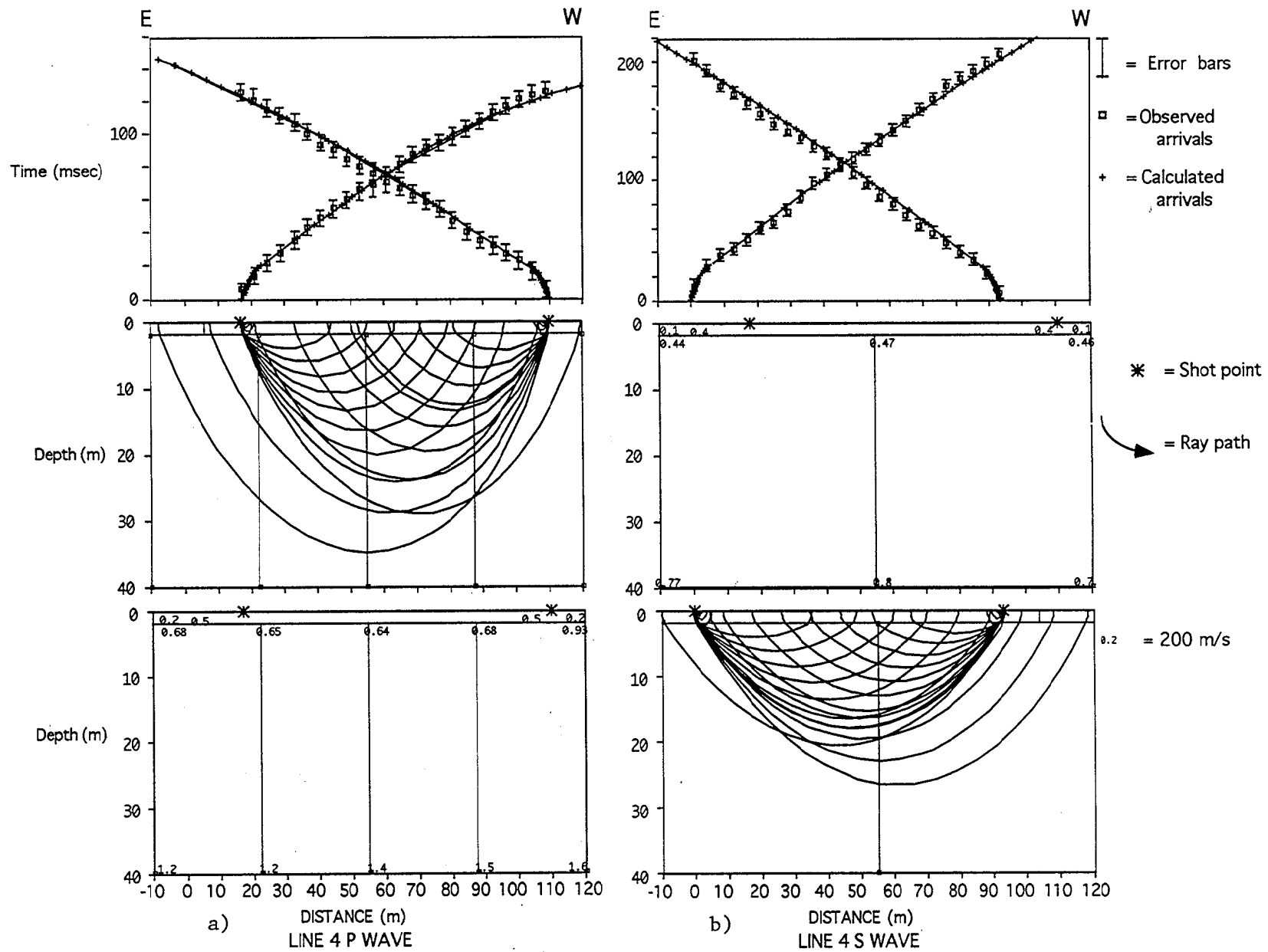


Figure 18 : Line 4 travel-time plots, ray paths, and velocity model (km/sec)



a) CPT-1, at the helipad location, northwest of Thornton



b) CPT-2, in the ravine, southwest of Thornton

Figure 19. The sites of CPT tests 1 through 4



c) CPT-3, at the southwest end of the Thornton west parking area



d) CPT-4, southeast of the hospital

Figure 19 (cont.) : The sites of CPT tests 1 through 4



UCSD

Site : SCRIPPS INSTITUTE  
Location : CPT-1

Client : LLNL  
Date : 10:31:96 09:05

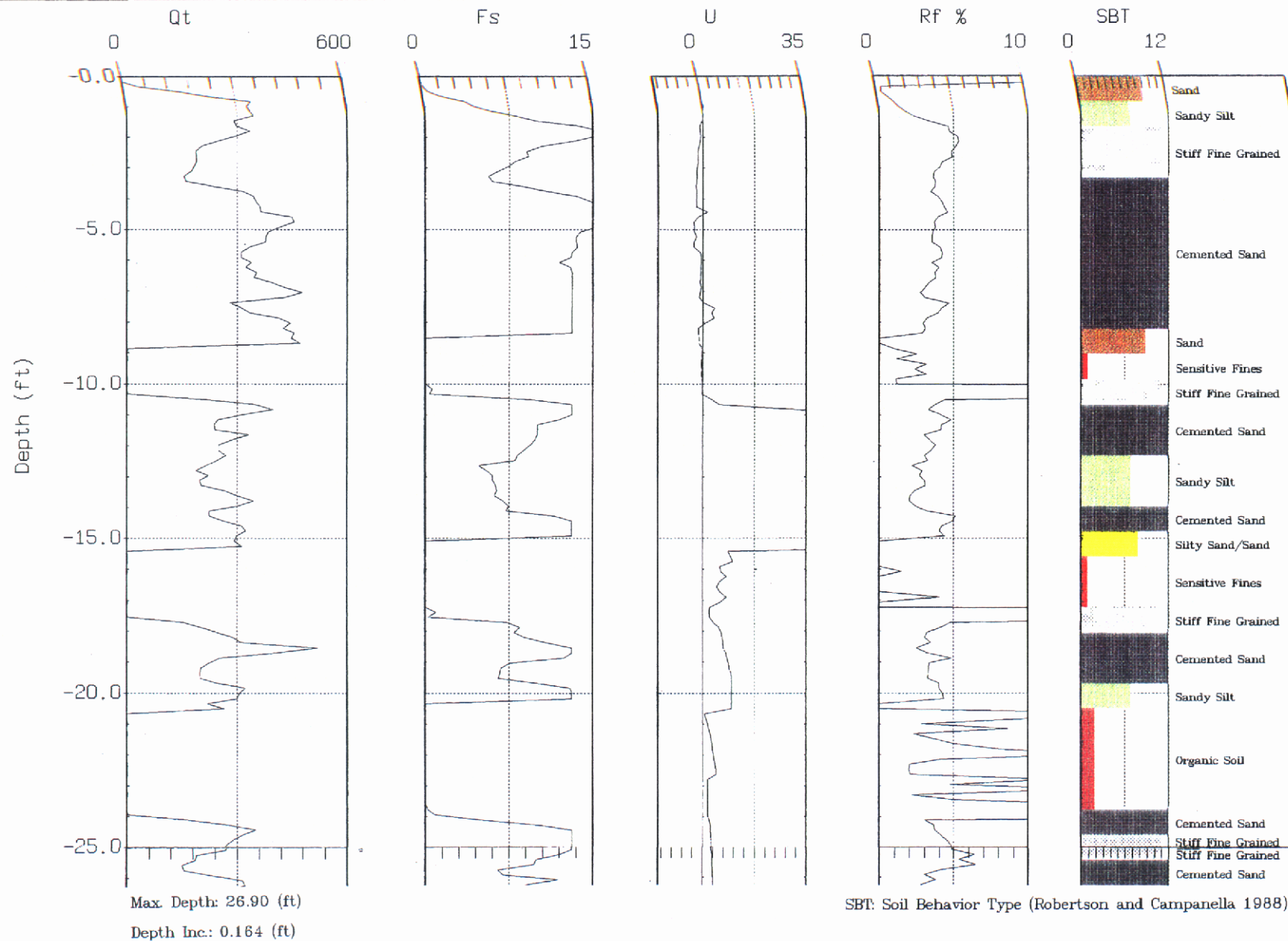


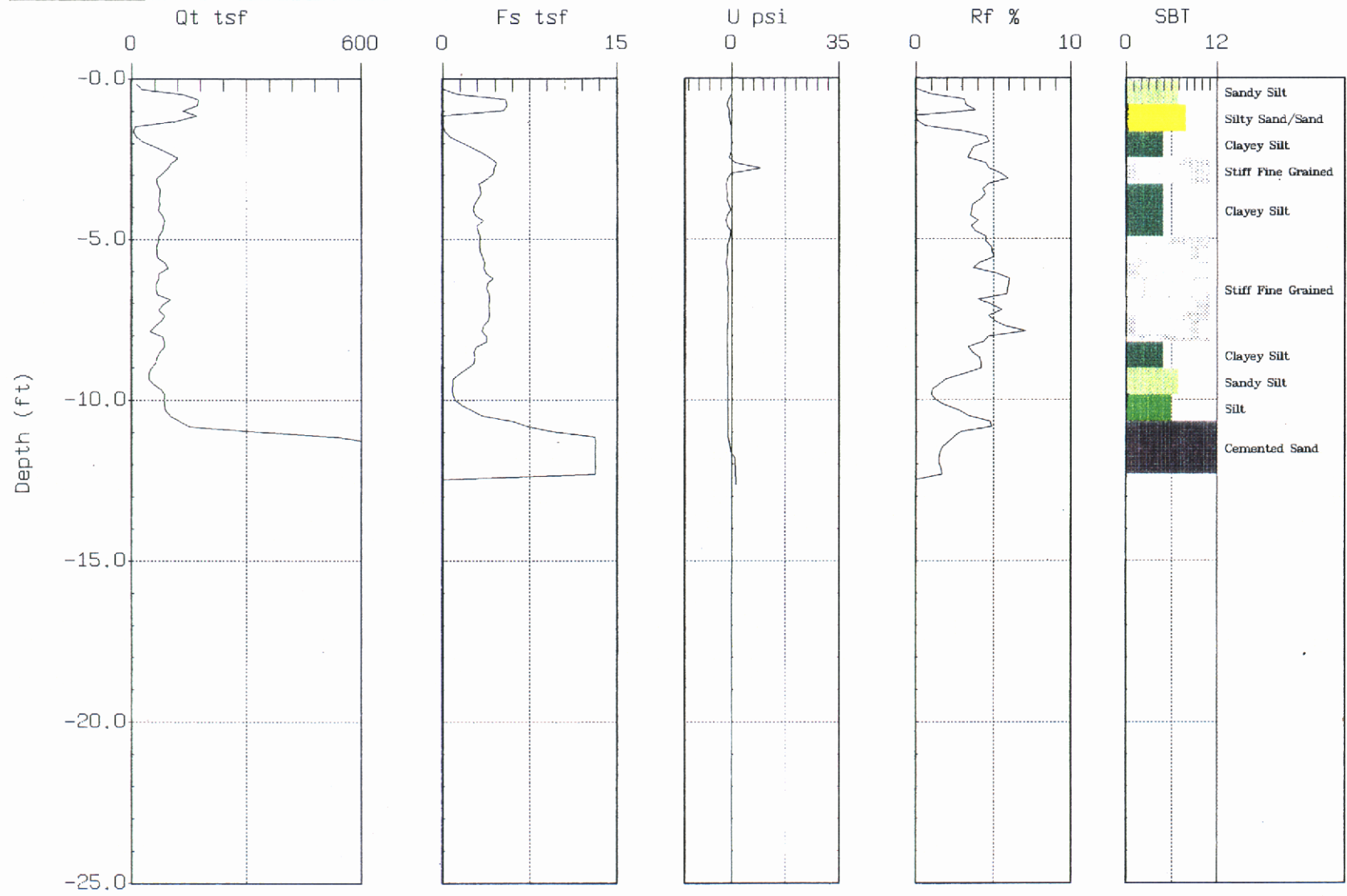
Figure 20. Cone penetration test results for CPT-1.



UCSD

Site : SCRIPPS INSTITUTE  
Location : CPT-3

Client : LLNL  
Date : 10:31:96 12:34



Max. Depth: 12.63 (ft)

Depth Inc.: 0.164 (ft)

SBT: Soil Behavior Type (Robertson and Campanella 1988)

Figure 22. Cone penetration test results for CPT-3.



UCSD

Site : SCRIPPS INSTITUTE  
Location : CPT-4

Client : LLNL  
Date : 10:31:96 13:19

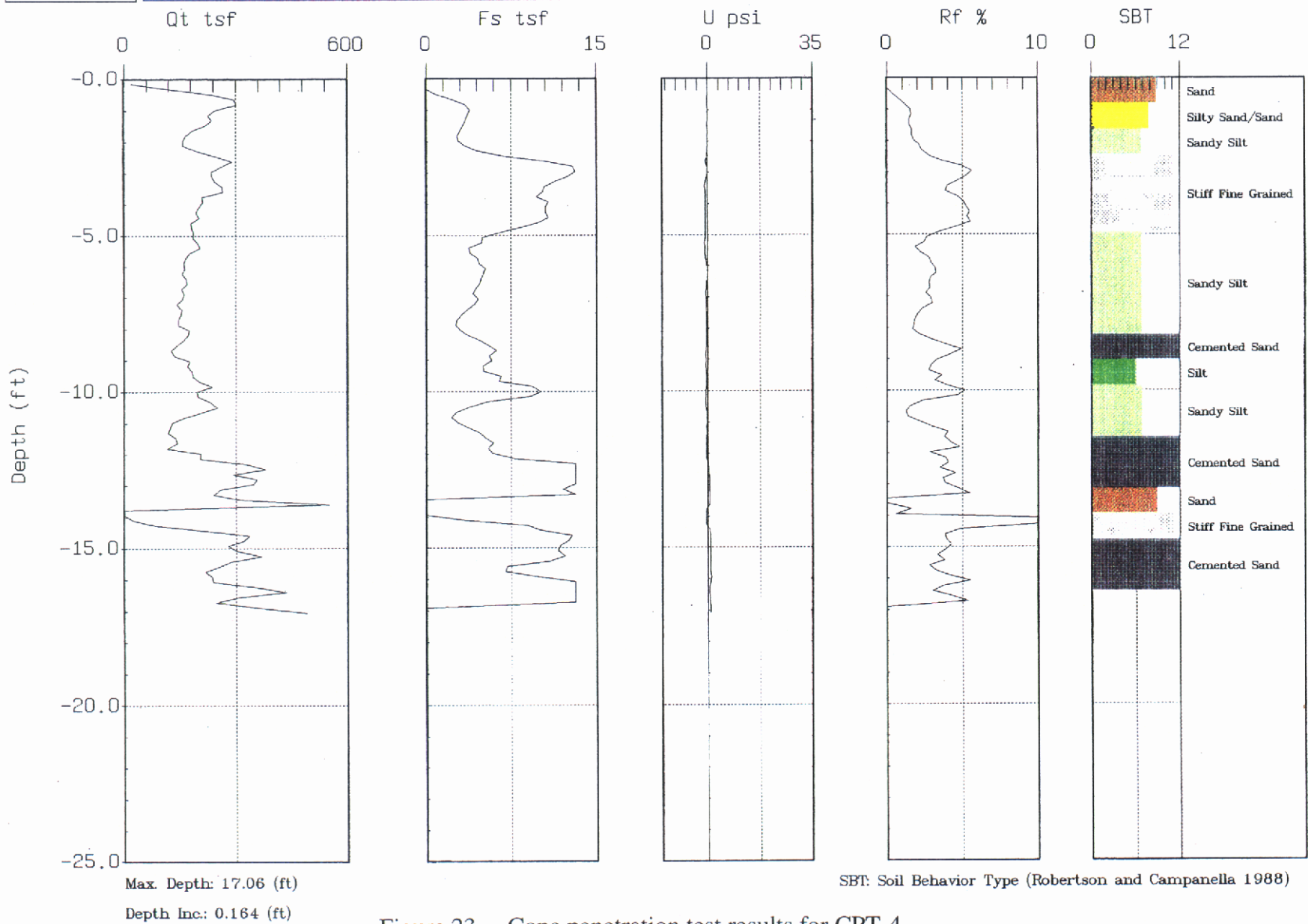


Figure 23. Cone penetration test results for CPT-4.

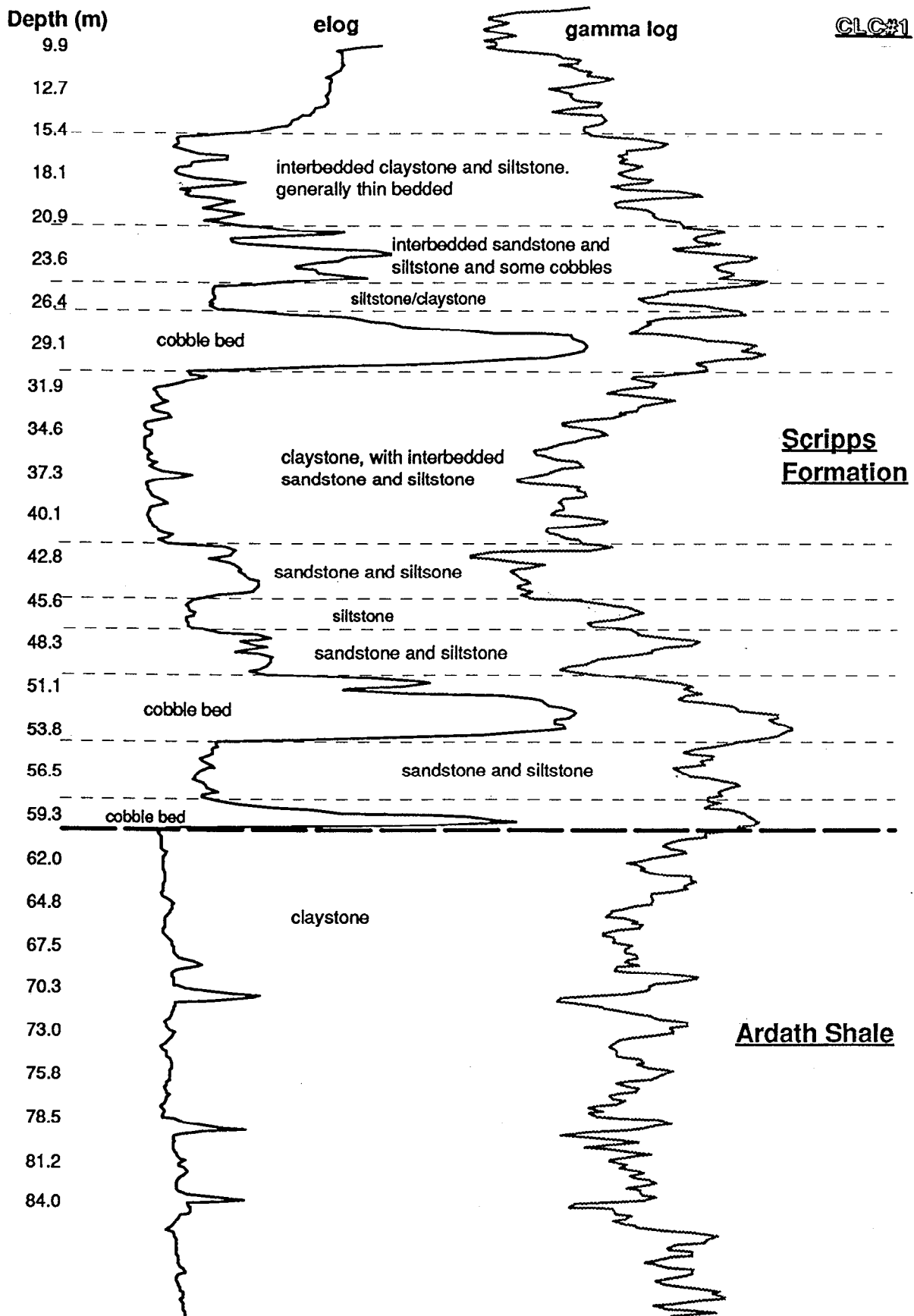


Figure 24. Lithologic section in deep hole CLC#1, as interpreted from cuttings samples, Pitcher samples, and geophysical logs.

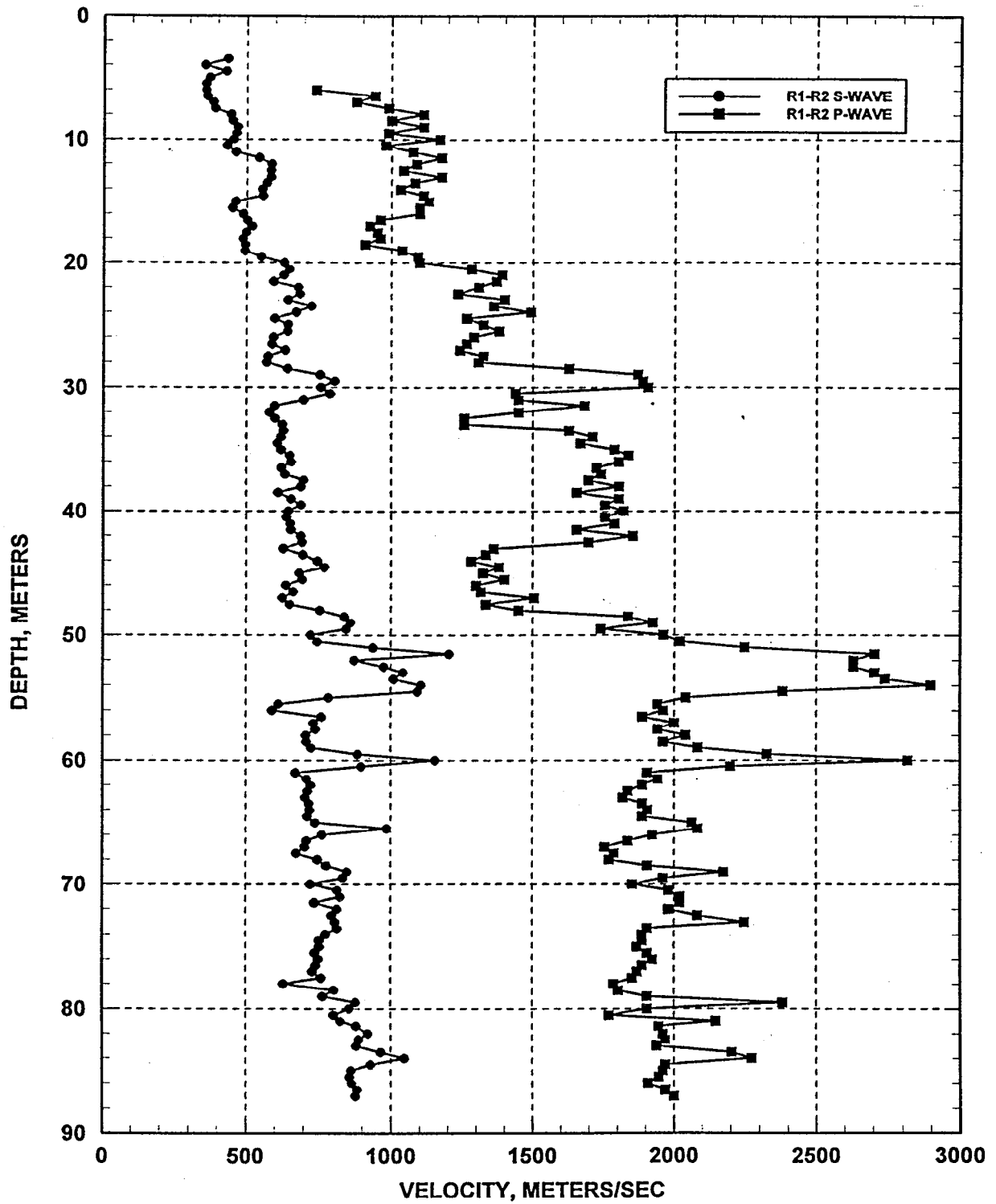


Figure 25. Borehole CLC#1, suspension P- and SH wave velocities.

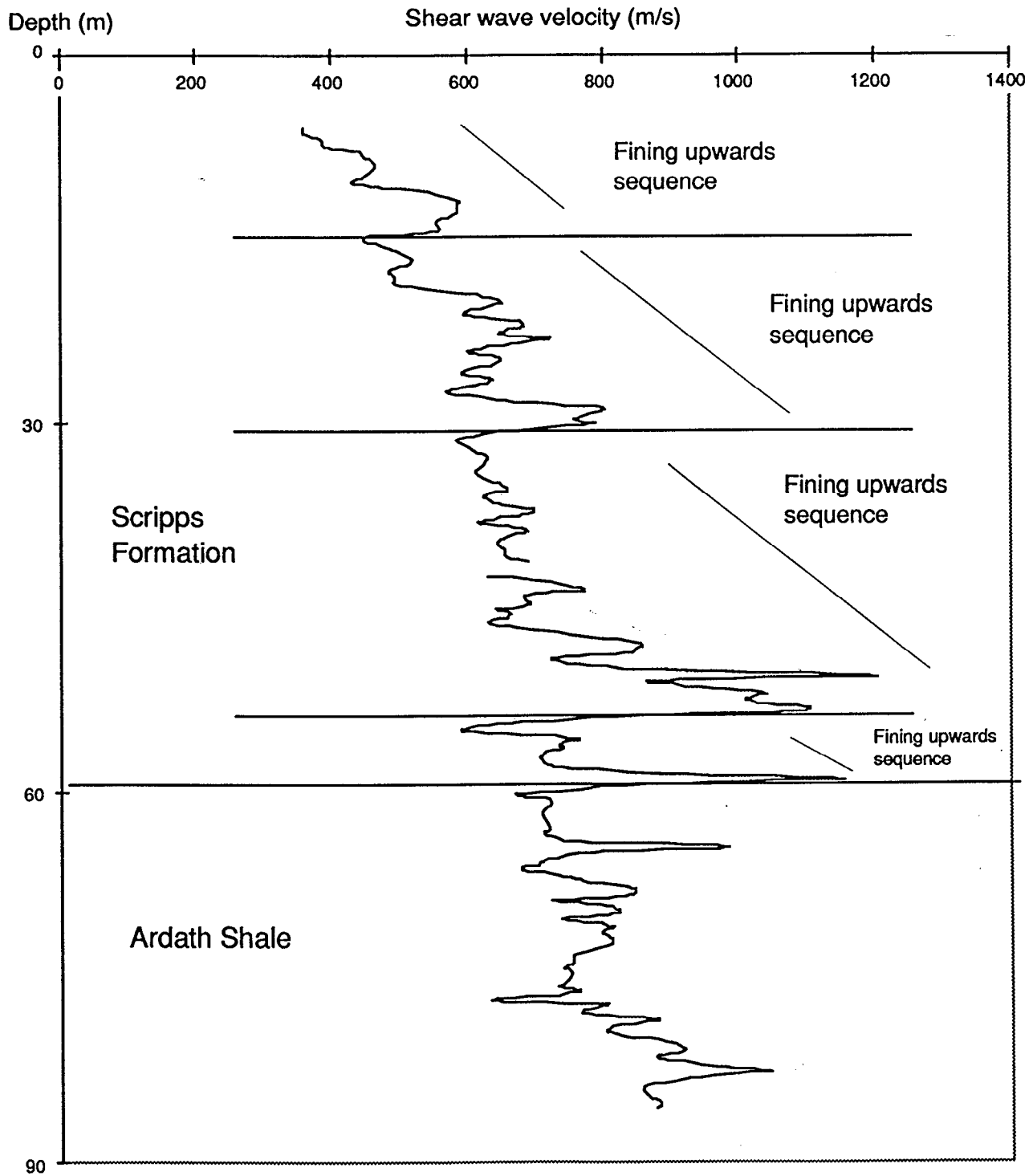


Figure 26. Fining upwards sequences in the Scripps Formation, along with the shear-wave velocity log.

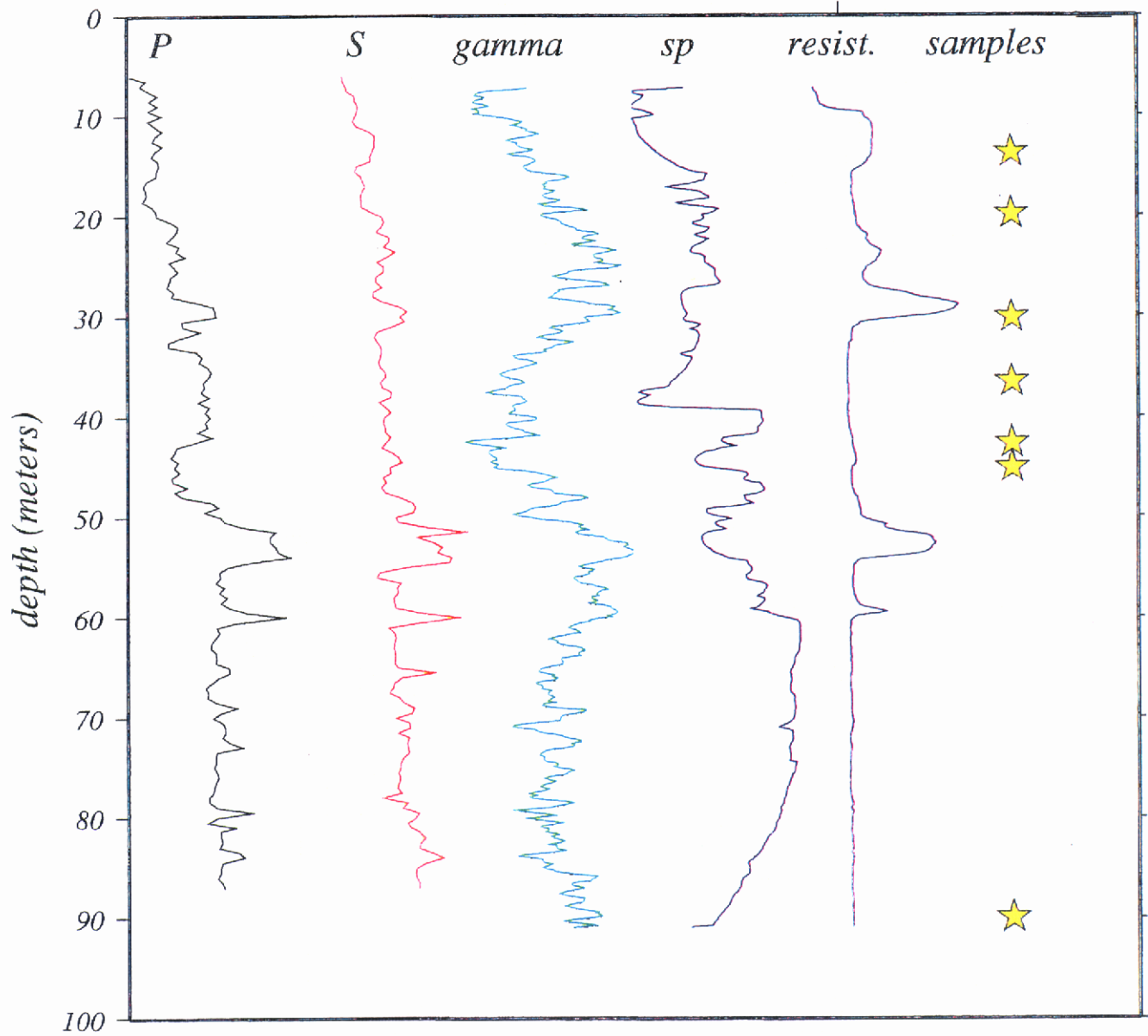


Figure 27. Summary depth profile of the various logs and sample locations

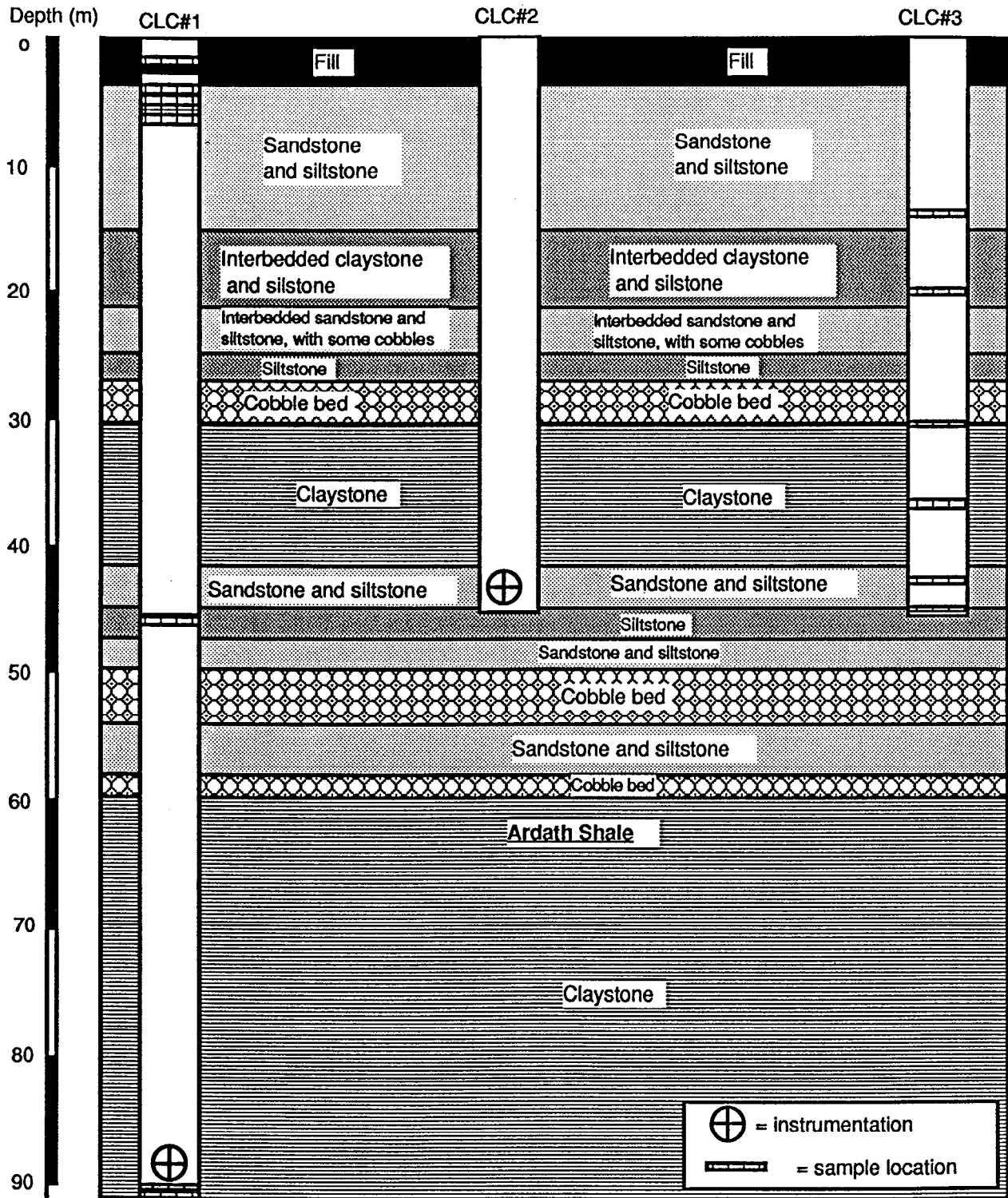


Figure 28. Schematic showing stratigraphy in holes CLC#1, CLC#2, and CLC#3, with locations of Pitcher samples and downhole instrumentation.

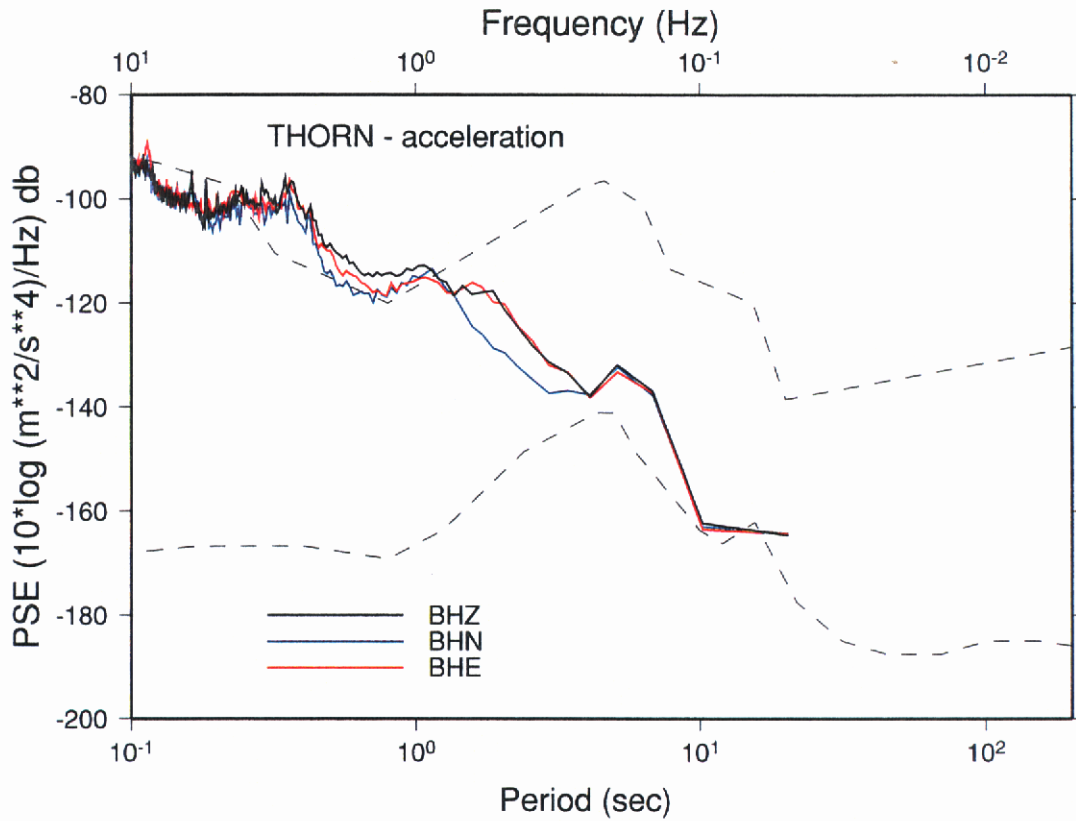


Figure 29. Summary of results of the seismic background noise survey at Thornton hospital.

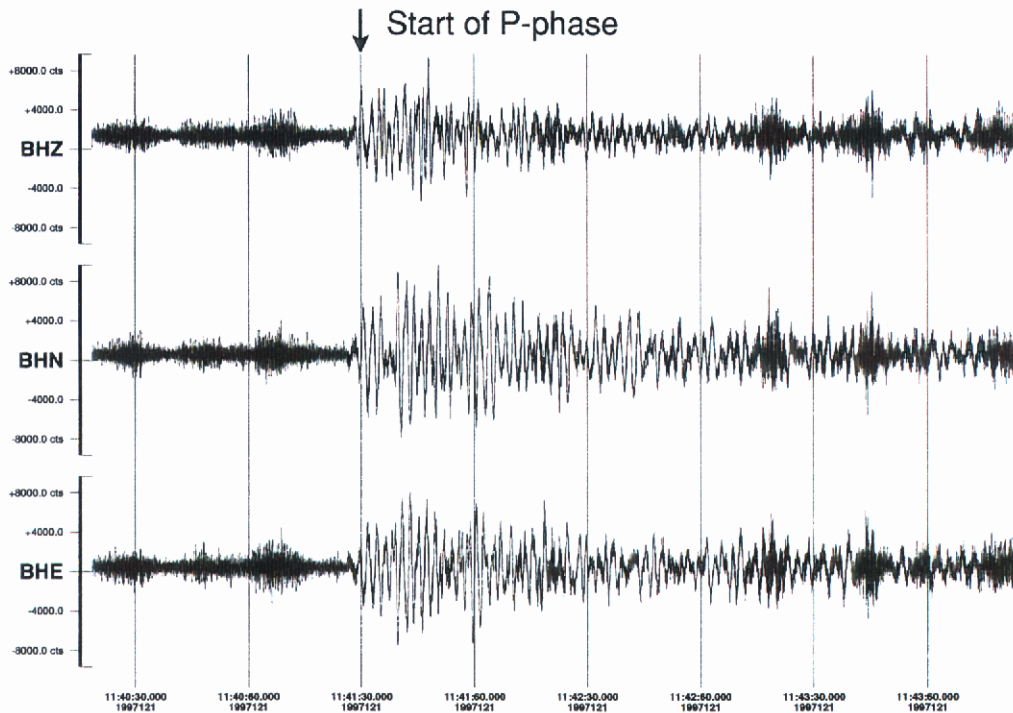


Figure 30. P-wave broadband records from an mb 5.2 event at 1840 km, during the noise survey

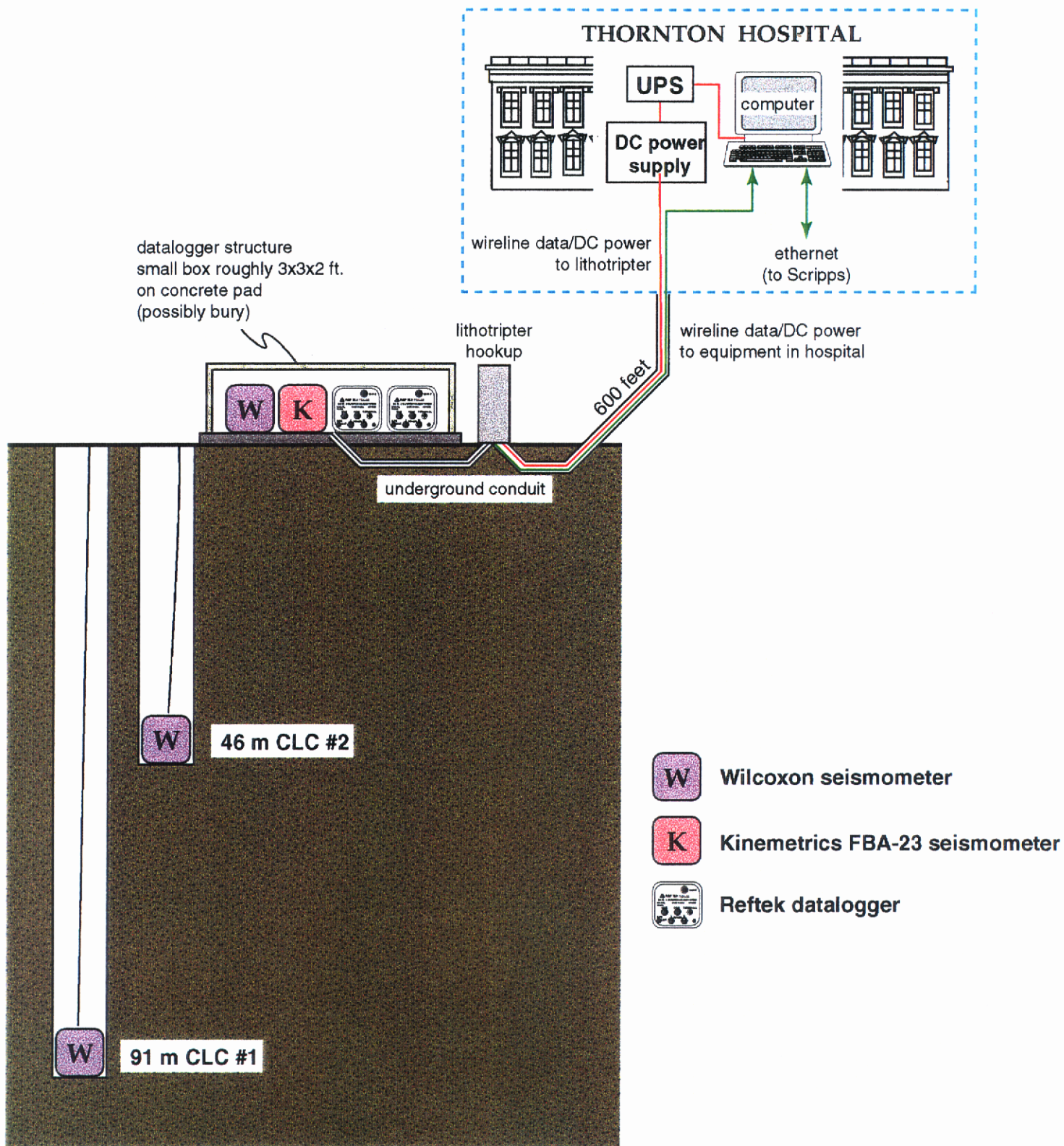


Figure 31. Conceptual design of the Thornton hospital seismic station.

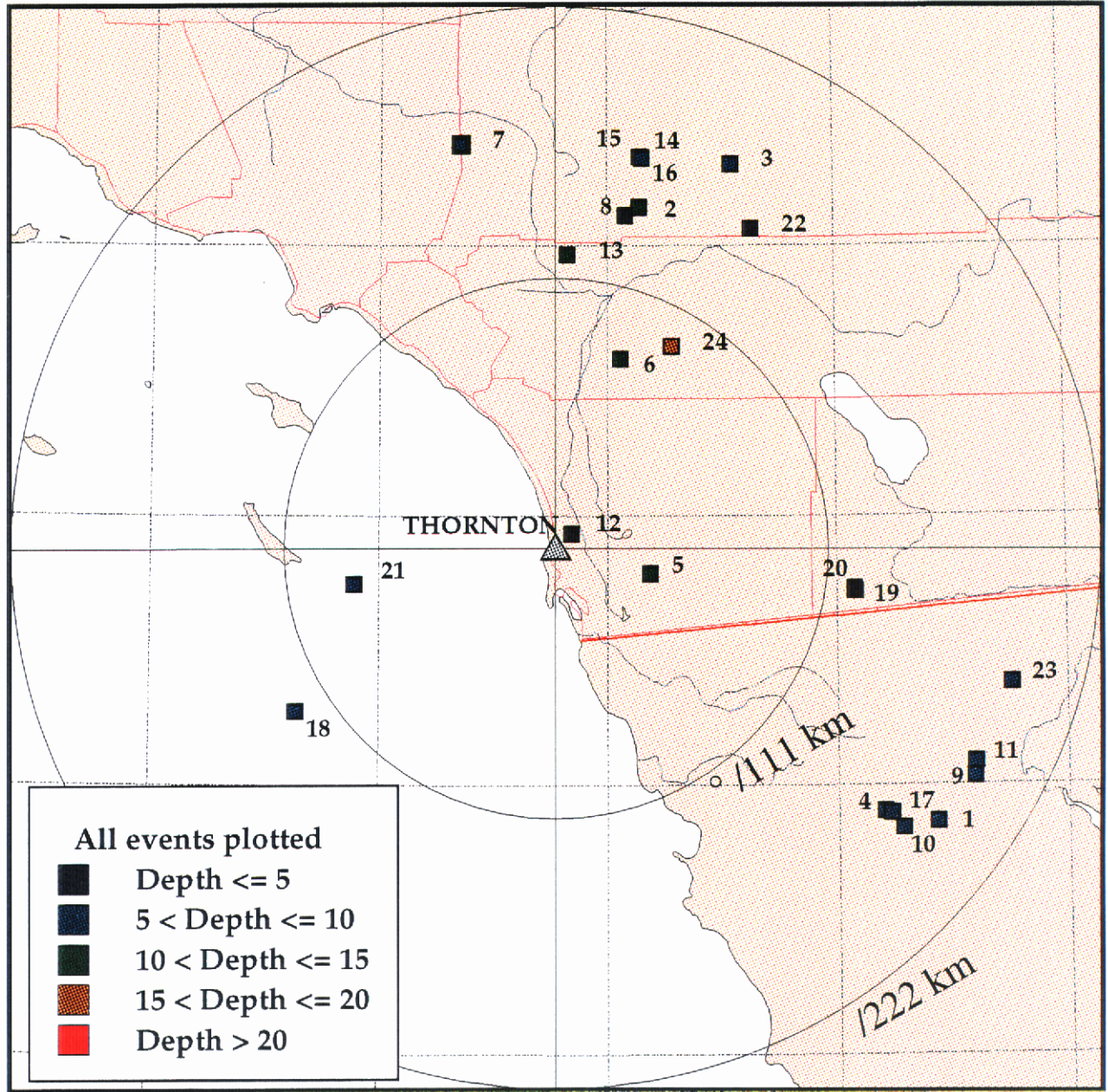


Figure 32 : Epicentral locations of seismic events recorded at Thornton up to July 19, 1999.

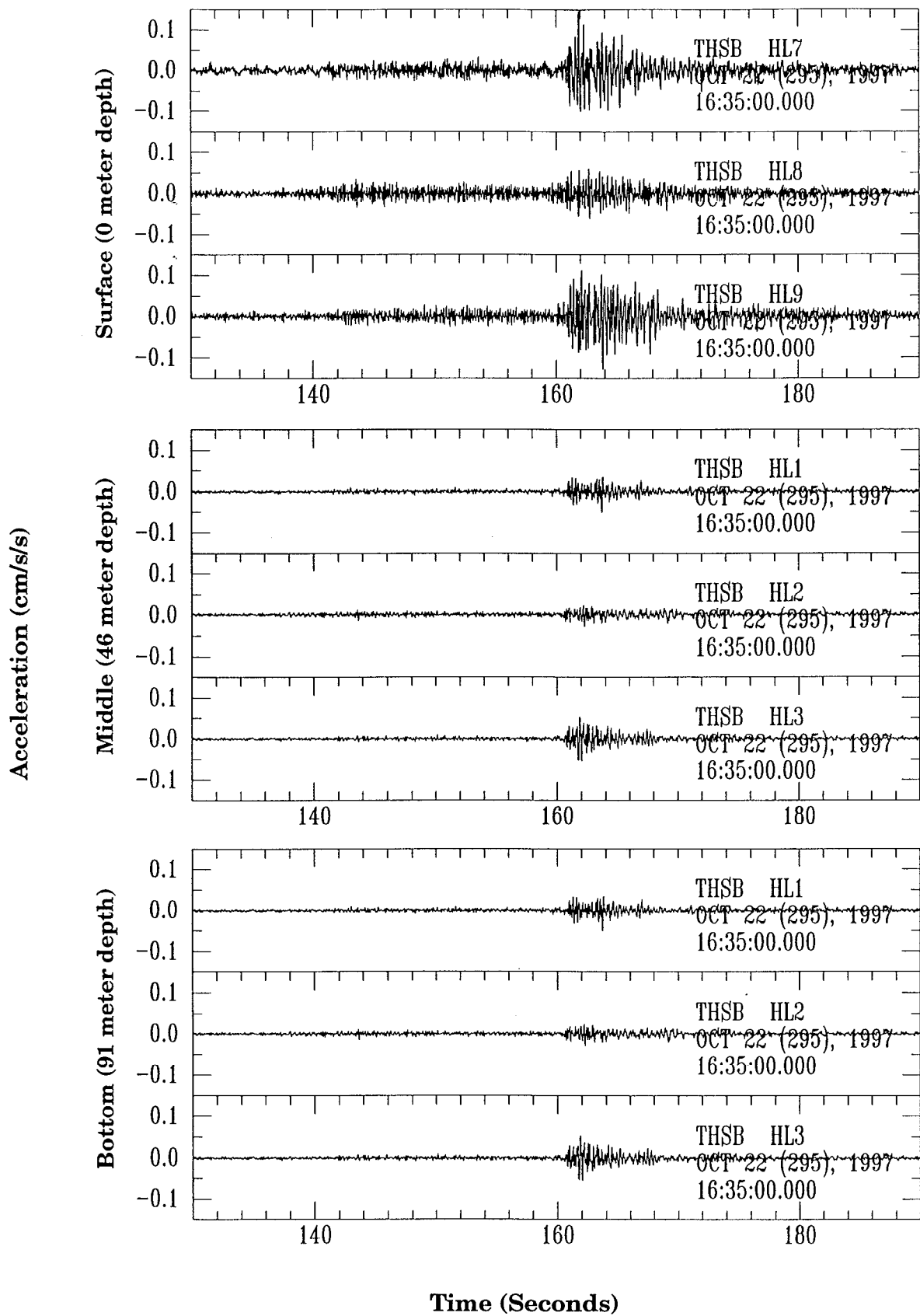


Figure 33 : Records from a M 3.0 earthquake at a distance of 172 km, on October 22, 1997.

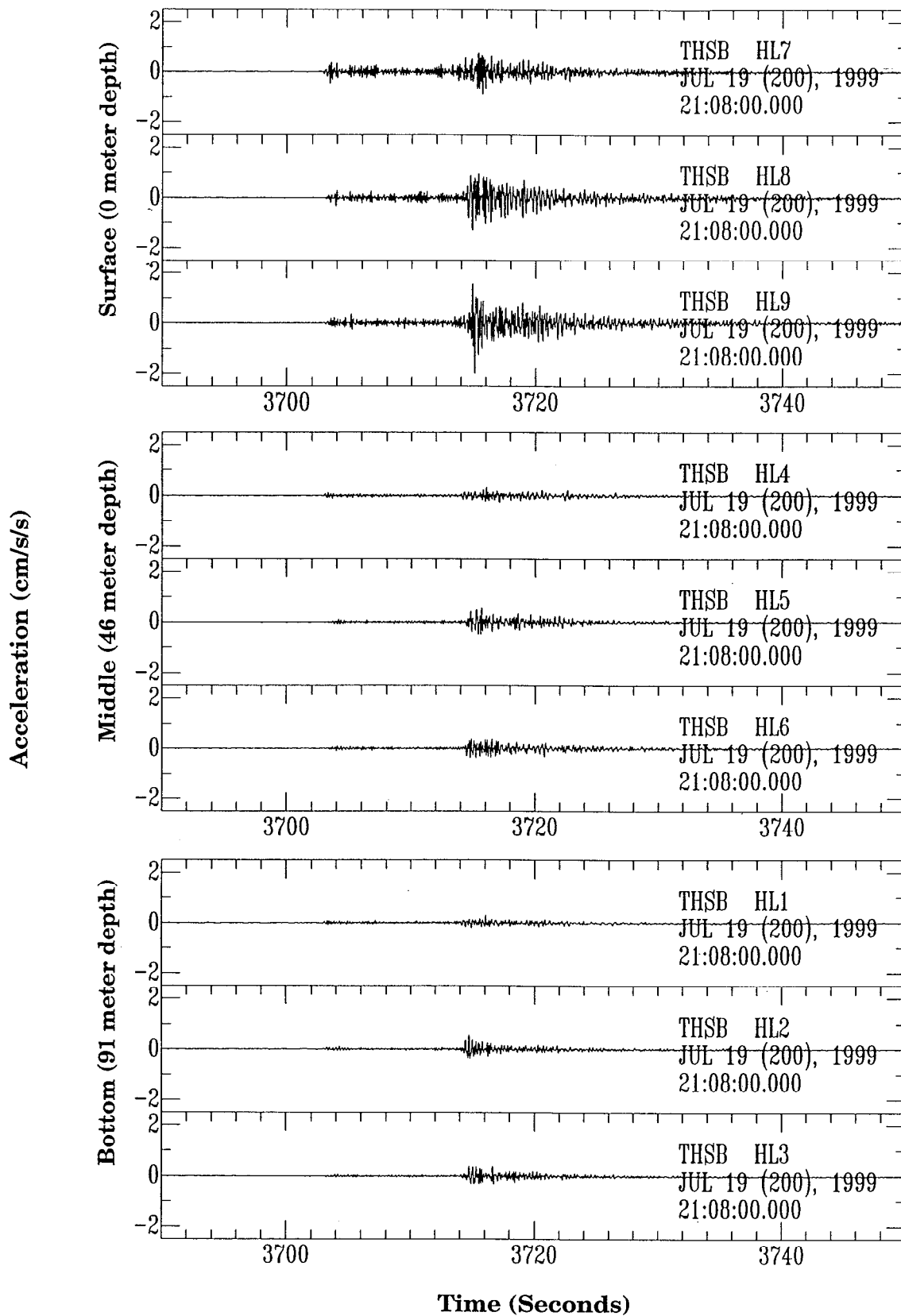


Figure 34 : Records from a M 4.4 earthquake at a distance of 96 km, on July 19, 1999.

UCSD Event 24 - M 4.4 - 7/19/99

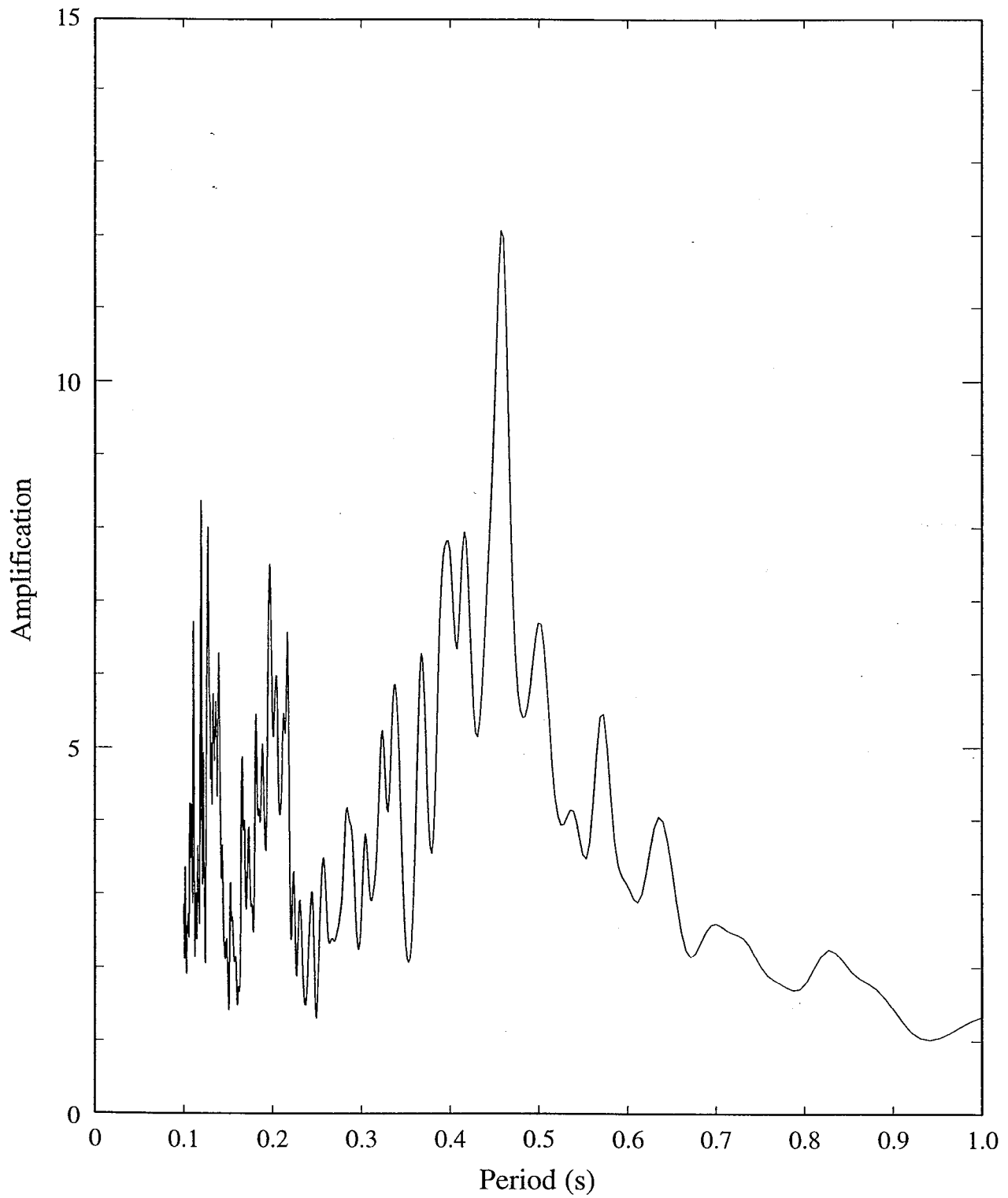


Figure 35 : Amplification of spectral horizontal acceleration, from 91-m depth to surface, at the Thornton site.